UNIVERSITY OF OKLAHOMA

GRADUATE COLLEGE

BUCKLING AND FLEXURAL VIBRATION OF RECTANGULAR PLATES SUBJECTED TO HALF SINUSOIDAL LOAD ON TWO OPPOSITE EDGES

A Dissertation

SUBMITTED TO THE GRADUATE FACULTY

in partial fulfillment of the requirements for the

degree of

Doctor of Philosophy

BY

KRISHNA KANTH DEVARAKONDA

Norman, Oklahoma

2004

BUCKLING AND FLEXURAL VIBRATION OF RECTANGULAR PLATES
SUBJECTED TO HALF SINUSOIDAL LOAD ON TWO OPPOSITE EDGES

A Dissertation APPROVED FOR THE
SCHOOL OF AEROSPACE AND MECHANICAL ENGINEERING

BY

Charles W. Best
Dr. Charles W. Best

Dr. Alfred G. Striz

Dr. James D. Baldwin

Feng-Chyuan Lai
Dr. Feng-Chyuan Lai

S. Gutman
Dr. Semion Gutman

ACKNOWLEDGMENTS

I would like to sincerely thank my chief advisor Dr. Charles W. Bert for his guidance, encouragement and support throughout my research. It is an honor for me to say that I learned a great deal on solid mechanics during my wonderful association with Dr. Bert both in and outside the classroom. His vision and dedication in mechanical engineering is a guiding beacon for me to carry the responsibility forward.

I would like to express my sincere appreciation to Dr. J.D. Baldwin for his support in providing me the finite element package. I fondly remember all those occasions when he encouraged me during various difficult times. I extend my sincere thanks to Dr. A.G. Striz for his help and advice on the finite element analysis. I remain thankful to Dr. Feng Lai for his friendly advice and Dr. S. Gutman for his advice regarding power series solution of differential equations. I am blessed to have such a wonderful committee.

I am very thankful to other giants of solid mechanics with whom I had discussions concerning my research. I thank Prof. A.W. Leissa (formerly of Ohio State University) for his advice on the Frobenius method and Prof. J.N. Reddy (of Texas A&M University) on his advice on the in-plane elasticity solution. In this connection, I would like to convey once again my thanks to Dr.Charles W. Bert for arranging time to meet with them. Thanks are also due to Prof. D. J. Gorman (formerly of the University of Ottawa) for his helpful suggestions on the superposition method.

The help of many past and present staff members at the AME office is very much appreciated. I thank the support of all my friends with whom I shared and discussed various aspects of my research. Among them I thank Mr. Gopinath Venkatesan for providing me some crucial references on the in-plane elasticity solution.

I thank my parents and my in-laws for their love, support and encouragement which sustained me during the development of this work. Last but not least, my special thanks are to my wife Sapna for her understanding and support throughout my research. I remain indebted to her for all the sacrifices she made in helping to make this manuscript become a reality. My special thanks goes to my daughter Maheeka whose addition to the family recently is a true blessing. Her smile is the driving force for me to overcome all the hardships of life.

TABLE OF CONTENTS

LIST OF TABLES

LIST OF FIGURES

NOMENCLATURE

A_{mn}, C= constants of polynomial solution

A_n, B_m = constants in the Pickett solution

a, b = plate size along x,y co-ordinate directions respectively

C_1,C_2,C_3,C_4 = constants in the superposition method

D = flexural rigidity

D_{1m}, D_{4m} = constants

F_{1m} = Fourier expansion term

h = plate thickness

k = aspect ratio = a/b

N_{xx} = normal stress resultant in the x-direction

N_{yy} = normal stress resultant in the y-direction

N_{xy} = shear stress resultant

R = uniform x-direction normal stress

r = multiplication factor

t = time

w = transverse deflection

α = constant in the polynomial solution

α_1, α_2, α_3 = constants in the Timoshenko solution

φ= Airy stress function

φ_1,φ_2,φ_3,φ_4 = Airy stress functions of the superposition method

η = dimensionless y co-ordinate = y/b

ξ = dimensionless x co-ordinate = x/a

ρ = plate density

σ_{x1}, σ_{y1}, τ_{xy1} = normal and shear stresses corresponding to stress function φ_1

σ_{x2}, σ_{y2}, τ_{xy2} = normal and shear stresses corresponding to stress function φ_2

σ_{x3}, σ_{y3}, τ_{xy3} = normal and shear stresses corresponding to stress function φ_3

σ_{x4}, σ_{y4}, τ_{xy4} = normal and shear stresses corresponding to stress function φ_4

σ_0 = maximum applied edge stress in the x-direction

σ_x = in-plane normal stress in the x-direction

σ_y = in-plane normal stress in the y-direction

τ_{xy} = in-plane shear stress

ω = transverse vibration frequency

Ω = dimensionless transverse vibration frequency

Ω_s = dimensionless fundamental natural vibration frequency

ABSTRACT

The problem of buckling of thin rectangular plates subjected to uniform and linearly varying in-plane load has been solved quite some time back beginning with the work of Bryan in 1890-91. Recently, Leissa and Kang obtained an exact solution in a series sense for the problem of buckling of rectangular plates subjected to *linearly* varying in-plane load. The case of buckling of rectangular plates subjected to *nonlinearly* varying in-plane load in the x direction received less attention, and the same problem was solved by van der Neut for the case of half-sinusoidal loading and by Benoy for the case of parabolic in-plane load. However, in their analyses, they considered an over-simplified in-plane solution by assuming the x-direction in-plane stress distribution to be the same at every plate section and the y-direction normal stress to be zero.

Based on the mechanics of the problem, one can expect that the x-direction in-plane stress distribution should exhibit the stress diffusion phenomenon as the plate aspect ratio is increased. The present work is threefold, wherein the first part deals with obtaining an in-plane elasticity solution for half sinusoidal edge loads on two opposite edges. Also present solution was compared with the in-plane solutions developed earlier in the literature as well as a numerical (finite element) solution. From the results thus obtained, it was concluded that the in-plane solutions were quite similar in terms of x-direction normal stresses. The y-direction normal stresses showed wide variations among the various methods and it was observed that some of the solutions produced some spurious stresses at the boundaries.

The second part of the present work investigates the buckling loads of rectangular plates subjected to half-sinusoidal in-plane loads for various edge conditions involving simply supported and clamped edge conditions. Using the Galerkin method, buckling loads are estimated for various plate sizes, and the results are compared with finite element solutions.

In the third part, the natural frequencies and mode shapes of rectangular plates subjected to the above mentioned edge loads on two opposite edges are obtained. Using the in-plane elasticity solution developed in part one, flexural vibration analysis is carried out and the results are compared with those from finite element analysis. Extensive results of dimensionless frequencies are tabulated for reference. Further research is recommended.

In loving memory of

My Teacher Late N. V. Krishna Rao

&

Uncle Late K. Venkanna

Who inspired me with their wisdom, love and affection throughout my education

CHAPTER ONE

INTRODUCTION

The problem of buckling of a rectangular elastic plate subjected to in-plane compressive or shear loading is important in the shipbuilding, aircraft, and automotive industries. The first work in this area was due to Bryan (1890-1891); see Timoshenko and Gere (1961), page 351. Bryan considered the case of uniformly distributed compressive loading with all four edges simply supported. Buckling of rectangular plates when all the edges are clamped was first analyzed by Taylor (1933). Shuleshko (1956, 1957) obtained buckling loads of rectangular plates with combinations of clamped, free, and simply supported edge conditions under uniaxial and biaxial edge loads.

El-Bayoumy (1971) obtained buckling loads for plates with all edges clamped using an extended Kantorovich method (which is an iterative version of the Kantorovich method, ref. Kerr 1969) and showed that accurate results for all aspect ratios can be obtained in a relatively small number of iterations. The cases of more complicated boundary conditions have been solved by innumerable investigators through the years and were summarized in books (Timoshenko and Gere 1961, Brush and Almroth 1975, Bazant and Cedolin 1991).

The case of linearly varying edge loading was first considered independently in 1910 by Timoshenko and in 1914 by Boobnov, using approximate methods; see Timoshenko and Gere (1961), page 373. This loading case was also analyzed, using approximate methods, by Way (1936), Favre (1948), Grossman (1949), Noel (1952), McKenzie (1964), and Dawe (1969).

For plate problems subjected to generalized in-plane load conditions, Bassily and Dickinson (1978) used the Ritz method for both an in-plane elasticity solution and an out-of-plane solution using beam functions. However, for the case of free edges, the Ritz method places no restrictions on the trial functions, as all the boundary conditions are natural or stress type conditions. Consequently, one cannot be assured of boundary condition satisfaction for the case of free edges. In order to overcome this, degenerate beam functions were proposed by Bassily and Dickinson (1975), and Bhat (1985) proposed sets of simple orthogonal polynomials.

For mixed boundary conditions, one can consider the superposition method instead of approximate methods such as the energy method. The superposition method as given by Timoshenko (Timoshenko and Goodier 1970) and used extensively by Gorman (ed. Guran and Inman 1999, and Gorman 2000) involves subdividing the given problem into building blocks and superposing the resulting solutions. With reference to mixed boundary conditions, one can consider the building blocks in such a way that each problem considers a part of the boundary conditions. Using such a superposition method, Gorman (2000) obtained buckling loads for rectangular plates having two opposite edges free and the other edges elastically supported.

Conventionally, variational methods such as the Rayleigh-Ritz and Galerkin methods are extensively used (Reddy 1999) for plate problems. Among other approximate methods used for buckling analysis are Bolotin's method (Dickinson 1975), the complimentary energy method (Sundararajan 1980), and the extended Kantorovich method (Kerr 1969). Additionally, numerical methods such as the finite difference method and the finite element method are extensively used (Szilard 1974) for plate analysis. Recently, Chen (1998) evaluated buckling loads using a finite difference technique wherein the governing differential equation is used for the finite differences. He showed that use of finite differences on the governing partial differential equation is simpler than the finite element method.

Grimm and Gerdeen (1975) simplified the extended Kantorovich method by using numerical integration for solving the iterative equations and obtained buckling loads for various edge conditions subjected to uniform and nonuniform edge loads. It is interesting to note that they considered a half cosine edge load distribution only on one edge as given in Massonnet (1962, see page 37-10). Using the half cosine edge load on one edge and a combination of uniform and linearly varying edge loads on the other two edges, they obtained buckling loads for various plate aspect ratios. The accuracy of the numerical results is established by comparing the solutions where classical solutions are available.

Experimental results on plate buckling were obtained simultaneously throughout the early 19th century, and the results were summarized in Timoshenko and Gere (1961) and in a review article by Walker in 1984.

Among the distributed edge load buckling problems, Brown (1991) was the first one to have considered tangential edge loads acting on the surface of the plate. Using the conjugate-displacement method, he obtained buckling loads for various edge conditions and tangential loads which were uniform and linearly varying along the plate length. In a related work, Wang et al. (2002) considered buckling of rectangular plates subjected to intermediate and end uniaxial loads. By decomposing the plate problem into two sub problems they obtained buckling solutions for the total plate by using continuity conditions at the separated edges.

Recently, Leissa and Kang (2001) and Kang and Leissa (2001) considered the plate buckling problem subjected to linearly varying in-plane load and obtained exact solution in a series sense. By considering the transverse displacement as sinusoidal in one direction, the governing differential equation can be solved by assuming a power series solution. Extensive results were tabulated for linearly varying in-plane edge load conditions including moment loads. Much more complete results of rectangular plate buckling under various boundary and load conditions were summarized in a handbook by Bloom and Coffin (2001).

There have been very few previous buckling solutions for the case of nonlinearly distributed edge loadings. Perhaps this scarcity is due to the additional complexity of having to first solve for the internal pre-stress distribution as a problem in plane stress elasticity. The first work in this area was due to Timoshenko (1924), who obtained an in-plane solution for the case of parabolic in-plane loading by assuming stress functions which satisfy all the required stress boundary conditions. As the solution thus presented cannot possibly satisfy the compatibility equations, one can conclude that it is an approximate solution. However, the present study indicated that the Timoshenko solution is exactly identical to the in-plane solution obtained by the Galerkin method using the same trial functions.

Later, Pickett (1944) proposed a solution by the superposition method which satisfied the governing differential equation and the compatibility equations, but some residual stresses remained at the boundaries. Apparently unaware of the in-plane stress solutions as developed by Timoshenko and Pickett, van der Neut (1958) considered uniaxial compressive loading with a half sine distribution. In his analysis, he subdivided the parabolic in-plane stress distribution into uniform and nonuniform components. By equating the additional work done due to the non-uniform component with the elastic energy due to uniform stresses, he estimated the buckling load. Moreover, no attempt has been made to solve the in-plane elasticity problem. Using parabolic in-plane stress distributions on two opposite edges, Benoy (1969) obtained buckling loads for plates having simply supported and clamped boundary conditions.

It should be pointed out that the works of van der Neut (1958) and Benoy (1969) both suffered from these serious deficiencies:

- The x-direction in-plane normal stress distribution was tacitly assumed to depend only on the y-position coordinate. (In actuality, there is a stress-diffusion phenomenon which causes this stress distribution to vary with x as well as y.)
- The contributions of the y-direction in-plane normal stress distribution and the in-plane shear stress distribution have been ignored.

Recently, Hu et al. (1999) obtained buckling loads for rectangular plates subjected to parabolically varying in-plane loads. Assuming a parabolic distribution, they successively integrated such that the in-plane stresses satisfied the governing differential equation in terms of the Airy stress function. Although their solution contained y-direction normal stresses and shear stresses, they remained the same throughout the plate. Moreover, the x-direction stress distribution was only a function of y, similar to the analysis of Benoy.

It is to be noted that the in-plane stress solutions as proposed by Timoshenko and Pickett do exhibit the stress diffusion phenomenon and can be considered quite suitable for buckling analysis. The goal of the present work is three fold. The first objective is to obtain an in-plane stress solution which satisfies the governing differential equation in terms of an Airy stress function and simultaneously satisfies all of the boundary conditions. Using the in-plane stress solutions thus developed, the second objective is to carry out more accurate buckling analysis and finally the flexural vibration analysis of has to be carried out.

Free flexural vibration analysis of thin rectangular plates has been studied extensively in the literature (Leissa 1969 and 1973). The vibration of plates subjected to only uniform in-plane forces was studied by Weinstein and Chien (1943), Lurie(1952), and Kaul and Tewari (1958). The same problem under uniform in-plane normal stress as well as shear stress was considered by Dickinson (1971) using the Ritz method. Simons and Leissa (1971) considered arbitrary in-plane acceleration loads and used beam eigen functions in the Ritz method. Mei and Yang (1972) used the finite element method for plate vibrations under combinations of in-plane loads including pure bending and linearly varying loads. Bassily and Dickinson (1973) used a perturbation technique for vibration problems involving arbitrary in-plane loads. Chan and Foo (1979) used the finite strip method for uniformly loaded plates and compared results with the available solutions in the literature.

Kielb and Han (1980) considered uniform in-plane loads and obtained vibration frequencies for all possible combinations of simply supported and clamped edge conditions.

Laura et al., (1977) considered rectangular plates subjected to parabolic tensile in-plane edge loading as proposed by Timoshenko and Goodier(1970). In their analysis, they considered transverse deflections in terms of polynomial functions in terms of x and y coordinate functions. However, they failed to present the frequencies and the associated mode shapes for this in-plane load condition. Recently, Leissa and Kang (2001) and Kang and Leissa (2001) obtained exact series solutions for buckling and natural frequencies of rectangular plates subjected to *linearly* varying in-plane loads.

CHAPTER TWO

IN-PLANE ELASTICITY SOLUTION

2.1 Problem Definition

In the present study, the rectangular plate buckling and vibration analysis problems subjected to nonlinear uniaxial in-plane loading are considered. Prior to analyzing the buckling and vibration characteristics of the rectangular plate, one has to find a satisfactory in-plane elasticity solution for a nonlinearly distributed in-plane load. The nonlinear in-plane load applied along two parallel edges is considered to have either parabolic or half sinusoidal variation in the present analysis. With reference to Figure 2.1, a thin rectangular plate having sides 2a, 2b along the x,y-coordinates, respectively, is subjected to either half sinusoidal or parabolic in-plane loading along the x-type edges. The placement of the origin of the coordinate system at the plate center is for mathematical convenience and, therefore, any other point such as the lower left corner could be used as well. In the present nonlinear edge load distribution, the maximum magnitude of the in-plane load occurs at the center of the edge (i.e., x = ±a, y = 0) while the y = ± b edges are stress free. Also, one can notice that all the plate edges remain free of in-plane shear stresses. Thus, the boundary conditions can be written as

$$at\,x=\pm a$$
$$\sigma_x = f\left(y^2\right) for\ parabolic\ distribution$$

$$or\ \cos\left(\frac{\pi y}{2b}\right) for\ half\ sinusoidal\ distribution \tag{2.1}$$

$$at\,x=\pm a,\quad \tau_{xy}=0 \tag{2.2}$$

$$at\ y=\pm b,\ \sigma_y\ and\ \tau_{xy}=0 \qquad (2.3)$$

Owing to the symmetry of the loading and boundary conditions, the coordinate system located at the plate center has certain advantages over any other location. Mathematically, one has to consider only the symmetric functions of x and y for the possible in-plane solution.

Based on the mechanics of the problem at hand, one can visualize that the in-plane σ_x stress distribution should vary along the x-axis and in particular it should show a stress diffusion phenomenon at higher plate aspect ratios. The aspect ratio is considered as the plate length (x-direction dimension) over plate width (y-direction dimension). In accordance with Saint-Venant's principle, for high aspect-ratio plates the in-plane σ_x stress distribution should become nearly uniform towards the plate center. One can expect that this stress diffusion to be greater as aspect ratio is increased. In a mathematical sense, the σ_x stress is a general function of x ,y throughout the plate.

Among the various solution methods for in-plane analysis, a polynomial stress function solution and a superposition method are considered in the present analysis. It is to be noted that some approximate in-plane solutions for a parabolically loaded rectangular plate are available in the literature. The first work in this area was due to Timoshenko (1924), who obtained an in-plane solution for the case of parabolic in-plane loading by assuming stress functions which satisfy all the required stress boundary conditions. As the solution thus presented cannot possibly satisfy the compatibility equations, one can conclude that it is an approximate solution. Pickett (1944) proposed a solution which satisfied the stress equilibrium equation and the compatibility equations, but some residual stresses remained at the boundaries. It is to be noted that the in-plane stress solutions as proposed by Timoshenko and Pickett do exhibit the stress diffusion phenomenon and can be considered quite suitable for the buckling analysis.

Apparently unaware of the in-plane stress solutions as developed by Timoshenko and Pickett, van der Neut (1958) considered a uniaxial compressive loading with a half sine distribution. Benoy (1969) considered a uniaxial compressive loading with a parabolic distribution and obtained an approximate energy solution.

It should be pointed out that the works of van der Neut (1958) and Benoy (1969) both suffered from the following deficiencies:

- The x-direction in-plane normal stress distribution was tacitly assumed to depend only on the y-position coordinate. In other words, the stress diffusion phenomenon is neglected.
- The contributions of the y-direction in-plane normal stress distribution and the in-plane shear stress distribution on buckling have been ignored.

2.2 Polynomial Solution

The plane elasticity problem for thin isotropic plates consists of obtaining solutions to the biharmonic equation in terms of the Airy stress function as shown in Equation (2.4).

$$\left(\frac{\partial^4}{\partial x^4}+2\frac{\partial^4}{\partial x^2 \partial y^2}+\frac{\partial^4}{\partial y^4}\right)\phi=0 \qquad (2.4)$$

where φ is the Airy stress function.

The stresses are determined by

$$\sigma_x = \frac{\partial^2 \phi}{\partial y^2}, \sigma_y = \frac{\partial^2 \phi}{\partial x^2}, \tau_{xy} = -\frac{\partial^2 \phi}{\partial x \partial y} \qquad (2.5a,b,c)$$

(The notation for the second subscript for x,y –direction stress definitions can be ignored for simplicity as there are no out-of-plane stress components)

Thus, for the present problem one has to find a solution for Equation (2.4) simultaneously satisfying the boundary conditions as specified in Equations (2.1) – (2.3). For continuous load conditions such as in the present problem, the polynomial method may give satisfactory results (Niedenfuhr 1957, Neou 1957). In essence the method consists of assuming the stress function as

$$\phi = \sum_{m=0}^{\infty} \sum_{n=0}^{\infty} A_{mn} \, x^m \, y^n \qquad (2.6)$$

Equation (2.6) when substituted in Equation (2.4) yields a polynomial equation which can be simplified using a systematic procedure suggested by Neidenfuhr and by Neou. Thus, Equation (2.4) with the stress function expressed by Equation (2.6) becomes

$$\begin{aligned} &\sum_{m=4}^{\infty} \sum_{n=0}^{\infty} m(m-1)(m-2)(m-3) x^{m-4} \, y^n \, A_{mn} + \\ &\qquad 2 \sum_{m=2}^{\infty} \sum_{n=2}^{\infty} m(m-1) n \, (n-1) x^{m-2} \, y^{n-2} \, A_{mn} + \\ &\qquad \sum_{m=0}^{\infty} \sum_{n=4}^{\infty} n(n-1)(n-2)(n-3) x^m \, y^{n-4} \, A_{mn} = 0 \end{aligned} \qquad (2.7)$$

Collecting similar powers of x and y, one can write Equation (2.7) as

$$\sum_{m=2}^{\infty} \sum_{n=2}^{\infty} \begin{bmatrix} (m+2)(m+1)m(m-1) A_{m+2,n-2} \\ +2m(m-1)n(n-1) A_{mn} \\ +(n+2)(n+1)n(n-1) A_{m-2,n+2} \end{bmatrix} x^{m-2} \, y^{n-2} = 0 \qquad (2.8)$$

Using Equation (2.8), one can obtain interrelations among constants A_{mn}.

With reference to the present problem, one has to consider terms up to order 4 so as to obtain stresses which are second order polynomials. It is to be noted that terms involving more than order 4 will result in higher order stresses in the plate. Balancing these higher order stresses in turn require additional terms. Thus one has to limit the order of the polynomial functions simultaneously balancing in such a way that the biharmonic equation (Equation 2.4) is satisfied. Following the polynomial method, one can obtain the stress function.

$$\phi = C\left(\frac{5}{3}y^4 + y^6 + 10x^2y^2 + 5x^4y^2 - 10x^2y^4 - 5x^4\right) \tag{2.9a}$$

where C is a constant to be determined from the boundary conditions.

The above stress function polynomial contains different orders of x and y which may cause some problems when equating the boundary conditions. For example, the σ_y stress is

$$\sigma_y = \frac{\partial^2\phi}{\partial x^2} = C\left(20y^2 + 60x^2y^2 - 20y^4 - 60x^2\right) \tag{2.10a}$$

At $y = \pm b$, σ_y cannot be equated to zero due to the varying orders of y in Equation (2.10a). In order to overcome this difficulty, one can multiply the lower order terms with plate dimension b without loss of generality. With reference to Equation (2.10a), if the first and last terms are multiplied with b^2, then the boundary condition can be satisfied exactly. The terms which are multiplied by b^2 in turn require other terms of the stress function φ to be multiplied as well. Thus, the modified stress function is

$$\phi = C\left(\frac{5}{3}b^2y^4 + y^6 + 10b^2x^2y^2 + 5x^4y^2 - 10x^2y^4 - 5b^2x^4\right) \tag{2.9b}$$

Using dimensionless parameters x/a = ξ, y/b = η, and k = a/b (aspect ratio of the plate) the above equation can be written as

$$\phi = C b^6 \left(\frac{5}{3}\eta^4 + \eta^6 + 10k^2\xi^2\eta^2 + 5k^4\xi^4\eta^2 - 10k^2\xi^2\eta^4 - 5k^4\xi^4 \right) \qquad (2.9c)$$

with stresses

$$\sigma_x = C b^4 \left(20\eta^2 + 30\eta^4 + 20k^2\xi^2 + 10k^4\xi^4 - 120k^2\xi^2\eta^2\right) \qquad (2.11a)$$

$$\sigma_y = C b^4 \left(20\eta^2 + 60k^2\xi^2\eta^2 - 20\eta^4 - 60k^2\xi^2\right) \qquad (2.11b)$$

$$\tau_{xy} = -C b^4 \left(40k\xi\eta + 40k^3\xi^3\eta - 80k\xi\eta^3\right) \qquad (2.11c)$$

Applying the σ_x boundary condition at the $\xi = \pm 1$ edges,

$$\sigma_x = C b^4 \left(20\eta^2 + 30\eta^4 + 20k^2 + 10k^4 - 120k^2\eta^2\right) \qquad (2.12a)$$

Now $\sigma_x = 0$ at the $\eta = \pm 1$ edges implies an additional constant term which has to be subtracted. Thus,

Let $\alpha = 50 + 10\,k^4 - 100\,k^2$

Then,

$$\sigma_x = C b^4 \left(20\eta^2 + 30\eta^4 + 20k^2\xi^2 + 10k^4\xi^4 - 120k^2\xi^2\eta^2 - \alpha\right) \qquad (2.13a)$$

At $\xi = \pm 1$, $\eta = 0$, $\sigma_x = -N_0$ (normalized stress resultant) implies

$$C b^4 = \frac{-N_0}{\left(120k^2 - 50\right)} \qquad (2.14)$$

Now combining all these equations together one has

$$\phi = \frac{-N_0 b^2}{\left(120k^2 - 50\right)} \left(\frac{5}{3}\eta^4 + \eta^6 + 10k^2\xi^2\eta^2 + 5k^4\xi^4\eta^2 - 10k^2\xi^2\eta^4 - 5k^4\xi^4 - \frac{\alpha\eta^2}{2} \right) \qquad (2.15)$$

$$\sigma_x = \frac{-N_0}{(120k^2 - 50)}\left(20\eta^2 + 30\eta^4 + 20k^2\xi^2 + 10k^4\xi^4 - 120k^2\xi^2\eta^2 - \alpha\right) \quad (2.16a)$$

$$\sigma_y = \frac{-N_0}{(120k^2 - 50)}\left(20\eta^2 + 60k^2\xi^2\eta^2 - 20\eta^4 - 60k^2\xi^2\right) \quad (2.16b)$$

$$\tau_{xy} = \frac{N_0}{(120k^2 - 50)}\left(40k\xi\eta + 40k^3\xi^3\eta - 80k\xi\eta^3\right) \quad (2.16c)$$

Although the above equations satisfy the σ_x and σ_y boundary conditions exactly, the shear stresses remain non-zero at all edges. However, the integral boundary conditions as given below are satisfied.

$$\text{At } \xi = \pm 1, \int_{\eta=-1}^{+1} \tau_{xy}\, d\eta \equiv 0 \quad (2.17a)$$

$$\text{And at } \eta = \pm 1, \int_{\xi=-1}^{+1} \tau_{xy}\, d\xi \equiv 0 \quad (2.17b)$$

Equations (2.16) contains a singularity at an aspect ratio of $k^2 = 5/12$ or $k = 0.64549$. For practical purposes, one can neglect this singularity for the following reason. The singular aspect ratio has large decimal digit accuracy which means that even for the aspect ratio of 0.64, a finite denominator can be obtained. However, mathematically one has to state that this solution is valid for every plate size except for the singular aspect ratio as given above.

2.2.1 Numerical Results

The in-plane stress resultants are shown in Figures 2.2 through 2.7. In Figure 2.2, the maximum stress resultant N_{xx} is shown along the plate half length. The maximum normalized stress (i.e., 1 at the edge) is seemingly diffusing rapidly towards the plate center. This diffusion is higher at higher plate aspect ratios (k) and, for $k = 3$, the diffusion resulted in unusually small values of the N_{xx} stress resultant near the plate central region.

In order to visualize the stress diffusion more clearly, Figures 2.3a through 2.3c show the N_{xx} stress resultant variations along the plate half width at various x = constant sections. Although the N_{xx} stress resultant is diffusing towards the plate center, it is non-uniform at any x = constant cross section as evident from Figures 2.3a through 2.3c. Near the top and bottom edges, the magnitude of the N_{xx} stress resultant is increased, and this increase is more prominent near the plate center and for lower plate aspect ratios. For a square plate (aspect ratio = 1), the maximum N_{xx} value at $\xi = 0$ and $\eta = 1$ is more than the maximum applied edge load.

In similar fashion, one can also observe the N_{yy} stress resultant distribution. However, as the N_{yy} stresses satisfied the boundary conditions on the top and bottom edges identically, the N_{yy} distribution throughout the interior of the plate does not matter much. The same reasoning applies to the shear stress distribution in the interior regions of the plate but, along the four edges, the shear stress distribution has to be studied closely. Figures 2.4 shows the shear stress distribution on x-type edges (left and right edges), whereas Figure 2.5 shows the same for the y-type edges (top and bottom edges).

In Figures 2.4 and 2.5, the maximum magnitude of the shear stress is increasing for higher plate aspect ratios. One can see clearly that, for a plate aspect ratio of 3, the maximum shear stress is of the order of the maximum normal stress applied at the left and right edges. Thus, the shear stresses are maximum at the plate corners for rectangular plates. However, this is not the case for a square plate where the maximum shear stress is occurring approximately at one fourth plate width from the top edge.

The stress distributions resulting from the polynomial solution are not satisfactory owing to the fact that the magnitude of the residual shear stresses are of a considerable ratio of the applied edge load. Moreover, these residual stresses are increasing for higher plate aspect ratios and, for an aspect ratio of 3, the maximum residual shear stress is approximately the same as the maximum applied normal load. One can conclude that the polynomial solution thus developed is more valid at lower plate aspect ratios.

2.3 Superposition Method

2.3.1 Two-Stress-Function Method

The superposition method as proposed by Timoshenko and Goodier (1970) consists of superposing two or more solutions of the governing differential equation [Equation (2.4)] wherein each solution satisfies part of the boundary conditions. In the present case, using the superposition method, one obtains residual stresses at various edges which can be removed by expanding these residual stresses in Fourier series and combining them with the other solutions. In the present case, the rectangular plate subjected to a half sinusoidal edge load is considered for the superposition method.

Considering the plate geometry as shown in Figure 2.1, it is convenient to consider dimensionless plate coordinates as $\xi = x/a$ and $\eta = y/b$, where $-1 \leq (\xi,\eta) \leq +1$. Thus, the applied edge load can be written as

$$\sigma_x = \sigma_0 \cos\left(\frac{\pi\eta}{2}\right) \tag{2.18}$$

Considering the Airy stress function φ_1 given by

$$\phi_1 = f(\xi)\cos\left(\frac{\pi\eta}{2}\right) \tag{2.19}$$

and substituting in Equation (2.4) results in the following general solution for the function f(ξ)

$$f(\xi)=C_1\cosh\left(\frac{k\pi\xi}{2}\right)+C_2\sinh\left(\frac{k\pi\xi}{2}\right)+C_3\,\xi\cosh\left(\frac{k\pi\xi}{2}\right)+C_4\,\xi\sinh\left(\frac{k\pi\xi}{2}\right) \tag{2.20}$$

where k = a/b (plate aspect ratio) and C_1 through C_4 are constants which are to be obtained from the boundary conditions. It is to be noted that the stress function solution as given by Equations (2.19) and (2.20) gives a zero normal stress at the $\eta = \pm 1$ edges.

Substituting the zero shear stress boundary conditions as well as the normal stress distributions as defined in Equation (2.18) at the edges $\xi = \pm 1$ yields a complete solution for the in-plane stresses:

$$f(\xi)=C_1\cosh\left(\frac{k\pi\xi}{2}\right)+C_4\,\xi\sinh\left(\frac{k\pi\xi}{2}\right) \tag{2.21}$$

where

$$C_1 = \frac{\frac{\pi a}{2b}\cosh\left(\frac{\pi a}{2b}\right)+\sinh\left(\frac{\pi a}{2b}\right)}{\frac{\pi a}{2b}+\sinh\left(\frac{\pi a}{2b}\right)\cosh\left(\frac{\pi a}{2b}\right)}\frac{\sigma_o b^2 h}{\pi^2} \tag{2.22a}$$

$$C_4 = -\frac{\frac{\pi a}{2b}\sinh\left(\frac{\pi a}{2b}\right)}{\frac{\pi a}{2b}+\sinh\left(\frac{\pi a}{2b}\right)\cosh\left(\frac{\pi a}{2b}\right)}\frac{\sigma_o b^2 h}{\pi^2} \tag{2.22b}$$

However, the above in-plane stress solution gives a residual shear stress distribution at the $\eta = \pm 1$ edges which can be eliminated using a superposed Fourier solution as discussed by Timoshenko and Goodier (1970) and by Gorman and Singhal (1993). In the present problem, a renormalized solution consisting of two superposed stress functions is sufficient to satisfy the required boundary conditions accurately.

The stress function solution in Equation (2.19) produces a residual shear stress distribution on the top and bottom edges of the plate in the x-direction which can be easily expanded as a Fourier sine series. In order to eliminate these shear stresses, one can start with a second stress function solution, which produces sinusoidal shear stress distribution in the x-direction. After eliminating the unsymmetric components, this stress function is given by

$$\phi_2 = \sum_{m=1,2..} \left(D_{1m} \cosh\left(\frac{m\pi\eta}{k}\right) + D_{4m}\, \eta \sinh\left(\frac{m\pi\eta}{k}\right)\right) \cos(m\pi\xi) \tag{2.23}$$

where D_{1m} and D_{4m} are constants to be determined from the boundary conditions and the residual stress balancing from the previous stress function solution φ_1.

Imposing the zero normal stress boundary condition at the $\eta = \pm 1$ edges, an interrelation between D_{1m} and D_{4m} can be obtained. Now, superposition of the shear stress distribution at the $\eta = \pm 1$ edges and equating the resultant to zero yields a complete solution. Let

$$\theta = \frac{\pi}{2ab}\left(\left(C_1 \frac{k\pi}{2} + C_4\right) \sinh\frac{k\pi\xi}{2} + C_4 \frac{k\pi}{2} \xi \cosh\frac{k\pi\xi}{2}\right) \tag{2.24}$$

and $F_{1m} = \int_{-1}^{1} \theta \sin(m\pi\xi)\, d\xi$, m = 1,2,..

$$D_{1m} = \frac{-F_{1m}\, ab}{m\pi\left[\left(\frac{m\pi}{k} - \frac{1}{\tanh(m\pi/k)}\right)\sinh\frac{m\pi}{k} - \frac{m\pi}{k}\frac{\cosh(m\pi/k)}{\tanh(m\pi/k)}\right]} \tag{2.25a}$$

and $D_{4m} = \dfrac{-D_{1m}}{\tanh \dfrac{m\pi}{k}}$ (2.25b)

It is to be observed that, whereas the initial stress-function solution (ϕ_1) is a one-term solution, the second stress-function solution (ϕ_2) is a series solution. However, at the most, the first three or four series terms are sufficient to obtain a close approximation for the vanishing residual shear stress distribution due to ϕ_1.

Although the stress-function solution ϕ_2 has zero normal stresses at the $\eta = \pm 1$ edges and zero shear stresses at the $\xi = \pm 1$ edges, it does produce a residual normal stress (σ_x) at $\xi = \pm 1$. However, it is observed that this σ_x stress distribution is once again sinusoidal with a very small magnitude. Consequently, a renormalization of the superposed σ_x distribution has to be carried out such that the resulting σ_x stresses are as specified by Equation (2.18). This renormalization is carried out using a small uniform stress and a multiplication factor. This methodology gives good results as shown in the next section.

Thus, the total solution is

$$\phi = (\phi_1 + \phi_2 + R)\, r \tag{2.26}$$

wherein ϕ_1 and ϕ_2 are as given above, R is the uniform stress and r is the renormalization factor such that the maximum in-plane σ_x stress is one. The stress solution corresponding to φ_2 is given below.

$$\sigma_{x1} = -\frac{\pi^2}{4b^2}\left(C_1 \cosh\left(\frac{k\pi\xi}{2}\right) + C_4\, \xi \sinh\left(\frac{k\pi\xi}{2}\right)\right)\cos\frac{\pi\eta}{2} \tag{2.27a}$$

$$\sigma_{y1} = \frac{1}{a^2}\left(\left(C_1 \frac{k^2\pi^2}{4} + C_4\, k\pi\right)\cosh\frac{k\pi\xi}{2} + C_4 \frac{k^2\pi^2}{4}\xi \sinh\frac{k\pi\xi}{2}\right)\cos\frac{\pi\eta}{2} \tag{2.27b}$$

$$\tau_{xy1} = \frac{\pi}{2ab}\left(\left(C_1\frac{k\pi}{2}+C_4\right)\sinh\frac{k\pi\xi}{2}+C_4\frac{k\pi}{2}\xi\cosh\frac{k\pi\xi}{2}\right)\sin\frac{\pi\eta}{2} \tag{2.27c}$$

$$\sigma_{x2} = \sum_{m=1,2,..}\frac{1}{b^2}\left[\left(D_{1m}\frac{m^2\pi^2}{k^2}+D_{4m}\frac{2m\pi}{k}\right)\cosh\left(\frac{m\pi\eta}{k}\right)+D_{4m}\frac{m^2\pi^2}{k^2}\eta\sinh\left(\frac{m\pi\eta}{k}\right)\right]\cos(m\pi\xi) \tag{2.28a}$$

$$\sigma_{y2} = -\sum_{m=1,2,..}\frac{m^2\pi^2}{a^2}\cos(m\pi\xi)\left[D_{1m}\cosh\left(\frac{m\pi\eta}{k}\right)+D_{4m}\,\eta\sinh\left(\frac{m\pi\eta}{k}\right)\right] \tag{2.28b}$$

$$\tau_{xy2} = \sum_{m=1,2,..}\frac{m\pi}{ab}\sin(m\pi\xi)\left[\left(D_{1m}\frac{m\pi}{k}+D_{4m}\right)\sinh\left(\frac{m\pi\eta}{k}\right)+D_{4m}\frac{m\pi}{k}\eta\cosh\left(\frac{m\pi\eta}{k}\right)\right] \tag{2.28c}$$

In the above equations, subscripts 1,2 indicate the respective stress functions, a, b are the plate dimensions in x, y directions, k is the plate aspect ratio.

In using the two-stress-function solution, however, one can observe that it deviates from the superposition method as developed by Timoshenko and used extensively by Gorman (1976). For the present problem, the complete superposition method requires a four-stress-function solution wherein each stress function has to have enough terms to obtain satisfactory convergence. In the present analysis, the superposition method using four-stress-function solution is also developed and the details are given subsequently.

2.3.1.1 Numerical Results

Numerical results of the two-stress-function solution are plotted in Figures 2.6 through 2.9. In Figure 2.6, the N_{xx} stress resultant is shown along the plate half length for various plate aspect ratios. Similar to the polynomial solution, the magnitude of the N_{xx} stress resultant decreased towards the plate center. However, the important difference is that the rate of decrease is less severe compared with the polynomial solution. Thus, with reference to Figure 2.2 and Figure 2.6, one can see clearly that for all aspect ratios considered (i.e., k = 1,2,3), the two-stress-function solution resulted in higher stresses throughout the plate. Although the rate of decrease is more for higher plate aspect ratios, the lowest magnitude of the N_{xx} stress resultant (at the plate center) is considerably higher (0.658 as opposed to 0.0388 for the polynomial solution) in case of the two-stress-function solution.

Figure 2.7a,b,c shows the N_{xx} stress resultant distribution against the plate width at various plate sections. Once again, in comparison with the corresponding results of the polynomial solution (Figures 2.3a,b,c), the two-stress-function results exhibit a smooth reduction which can be correlated with the aspect ratio. For smaller plate aspect ratios, the cross sectional stress distribution changed very little between the plate edges and the plate center (Figure 2.7a). As the aspect ratio is increased (Figures 2.7b and 2.7c), the N_{xx} stress resultant is becoming more uniform in comparison with the nonlinear edge distribution. Similar correlation cannot be obtained for the case of the polynomial solution (Figures 2.3a, b, c). In order to visualize the stress diffusion at higher aspect ratios, a three dimensional plot is shown in Figure 2.8 for the N_{xx} normal stress resultant distribution. The height of the surface represents the numerical value of the stress resultant and one can see clearly that, for most of the plate region, the N_{xx} remained uniform (flat region). However, near the plate edges where the load is applied, the normal stress resultant rapidly becomes nonlinear in the y-direction.

Figure 2.9 shows the N_{xy} shear stress resultant distribution along the plate half length at the $\eta(y/b) = \pm 1$ edges. Due to the trigonometric terms in the Airy stress function solution, the shear stress distribution is also sinusoidal as shown in Figure 2.9. However, the magnitude of the shear stress resultant is considerably smaller than the corresponding results from the polynomial solution (see Figure 2.5). At higher aspect ratios, the magnitude is increasing but even for the case of aspect ratio 3, the maximum magnitude is four hundredth the value of the maximum normal stress resultant. In comparison, the polynomial solution gave a shear stress resultant of the same order as the maximum normal stress resultant. It is to be noted that, along the $x/a = \pm 1$ edges, the shear stress resultant is identically zero for the two-stress-function solution.

2.3.1.2 Convergence Studies

In case of the two stress-function solution, convergence is studied in terms of the residual shear stress distribution on the $\eta = \pm 1$ edges. This is due to the fact that the second stress function solution is primarily used to cancel the residual shear stresses due to the original stress function solution at the $\eta = \pm 1$ edges. With reference to Equations (2.24) and (2.25a,b), the number of terms required in the stress function solution φ_2

depends on the accuracy requirements of the residual shear stress distribution at the $\eta = \pm 1$ edges. For plate aspect ratios up to three, it is observed that the residual shear stresses can be made sufficiently small for up to three series terms in the stress function solution φ_2.

Figure 2.10 is a plot for the resultant shear stress distribution at the $\eta = \pm 1$ edges for the original stress function solution (one term solution) and using three Fourier expansion terms in the second stress function solution (four term solution) for a plate aspect ratio of 3. It is clearly evident from this figure that the shear stresses are considerably reduced even for a three term Fourier expansion in the second stress function solution. However, each Fourier expansion term introduces additional residual normal stresses in the x-direction and, therefore, a balance is required between these two opposing effects. It is observed from this analysis that a three term expansion is sufficient for obtaining a maximum shear stress resultant value of four hundredth the magnitude of the normal stress. It is to be noted that at lower aspect ratios the accuracy is much better with three term Fourier expansions.

2.3.2 Complete Stress Function Solution

Considering the stress function in terms of trigonometric terms, a two-stress-function solution was proposed in the previous section. One can notice that each stress function introduces a residual stress at the boundary which needs to be cancelled by way of Fourier expansion. In the previous section, the residual stresses due to the second stress function are cancelled by renormalization. Alternately, instead of renormalizing, one can proceed in a similar fashion and introduce additional stress functions in such a way that all the residual stresses at all the boundaries are balanced. This method as proposed by Timoshenko and widely used by Gorman yields a series solution, and the resulting solution is considerably more complicated. For the present problem, the two stress functions introduced in the previous section remain the same. In order to remove the residual stresses due to the second stress function, a third stress function is considered which is

$$\phi_3 = \sum_{n=1,2..} \left(E_{1n}\cosh(kn\pi\xi) + E_{4n}\,\xi\sinh(kn\pi\xi)\right)\cos(n\pi\eta) \tag{2.29}$$

where E_{1n} through E_{4n} are constants and E_{2n} and E_{3n} terms are discarded due to symmetry conditions.

The stresses are

$$\sigma_{xx3} = \sum_{n=1,2,..} \frac{-n^2\pi^2}{b^2}\left[E_{1n}\cosh(kn\pi\xi) + E_{4n}\,\xi\sinh(kn\pi\xi)\right]\cos(n\pi\eta) \tag{2.30a}$$

$$\sigma_{yy3} = \sum_{n=1,2,..} \frac{1}{a^2}\left[\left(E_{1n}\,k^2n^2\pi^2 + 2\,E_{4n}\,kn\pi\right)\cosh(kn\pi\xi) + E_{4n}\,k^2n^2\pi^2\,\xi\sinh(kn\pi\xi)\right]\cos(n\pi\eta) \tag{2.30b}$$

$$\tau_{xy3} = \sum_{n=1,2,..} \frac{n\pi}{ab}\left[\left(E_{1n}kn\pi + E_{4n}\right)\sinh(kn\pi\xi) + E_{4n}\,kn\pi\xi\cosh(kn\pi\xi)\right]\sin(n\pi\eta) \tag{2.30c}$$

By expanding the residual σ_{xx} stresses (at the $\xi = \pm 1$ edges) due to the second stress function in the Fourier cosine series, one can equate to the above σ_{xx} stresses and obtain an interrelation between E_{1n} and D_{1m}.

The above stress solution satisfies the zero shear stress boundary condition at the $\eta = \pm 1$ edges. Equating the shear stresses at the $\xi = \pm 1$ edges gives an interrelation between E_{1n} and E_{4n}.

$$E_{1n}\, k\, n\, \pi \sinh(kn\pi) + E_{4n}\left[\sinh(kn\pi) + kn\pi\cosh(kn\pi)\right] = 0 \qquad (2.31)$$

However, the above stress solution gives residual σ_{yy} stresses at the $\eta = \pm 1$ edges which can finally be removed by a fourth stress function.

$$\phi_4 = \sum_{p=1,2,..}\left(F_{1p}\cosh\left(\frac{p\pi\eta}{k}\right) + F_{4p}\,\eta\sinh\left(\frac{p\pi\eta}{k}\right)\right)\cos(p\pi\xi) \qquad (2.32)$$

The stresses are (2.33a,b,c)

$$\sigma_{x4} = \sum_{p=1,2,..}\frac{1}{b^2}\left[\left(F_{1p}\frac{p^2\pi^2}{k^2} + F_{4p}\frac{2p\pi}{k}\right)\cosh\left(\frac{p\pi\eta}{k}\right) + F_{4p}\frac{p^2\pi^2}{k^2}\eta\sinh\left(\frac{p\pi\eta}{k}\right)\right]\cos(p\pi\xi)$$

$$\sigma_{y4} = -\sum_{p=1,2,..}\frac{p^2\pi^2}{a^2}\cos(p\pi\xi)\left[F_{1p}\cosh\left(\frac{p\pi\eta}{k}\right) + F_{4p}\,\eta\sinh\left(\frac{p\pi\eta}{k}\right)\right]$$

$$\tau_{xy4} = \sum_{p=1,2,..}\frac{p\pi}{ab}\sin(p\pi\xi)\left[\left(F_{1p}\frac{p\pi}{k} + F_{4p}\right)\sinh\left(\frac{p\pi\eta}{k}\right) + F_{4p}\frac{p\pi}{k}\eta\cosh\left(\frac{p\pi\eta}{k}\right)\right]$$

Imposing zero shear stress boundary conditions on the $\eta = \pm 1$ edges,

$$F_{1p}\,(p\,\pi/k)\sinh(p\,\pi/k) + F_{4p}\left[\sinh(p\,\pi/k) + (p\,\pi/k)\cosh(p\,\pi/k)\right] = 0 \qquad (2.34)$$

Also, in the present solution, the relations between D_{1m} and D_{4m} in terms of C_1 and C_4 as given in Equations (2.24) and (2.25) are valid. Additionally, by considering the following two boundary conditions, one obtains two sets of equations involving E_{1n}, E_{4n}, and F_{1p}, F_{4p} in terms of C_x and D_{xx}. The resulting equations can easily be solved given any specified plate numerical parameters.

1. $\sigma_{yy} = 0$ at the $\eta = \pm 1$ edges,
2. $\sigma_{xx} = 0$ at the $\xi = \pm 1$ edges (this condition is only for residual stresses).

In each of the above boundary conditions, only one stress solution remains in either sine or cosine function of ξ or η, and the remaining stresses have to be expanded in Fourier (corresponding sine or cosine) series. Moreover, each sine or cosine original stress function in one boundary condition needs to be expanded in Fourier series for the other boundary conditions. Thus, the number of terms in the φ_3 and φ_4 solutions is to be exactly the same in order to get the complete solution. The complete solution is

$$\varphi = \varphi_1 + \varphi_2 + \varphi_3 + \varphi_4 \tag{2.35}$$

2.3.2.1 Numerical Results

Numerical results are compared against the two-stress-function solution. It is to be noted that, in using the four-stress-function approach, some of the residual stresses have to be expanded in Fourier cosine series as well as sine series. The cosine series expansion contains a zero order term, resulting in a uniform stress value to be required in order to get a satisfactory solution. Among the various cosine expansions, it is observed that only the σ_{xx} residual stress due to the φ_2 stress function solution requires this zero order term.

Figure 2.11 is a comparative plot of the N_{xx} stress resultant along the plate central line for various aspect ratios. The N_{xx} stress resultant closely agreed with the two-stress-function solution near the plate edges but remained lower in most parts of the plate. The rate of reduction in both cases is almost identical.

Figures 2.12a,b,c show the comparative N_{xx} stress resultant distribution at various plate sections. In all of these plots, the four-stress-function solution resulted in non-zero stresses at the plate corners. This can be explained due to a larger number of Fourier expansion functions as opposed to the two-stress-function solution. Moreover, near the plate edges (and corners), the Fourier expansions did not match the corresponding functions (analogous to the Gibbs phenomenon) causing residual N_{yy} stresses on top and bottom edges of the plate.

However, the N_{xx} stress resultants showed close agreement with the two-stress-function solution in the interior portion of the plate irrespective of the plate aspect ratio. Similarly, the N_{xy} shear stress resultant showed close agreement with corresponding two-stress-function solution. On the top and bottom edges ($y/b = 1$), a residual shear stress distribution is observed (Figure 2.13) whose magnitude is increased with plate aspect ratio. In comparison with the applied edge normal load, the residual shear stresses are very small.

As mentioned before, due to the nature of the Fourier cosine expansion, the four-stress-function solution did not satisfy the σ_{yy} boundary conditions especially near the corners. This is shown in Figures 2.14 and 2.15. It is to be noted that increasing the number of expansion terms does not improve the stress resultants at the corners. Moreover, the magnitudes of these residual y-direction normal stresses are considerable at the plate corners even though they remained very small throughout the plate. Similar edge discrepancies were observed in the literature (Gorman and Singhal (1993)) for problems involving Fourier expansions.

2.3.2.2 Convergence Analysis

Also, in using the four-stress-function approach, the convergence of the resulting in-plane solution generally depends on the number of terms considered in the Fourier expansion. However, in the present analysis it was observed that the in-plane stress response is very sluggish with the number of Fourier expansion terms. Thus, the stress solution consisting of a four-term expansion was compared for a plate with an aspect ratio of 3 with the corresponding solution using an eight-term Fourier expansion. As the resulting buckling solution showed a change of only about 0.1 percent, the four-term expansion is considered to be sufficient. Figure 2.16 is a plot of N_{xx} stress resultant using a four-term and an eight-term Fourier expansion. It is clearly evident from this figure that the magnitude of the N_{xx} stress resultant changed very little even when the number of Fourier terms is doubled. As a result, the four-stress-function solution involving four-term Fourier expansion is used in the remainder of this study.

2.4 Finite Element Analysis

The rectangular plate is modeled using an eight-node (MARC element number 72) quadrilateral shell element (Ref: MARC element library (1996)). Although this element formulation is a generalized one for shell analysis, plate analysis can be done with equal ease. This element has three degrees of freedom at each corner node and an additional rotational degree of freedom at each mid node on the four edges.

The plate model is analyzed using various different mesh sizes and the convergence of the results is established. However, in using the finite element analysis, the minimum buckling load is considered to be the parameter to check the convergence, details of which will be explained in Chapter 3. Based on the results, it was established that a mesh size consisting of 1200 elements (60 x 20 in the x,y directions respectively) is sufficient for a plate with an aspect ratio of 3. Similar element densities (number of elements in a given area) are used for other plate aspect ratios. Care is taken to ensure that the element shape remains as close to the square as possible. The X and Y (u,v correspondingly) displacements are restricted along the nodes on two mutually perpendicular lines intersecting the plate surface. At the left and right edges of the plate, a uniform initial edge load (per unit length) is applied. This uniform edge load varies for each element such that the magnitude of the edge load follows approximately a sinusoidal distribution. The edge load for each element is calculated such that the total edge load of the element is identically equal to that of total sinusoidal load corresponding to the element edge coordinates. In other words, the sinusoidal load is modeled as a stepwise uniform edge load. (Figure 2.17 shows such a distribution for a plate aspect ratio of 3). The edge load is applied so as to obtain a consistent load stiffness matrix formulation. A sample MARC input file is given in the Appendix III.

2.4.1 Numerical Results

Numerical results are obtained for plate aspect ratios of 1 and 3. Figure 2.18 shows the comparative N_{xx} stress resultant distribution along the plate center where one can observe that the FE solution gives smaller stresses than the two-stress-function approach. Figures 2.19a and 2.19b show the same N_{xx} distribution at various plate sections. In all these figures, the numerical closeness of FE solution and the two-stress-function solution can be easily observed. Thus the x-direction normal stress resultant agrees qualitatively and quantitatively with the two-stress-function solution. Due to the numerical nature of the stress calculations in the finite element analysis, a small negative N_{yy} normal stress is seen in Figure 2.20. The N_{yy} stress resultant shows reasonably close agreement with the two-stress-function solution. It is to be noted that the N_{xy} shear stress resultants are negligibly small along all the edges in the FE solutions.

2.5 Timoshenko Solution

Using stress functions which satisfy all the stress boundary conditions identically, Timoshenko (1924) proposed a solution for the case of a parabolically loaded rectangular plate using the Rayleigh-Ritz method. It is to be noted that, although he omitted the contribution of Poisson's terms from the energy functional, the effect of those terms turned out to be negligible by way of identical results with the solution by the Galerkin method. The stress function is

$$\phi=\frac{1}{2}N_0 y^2\left(1-\frac{y^2}{6b^2}\right)+\left(x^2-a^2\right)^2\left(y^2-b^2\right)^2\left(\alpha_1+\alpha_2 x^2+\alpha_3 y^2+\ldots\right) \qquad (2.36)$$

where (2a x 2b) is the plate size, $N_0 = h\ \sigma_0$, and α_1, α_2, α_3 are constants to be determined by minimizing the Rayleigh-Ritz energy functional (or using the Galerkin method). Using up to three terms, the stress solution is given by (in nondimensional coordinates ξ, η)

$$\sigma_x=-N_0\left(1-\eta^2\right)-N_0\left(\xi^2-1\right)^2\left[\begin{array}{r}\alpha_1\left(12\eta^2-4\right)+\alpha_2\,\xi^2\left(12\eta^2-4\right)+\\ \alpha_3\left(30\eta^4-24\eta^2+2\right)/k^2\end{array}\right] \qquad (2.36a)$$

$$\sigma_y=-N_0\left(\eta^2-1\right)^2\left[\frac{\alpha_1}{k^2}\left(12\xi^2-4\right)+\frac{\alpha_2}{k^2}\left(30\xi^4-24\xi^2+2\right)+\frac{\alpha_3}{k^4}\left(12\xi^2\eta^2-4\eta^2\right)\right]$$

(2.36b)

$$\begin{aligned}\tau_{xy}=&-16N_0\frac{\alpha_1}{k}\xi\eta\left(1-\xi^2\right)\left(\eta^2-1\right)\\ &-N_0\frac{\alpha_2}{k}\left(24\xi^5-32\xi^3+8\xi\right)\left(\eta-\eta^3\right)-N_0\frac{\alpha_3}{k^3}\left[8\left(\xi-\xi^3\right)\left(3\eta^5+\eta-4\eta^3\right)\right]\end{aligned}$$

(2.36c)

2.5.1 Numerical Results

Numerical results of the in-plane solutions using the two-stress-function approach are compared against the Timoshenko (also Galerkin) solutions. Figure 2.21 is a plot of N_{xx} at η (y/b) = 0, along the plate length, and Fig 2.22a,b shows the N_{xx} distribution at various plate sections. From these figures, one can see that the N_{xx} distributions of both the two-stress-function and Timoshenko (Galerkin) solutions are very close throughout the plate. Thus, the N_{xx} stress resultant diffusion into the plate is qualitatively as well as quantitatively in close agreement between the two methods.

Figure 2.23 shows the N_{yy} distribution across the plate width (η) at the $\xi = \pm 1$ edges. Although the two-stress-function solution and Timoshenko (Galerkin) solution showed similar pattern for a square plate, they differ considerably for higher plate aspect ratios.

2.6 Pickett Solution

Pickett (1944) considered a parabolically loaded rectangular plate and obtained a series solution for in-plane stresses which satisfy the equilibrium equations and the compatibility equation. The complete stress solution is reproduced below.

$$\sigma_{xx} = S + \sum_{n=1,2,..} \frac{A_n \cos(n\pi\eta)}{\cosh(\alpha)} [\alpha\xi \sinh(\alpha\xi) - (1 + \alpha\coth(\alpha))\cosh(\alpha\xi)]$$

$$- \sum_{m=1,2,..} \frac{B_m \cos(m\pi\xi)}{\cosh\beta} [\beta\eta \sinh(\beta\eta) + (1 - \beta\coth(\beta))\cosh(\beta\eta)] \tag{2.37a}$$

$$\sigma_{yy} = - \sum_{n=1,2,..} \frac{A_n \cos(n\pi\eta)}{\cosh\alpha} [\alpha\xi \sinh(\alpha\xi) + (1 - \alpha\coth\alpha)\cosh(\alpha\xi)]$$

$$+ \sum_{m=1,2,..} \frac{B_m \cos(m\pi\xi)}{\cosh\beta} [\beta\eta \sinh(\beta\eta) - (1 + \beta\coth\beta)\cosh(\beta\eta)] \tag{2.37b}$$

$$\tau_{xy} = \sum_{n=1,2,..} \frac{A_n \sin(n\pi\eta)}{\cosh\alpha} [\alpha\coth\alpha \sinh(\alpha\xi) - \alpha\xi \cosh(\alpha\xi)]$$

$$+\sum_{m=1,2,..}\frac{B_m\sin(m\pi\xi)}{\cosh\beta}\left[\beta\coth\beta\sinh(\beta\eta)-\beta\eta\cosh(\beta\eta)\right] \tag{2.38b}$$

where α = nπk and β = (mπ/k), A_n, B_m are constants to be found from the boundary conditions, ξ = x/a, η = y/b are normalized plate coordinates, k = a/b is the plate aspect ratio, and S is the x-direction normal stress intensity at the $\xi = \pm 1$ and $\eta = 0$ points. The in-plane boundary stress condition is

$$\sigma_{xx} = (3\ S/2)\ [1-\eta^2]$$

The nature of the above stress solution is quite similar to the four-stress-function approach as described earlier. At the boundaries, the stress boundary conditions are satisfied by expanding the stresses in Fourier series.

Thus,

$$A_n=\frac{\dfrac{6S(-1)^n}{n^2\pi^2}+\sum\limits_{m=1,2,..}(-1)^{n+m-1}\dfrac{4}{n\pi}\dfrac{m}{nk}\dfrac{\tanh\beta}{\left\{1+\left(\dfrac{m}{nk}\right)^2\right\}^2}B_m}{1+\alpha(\coth\alpha-\tanh\alpha)} \tag{2.39a}$$

$$B_m=\frac{\sum\limits_{n=1,2,..}(-1)^{n+m-1}\dfrac{4}{m\pi}\dfrac{nk}{m}\dfrac{\tanh\alpha}{\left\{1+\left(\dfrac{nk}{m}\right)^2\right\}^2}A_n}{1+\beta(\coth\beta-\tanh\beta)} \tag{2.39b}$$

Similar to the four-stress-function solution, equal numbers of terms for the n, m series have to be taken to obtain a solution.

2.6.1 Numerical Results

Again, the in-plane stress results are compared with corresponding values using the two-stress-function approach as shown in Figures 2.24, 2.25a, and 2.25b. From these figures, one can observe that the Pickett solution stresses are in close agreement with the two-stress-function approach as far as the x-direction normal stresses (σ_{xx}) are concerned.

Similar to the four-stress-function solution, the σ_{yy} stresses are non zero near the plate corners, thus violating the σ_{yy} boundary condition (refer to Figure 2.26). Moreover, the Pickett solution also exhibits higher y-direction normal stresses at the plate corners very similar to the four-stress-function method (refer to Figure 2.15). Thus, the Pickett solution, being a series solution involving trigonometric functions, showed similar results as the four-stress-function method.

2.7 Summary

The in-plane elasticity solution for thin rectangular plates subjected to half-sinusoidal edge loads on two opposite edges is solved analytically by two different methods and numerically by the finite element method. All the solutions are compared with solutions available in the literature. The two analytical methods are

1. Polynomial solution
2. Stress function solutions using two and four stress functions

Based on Saint-Venant's principle, one can expect that the stress distribution should exhibit a diffusion phenomenon as the plate aspect ratio is increased. In simple terms, the stress diffusion causes the in-plane stresses to be uniform in the plate interior although the edge stresses are nonlinear.

Even though the polynomial solution shows this stress diffusion, the stresses reduce much more rapidly towards the plate center as compared to all other solutions. Moreover, the residual shear stresses along all the plate edges were of the same order as the applied edge load, thereby violating the shear stress boundary conditions.

The two-stress-function method and the four-stress-function method show close agreement with the finite element solution as far as the N_{xx} stress distribution is concerned. However, the four-stress-function method yields some residual y-direction normal stresses, which are of considerable magnitude on the plate top and bottom edges. Also the Pickett solution shows similar residual edge normal stresses in the y-direction.

From the convergence studies of both the two-stress-function and four-stress-function methods it is evident that different criteria are causing them to converge. In the two-stress-function method, convergence is achieved by a balance between additional terms which both smoothes the residual edge shear stresses as well as increases the x-direction normal stresses. It is observed that, for plate aspect ratios of up to 3, three series terms yields sufficiently accurate results.

In case of the four-stress-function method, convergence is very slow with additional terms. Moreover, each additional term while smoothening one residual stress at some edge, contributes toward residual stresses on other edges. Also, due to the additional Fourier expansions involved, the functions do not satisfy the y-direction normal stresses at the plate corners.

Both, the Timoshenko solution and the Pickett solution show excellent agreement as far as x-direction in-plane stresses are concerned. It is to be noted that the Timoshenko, Pickett and the polynomial solutions are for the case of parabolic loading whereas the two-stress-function solution, the four-stress-function solution, and the finite element solution are for half sinusoidal edge loadings. Extensive plots are shown for all the in-plane stress distributions.

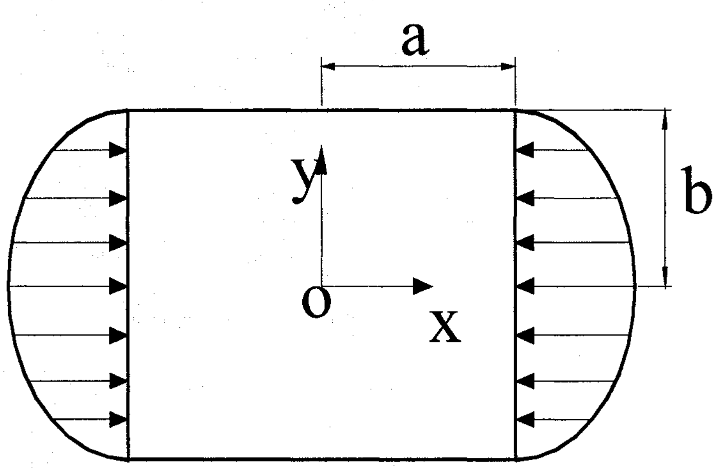

Figure 2.1: Geometry of the plate

Polynomial Solution results

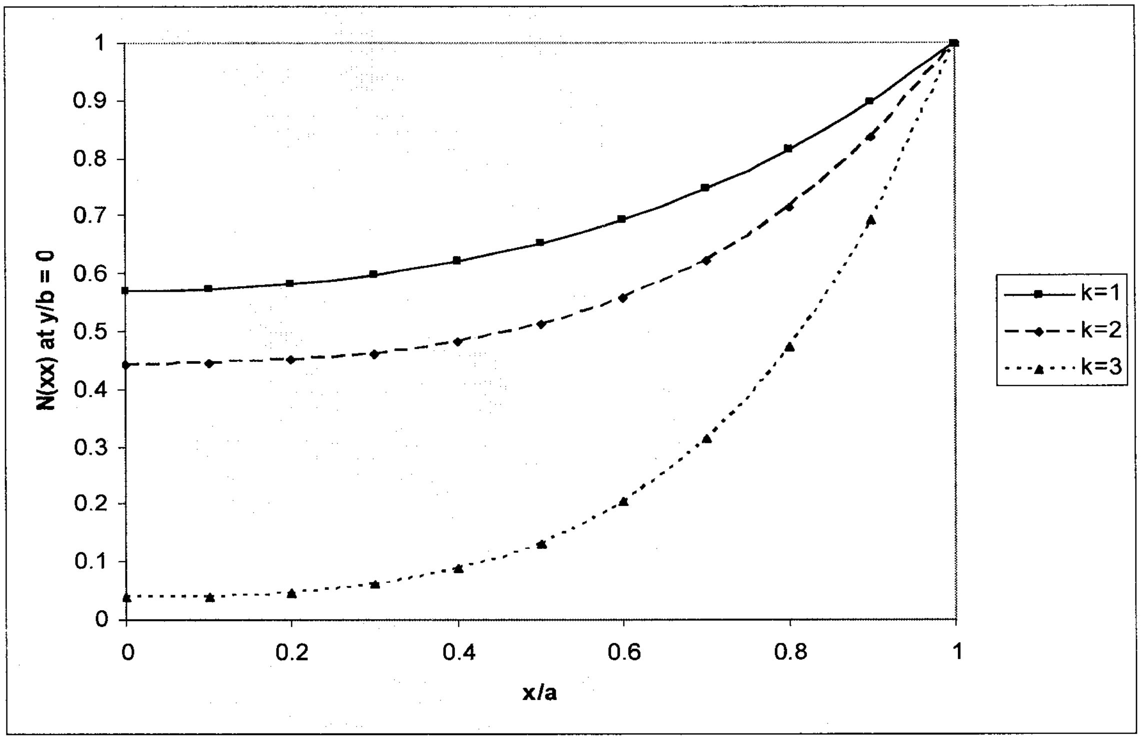

Figure 2.2: N_{xx} distribution at y/b=0 for various plate aspect ratios (k)

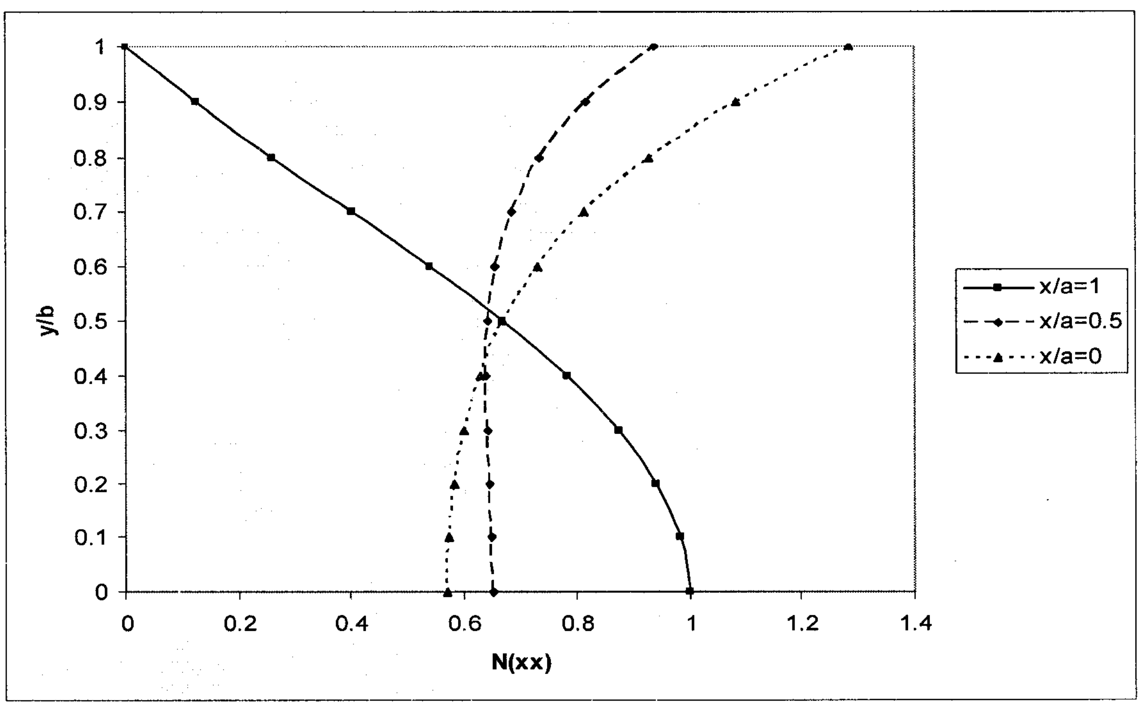

Figure 2.3a: N_{xx} distribution along plate half width (aspect ratio k = 1)

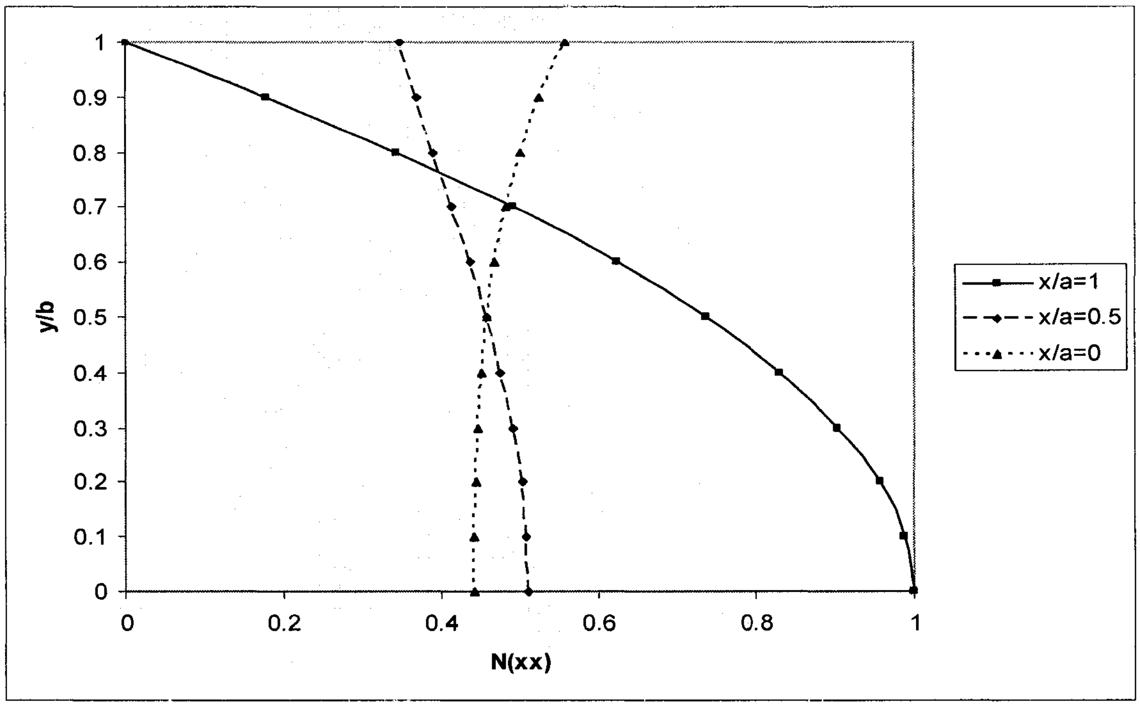

Figure 2.3b: N_{xx} distribution along plate half width (aspect ratio k = 2)

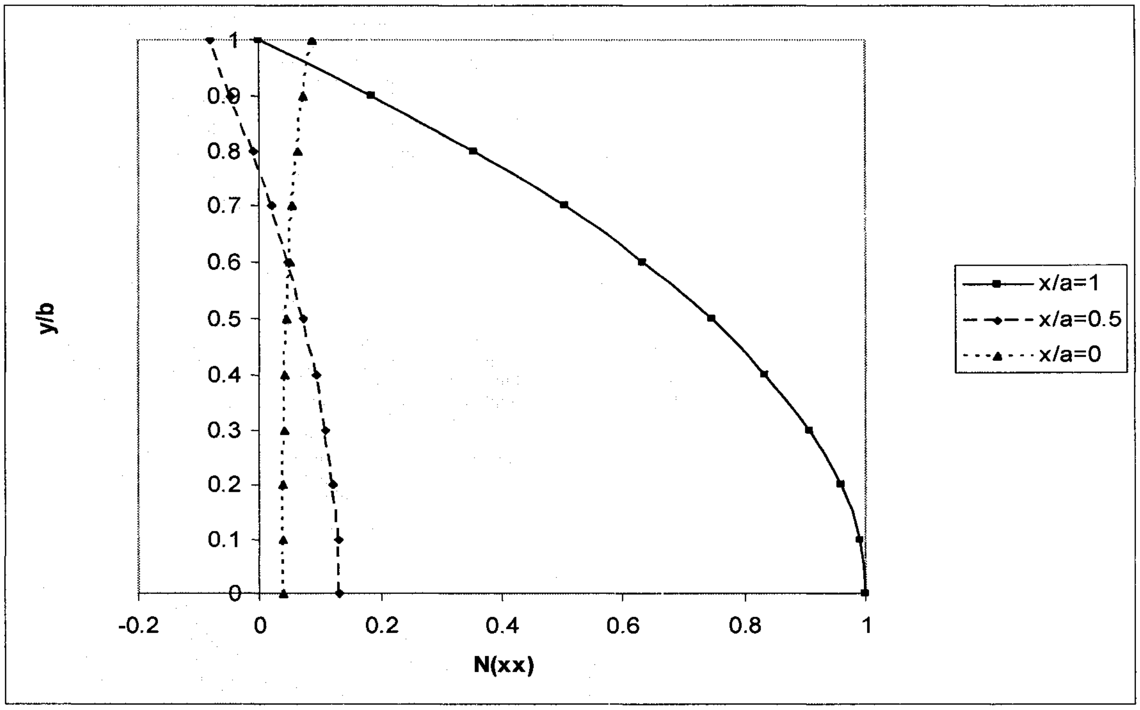

Figure 2.3c: N_{xx} distribution along plate half width (aspect ratio k = 3)

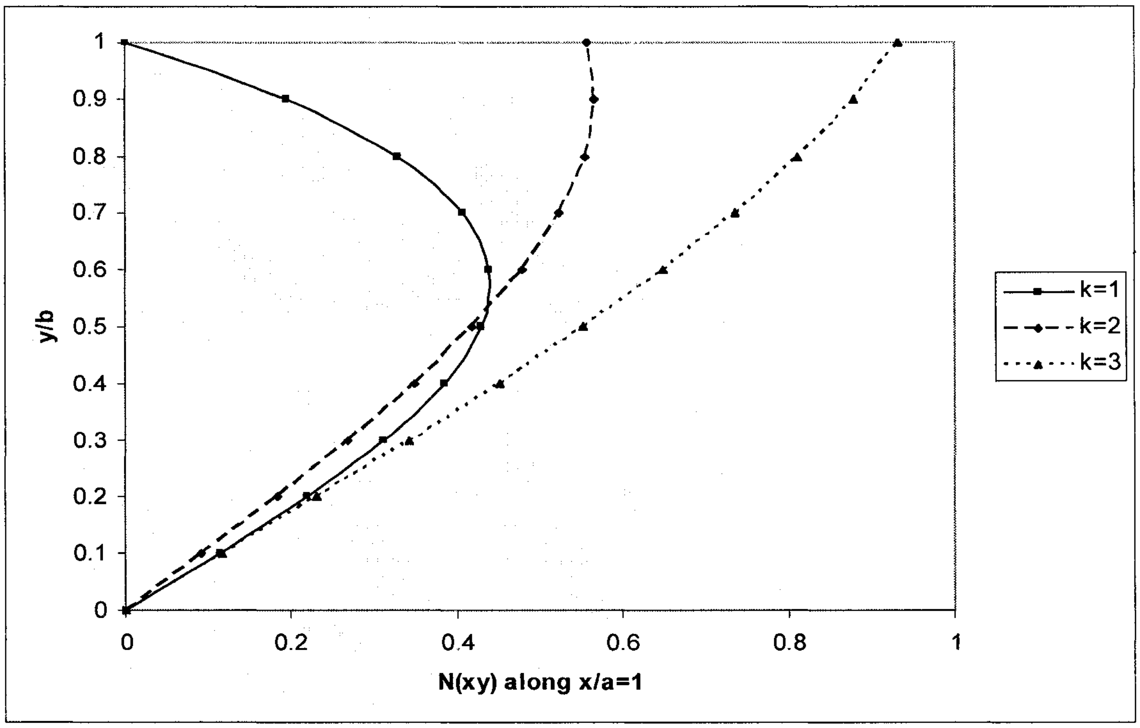

Figure 2.4: N_{xy} distribution along plate half width at (x/a) = ±1 edges

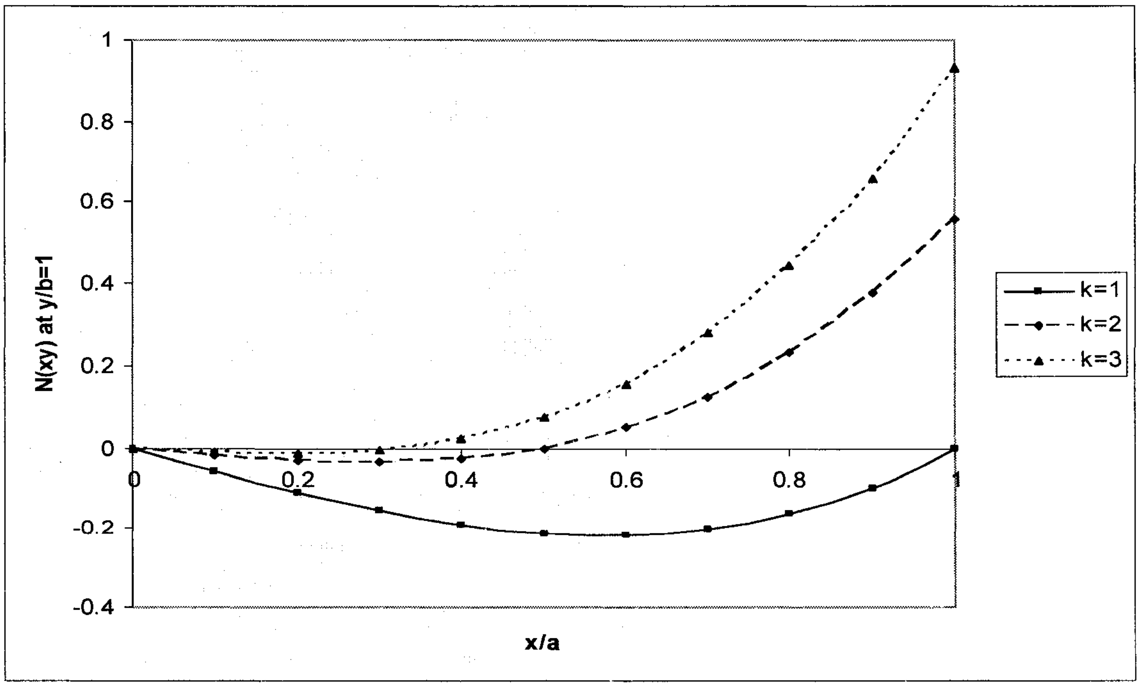

Figure 2.5: N_{xy} distribution along plate half length at (y/b) = ±1 edges

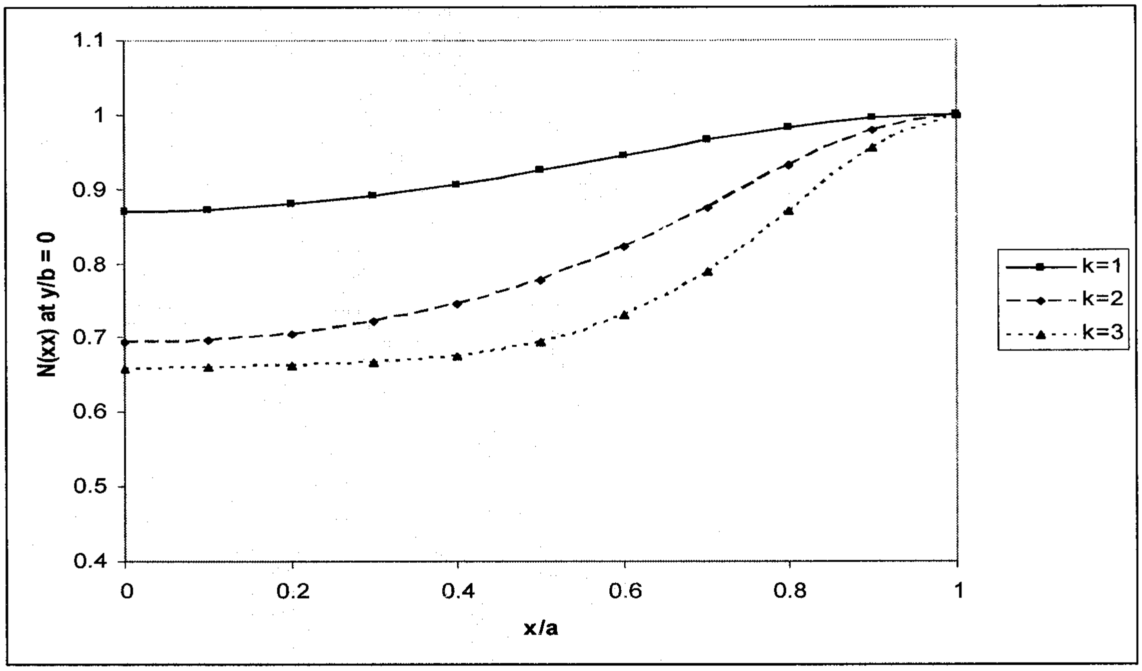

Figure 2.6: N_{xx} distribution at y/b =0 for various plate aspect ratios

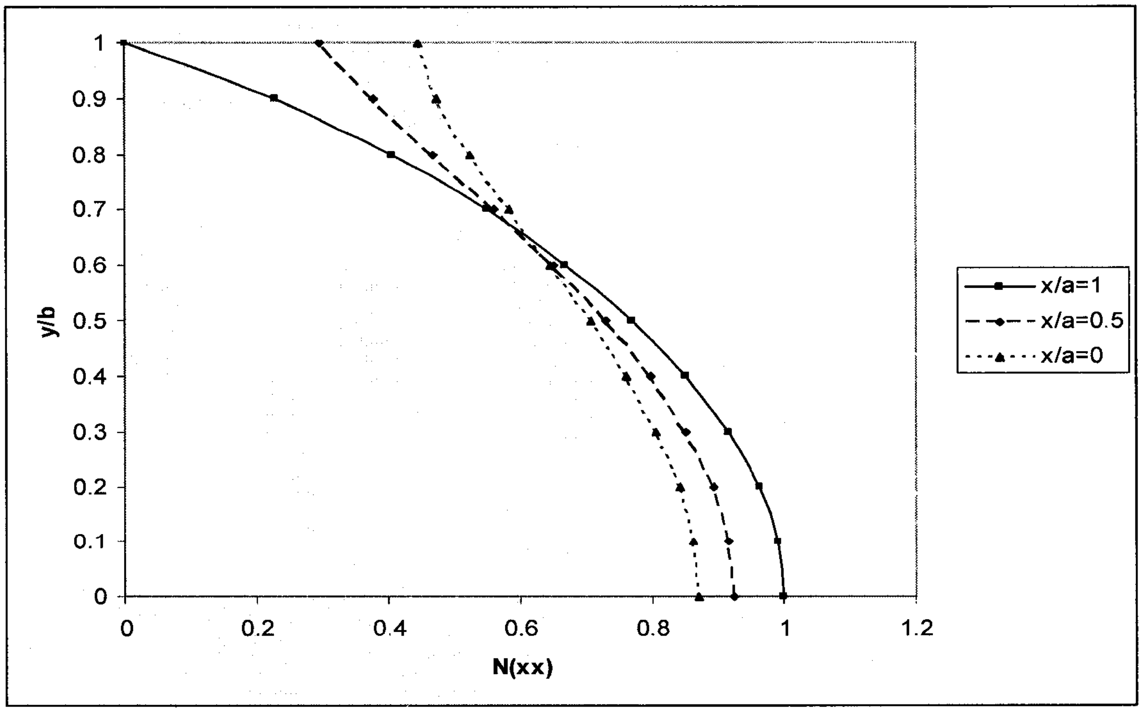

Figure 2.7a: N_{xx} distribution along plate half width (aspect ratio k = 1)

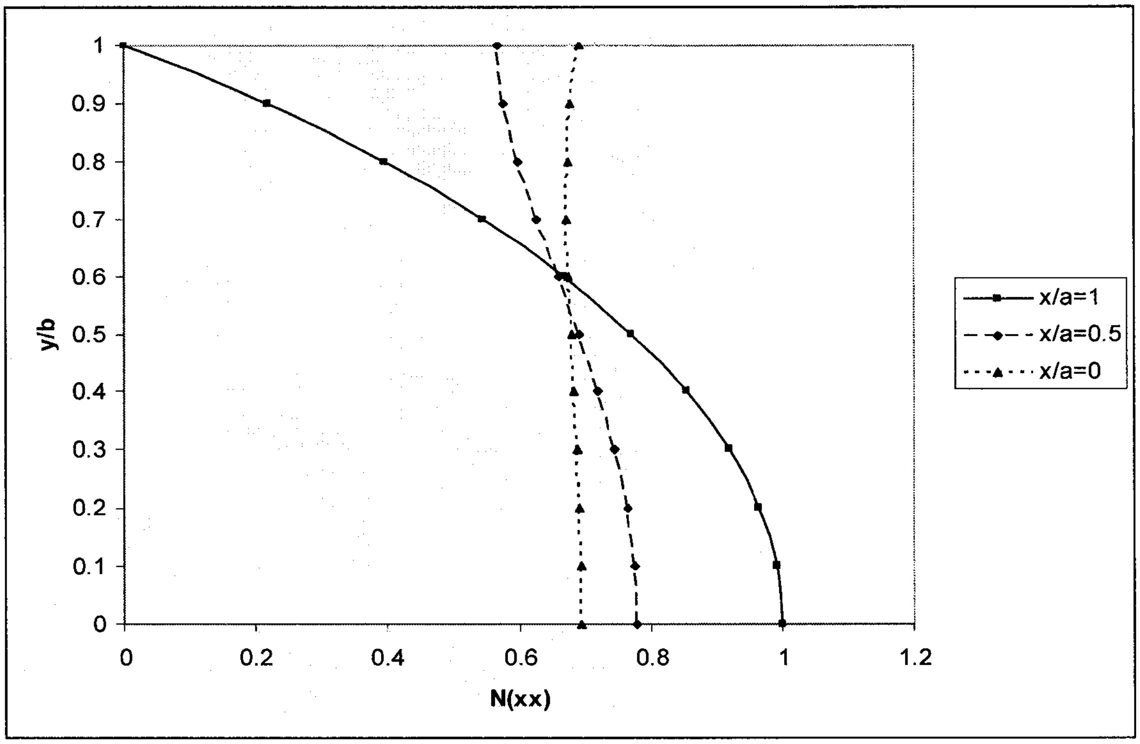

Figure 2.7b: N_{xx} distribution along plate half width (aspect ratio k = 2)

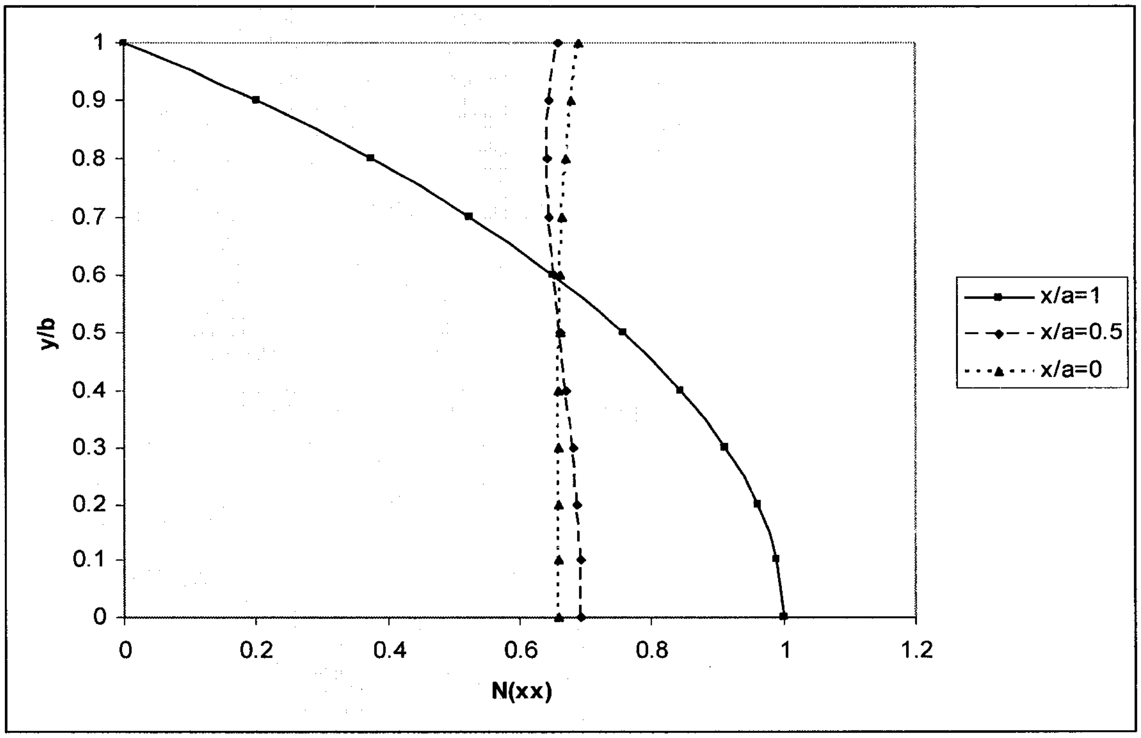

Figure 2.7c: N_{xx} distribution along plate half width (aspect ratio k = 3)

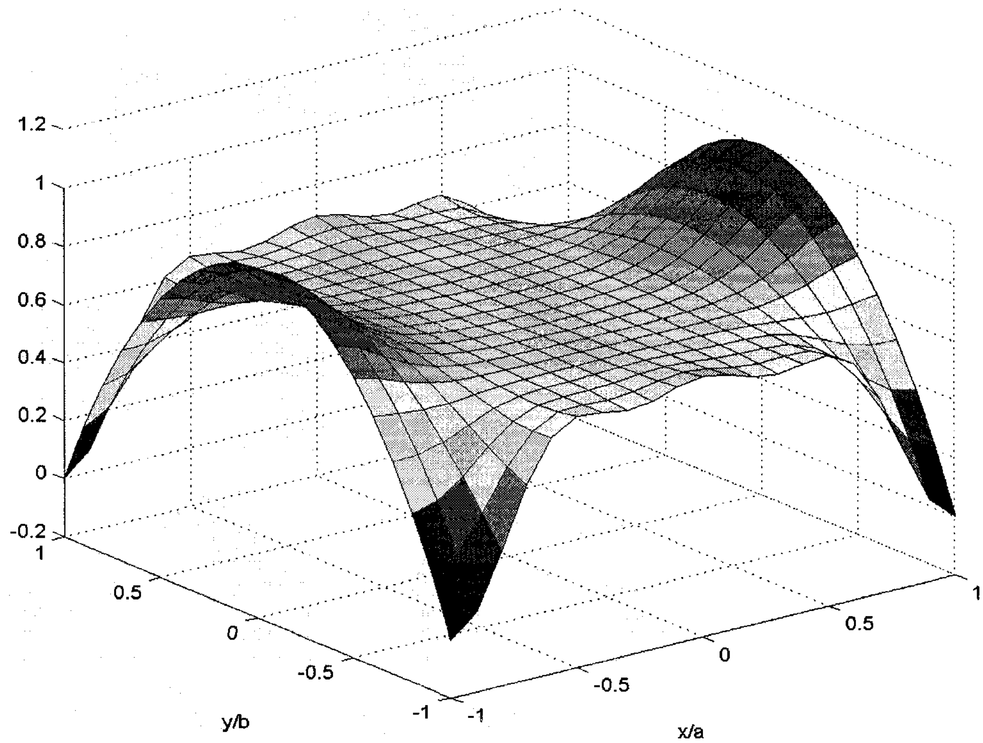

Figure 2.8: N_{xx} distribution as a 3-d plot for aspect ratio: 3 (height is the magnitude)

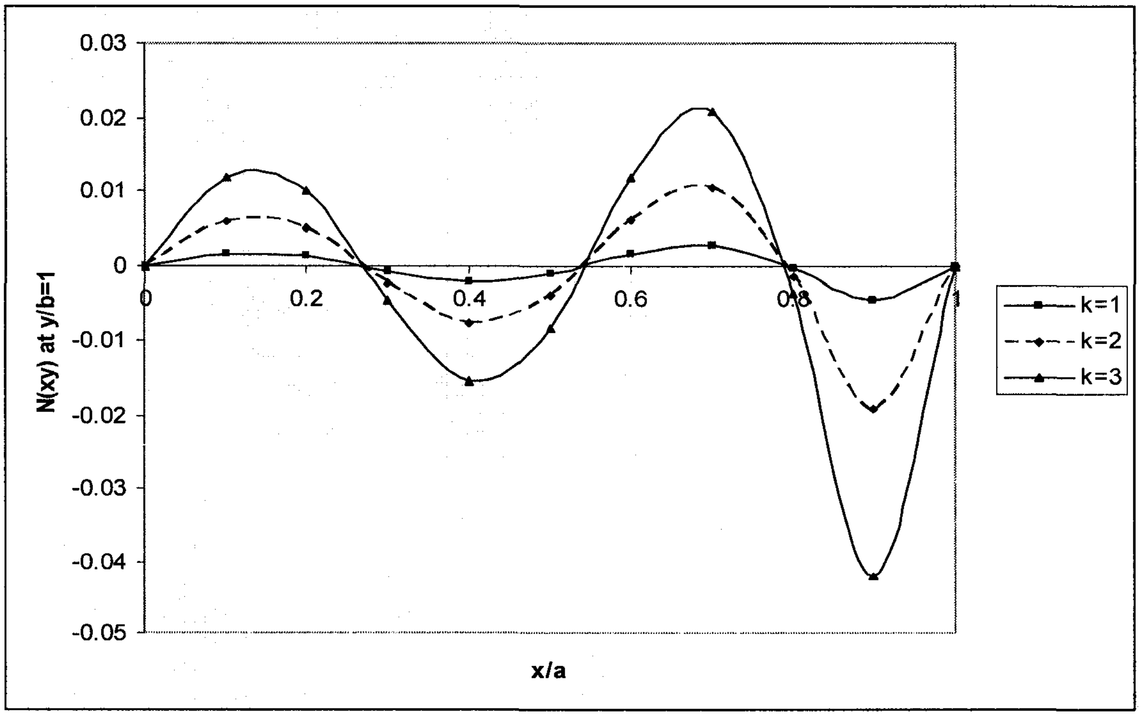

Figure 2.9: N_{xy} distribution along plate half length at (y/b) = ±1 edges

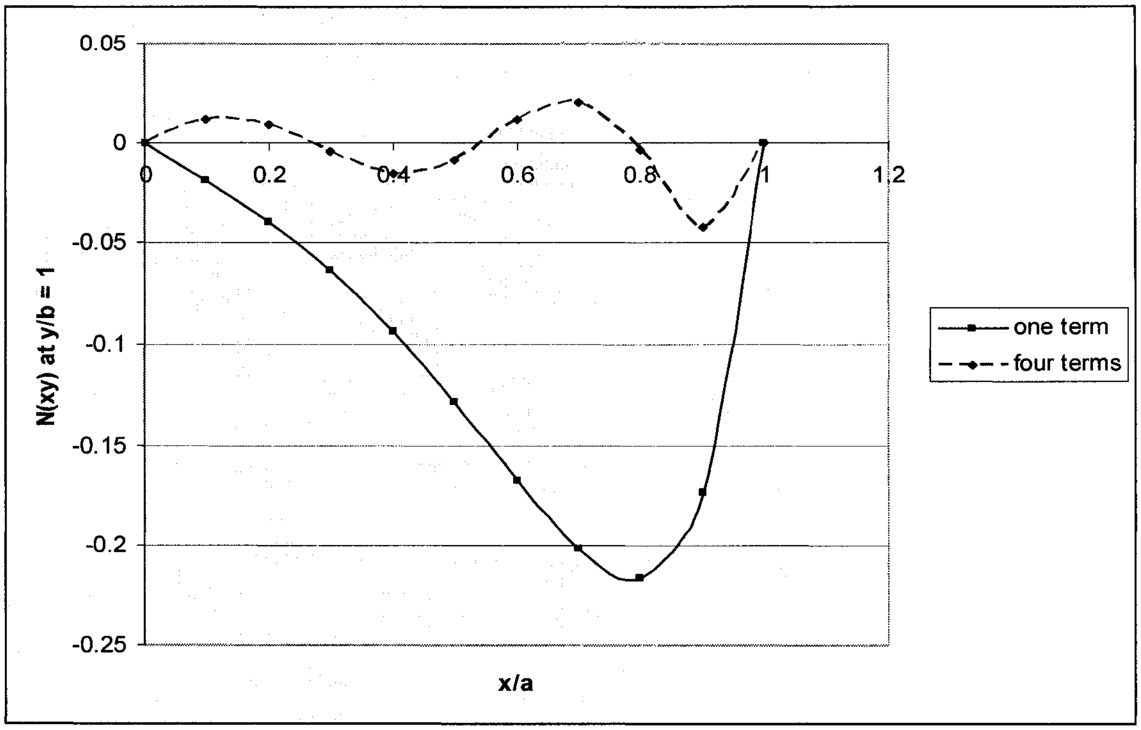

Figure 2.10: N_{xy} convergence at (y/b) = ±1 edges

Four-stress-function results

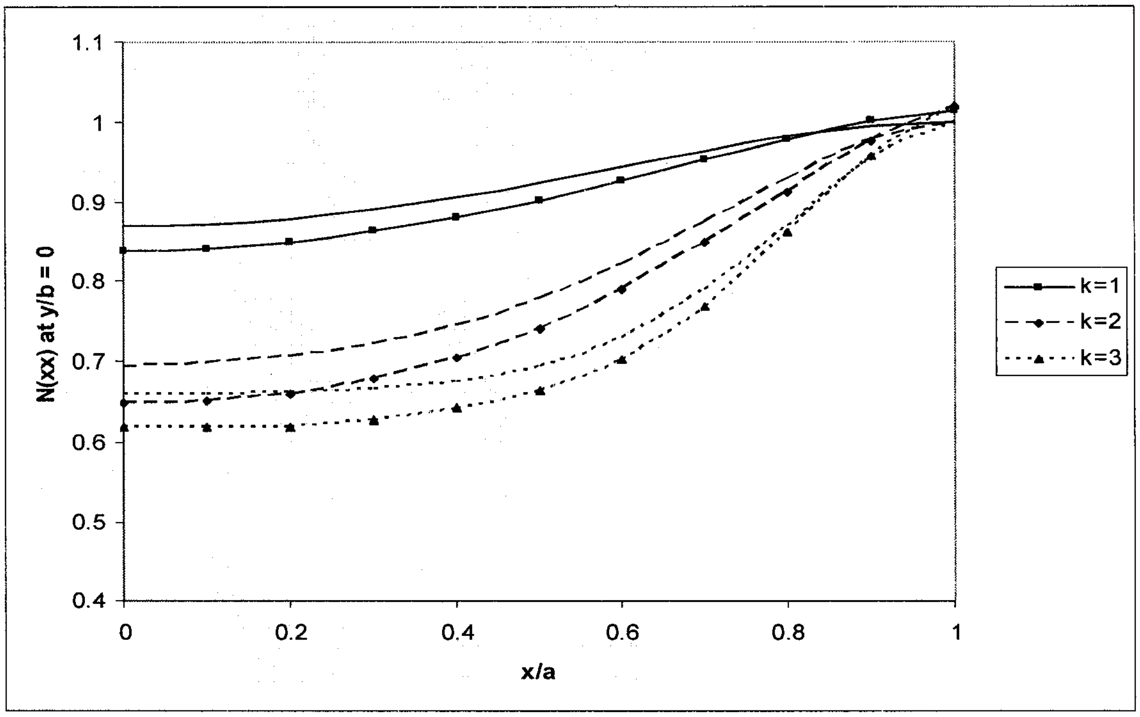

Figure 2.11: Comparative N_{xx} distributions at y/b =0 along plate half length (Lines without markers are two-stress-function solution results)

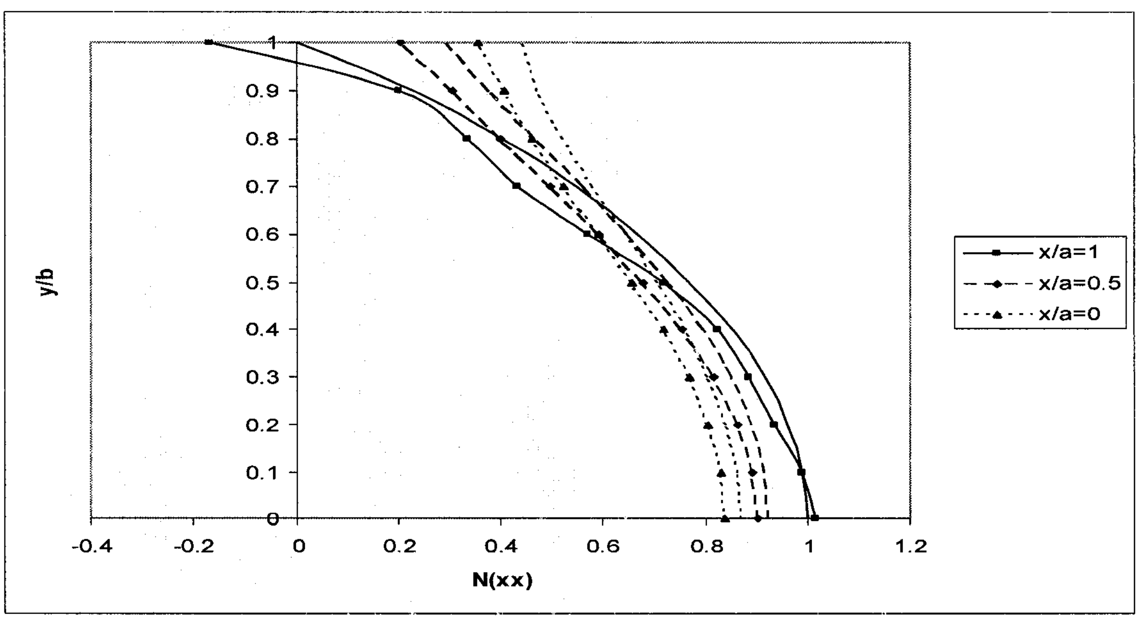

Figure 2.12a: Comparative N_{xx} distributions along plate half width (aspect ratio k = 1) (Lines without markers are two-stress-function solution results)

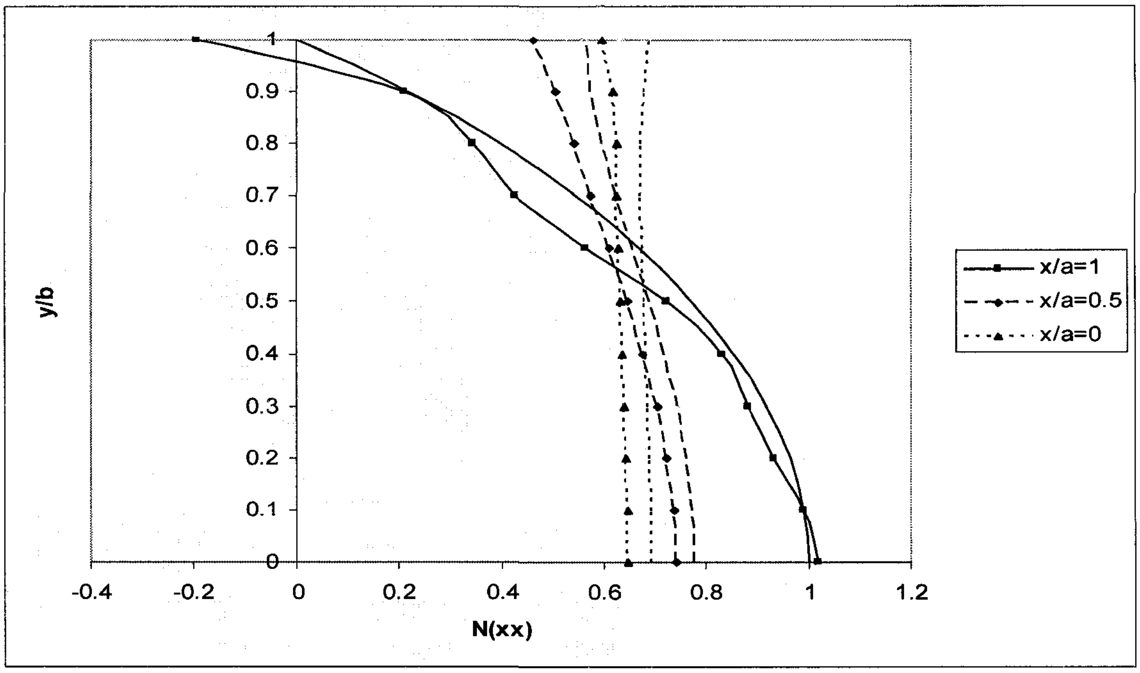

Figure 2.12b: Comparative N_{xx} distributions along plate half width (aspect ratio k = 2)
(Lines without markers are two-stress-function solution results)

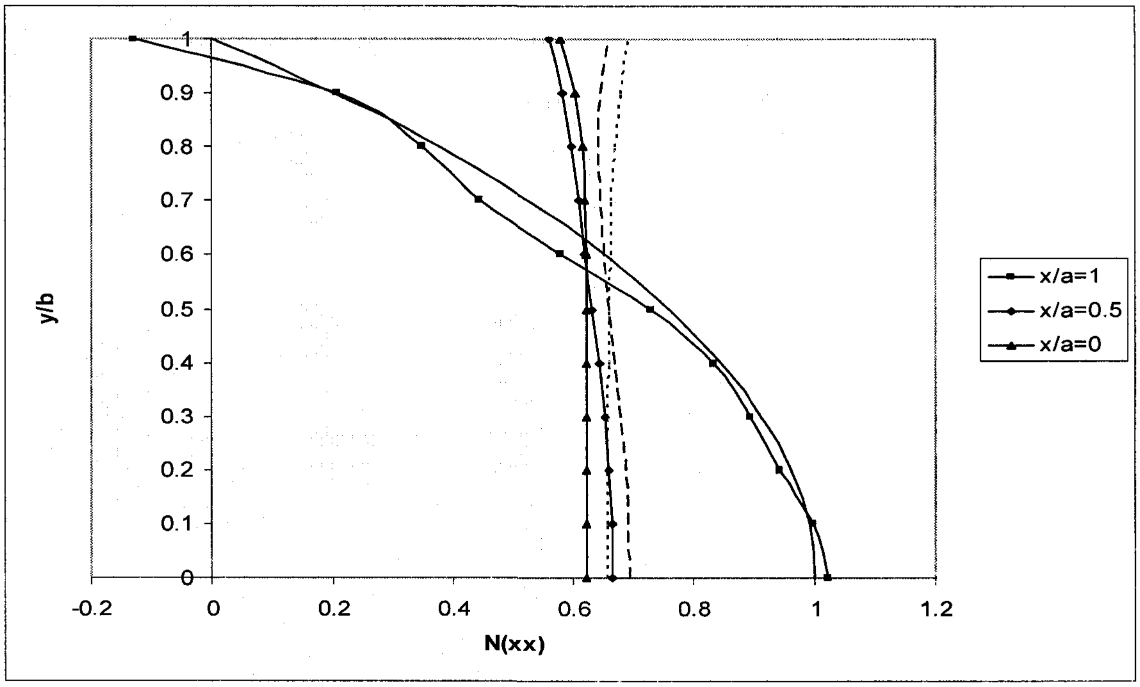

Figure 2.12c: Comparative N_{xx} distributions along plate half width (aspect ratio k = 3)
(Lines without markers are two-stress-function solution results)

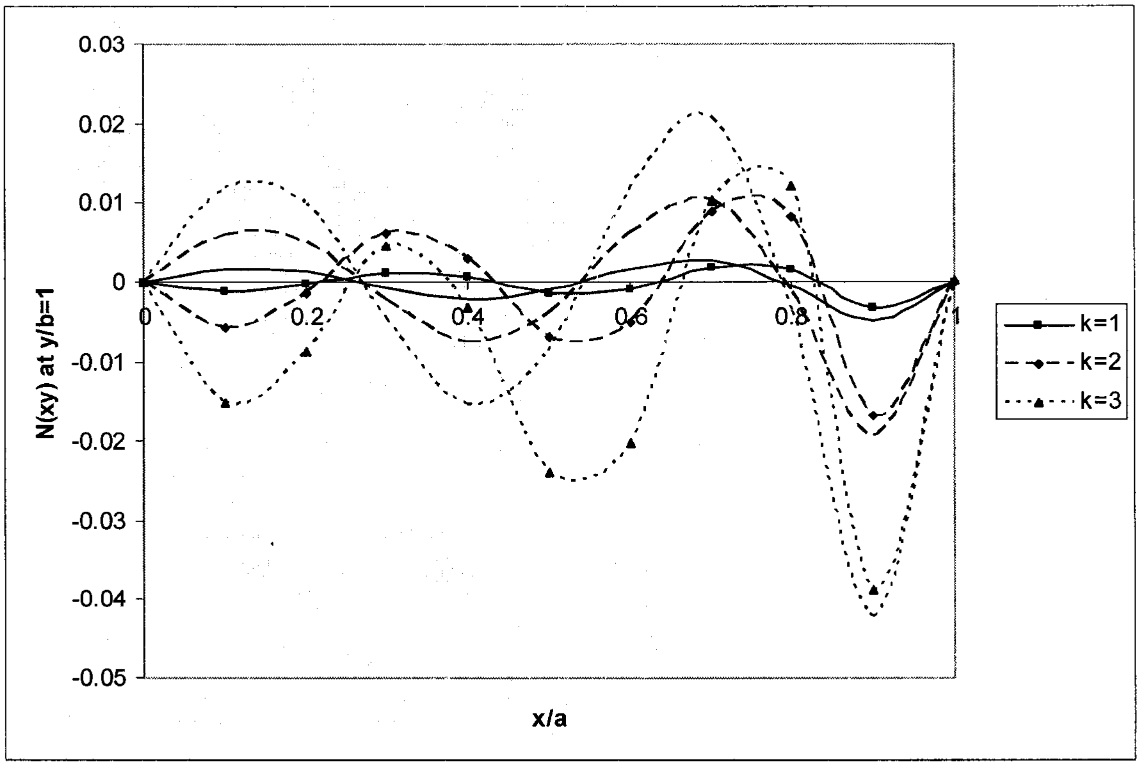

Figure 2.13: Comparative N_{xy} distributions along plate half length at (y/b) = ±1 edges (Lines without markers are two-stress-function solution results)

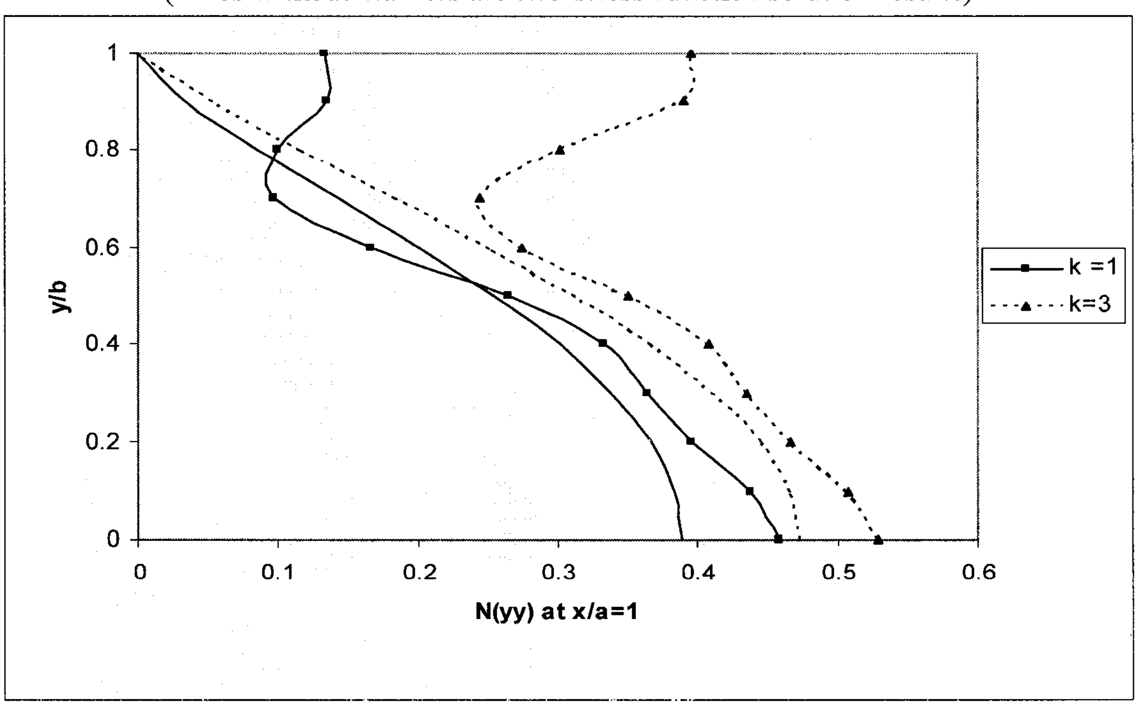

Figure 2.14: Comparative N_{yy} distributions at x/a = ±1 edges across plate half width (Lines without markers are two-stress-function solution results)

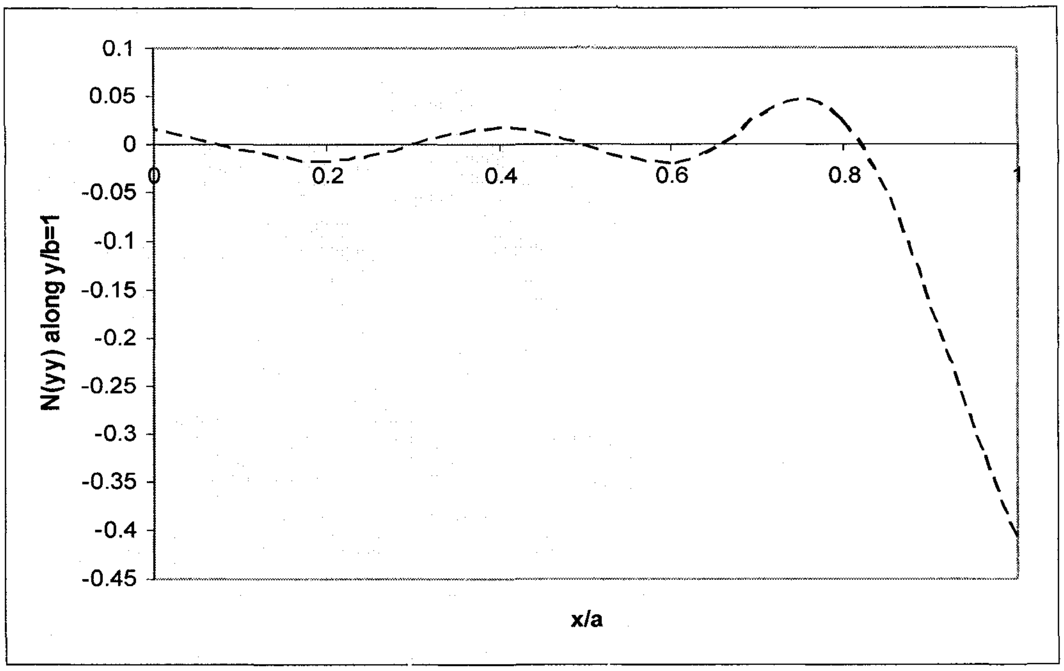

Figure 2.15: Y-direction normal stress (N_{yy}) distribution at y/b = ±1 edges (aspect ratio k = 3)

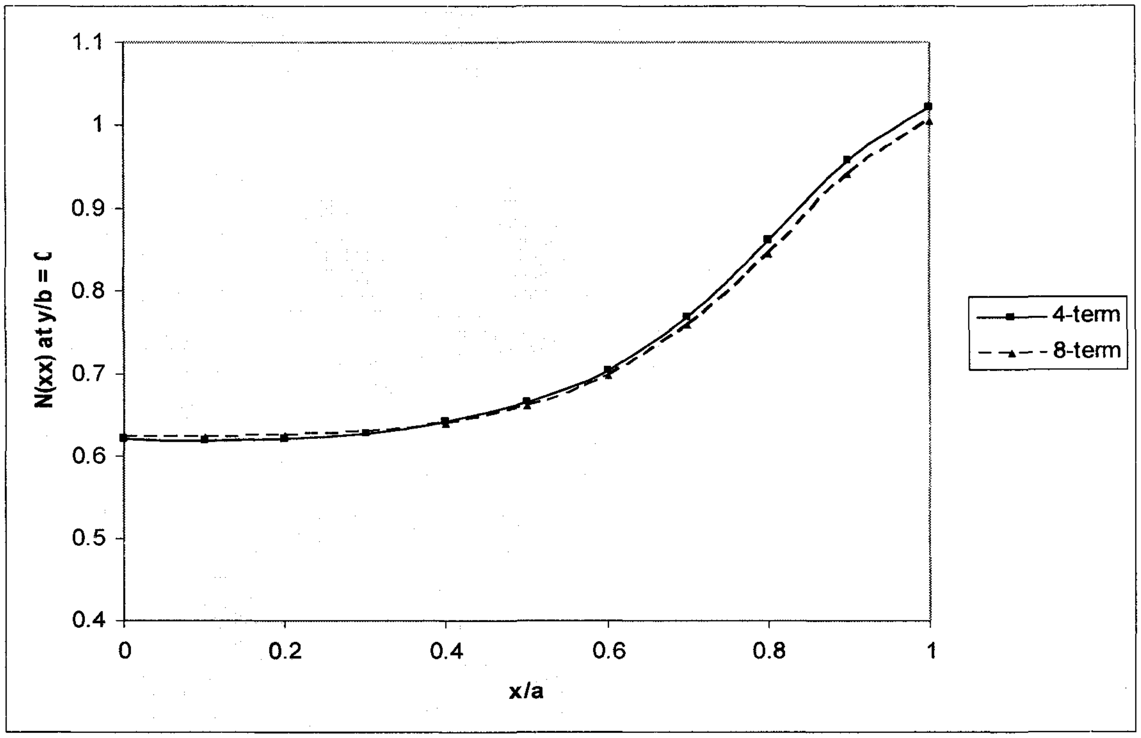

Figure 2.16: Convergence of N_{xx} stress resultant at y/b=0 (aspect ratio k = 3)

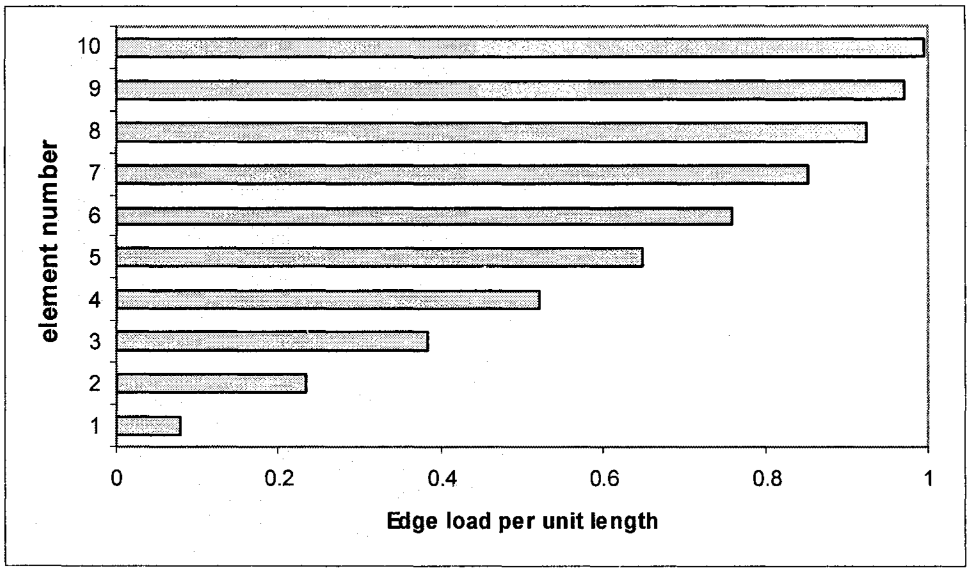

Figure 2.17: Applied edge load at each element (for one half plate width)
(aspect ratio k = 3)

Finite element analysis results

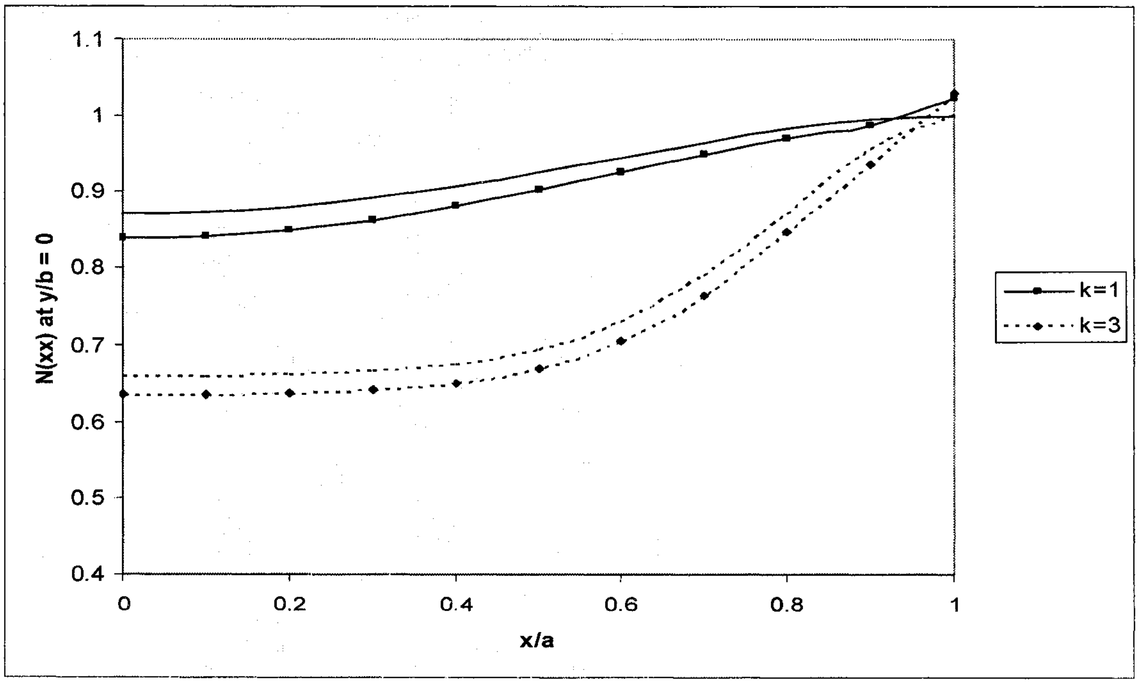

Figure 2.18: Comparative N_{xx} distributions at y/b =0 along plate half length
(Lines without markers are the two-stress-function solution results)

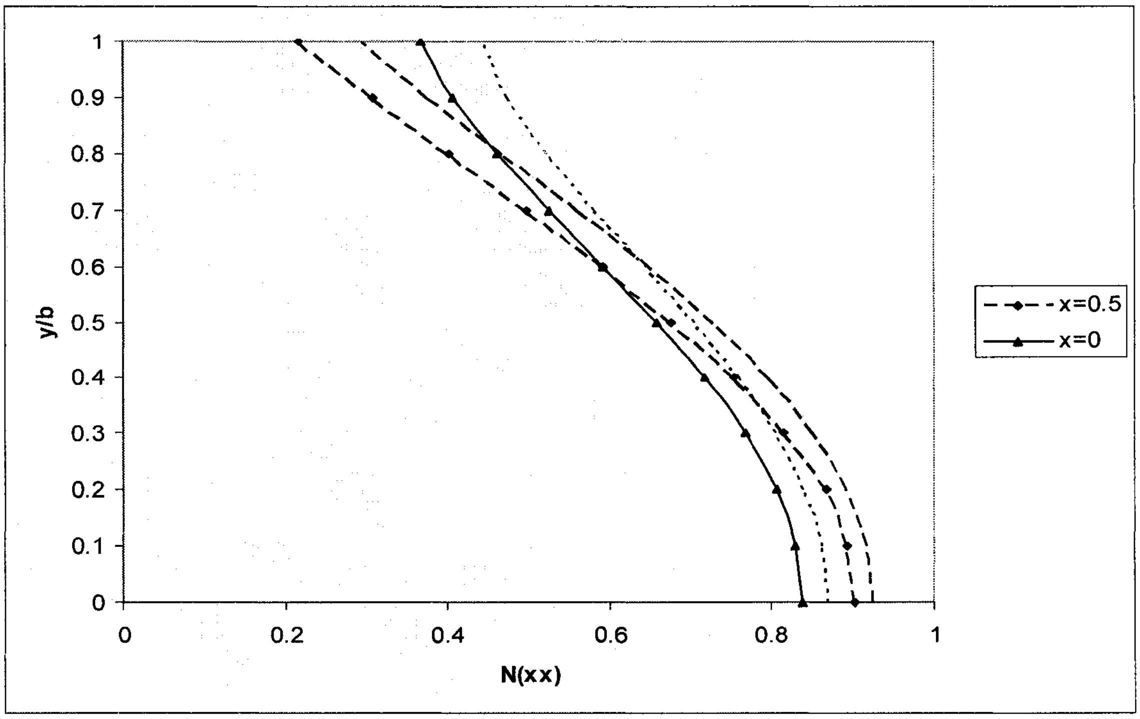

Figure 2.19a: Comparative N_{xx} distributions along plate half width (aspect ratio k = 1) (Lines without markers are two-stress-function solution results)

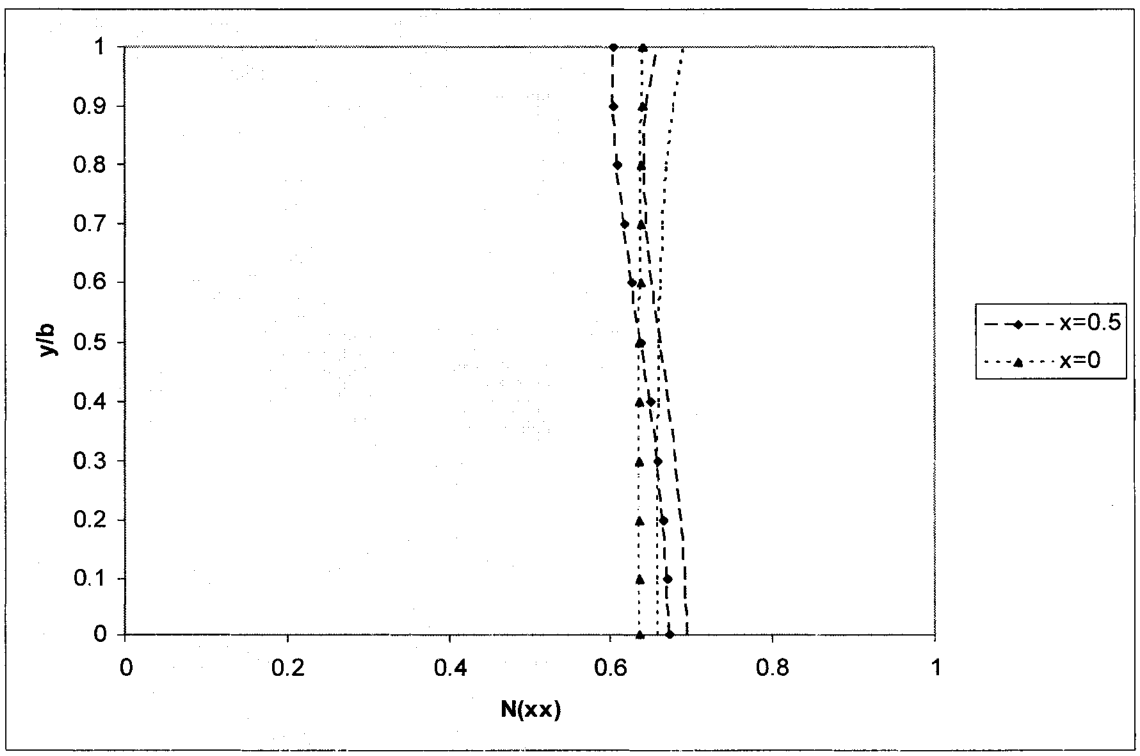

Figure 2.19b: Comparative normal stress (N_{xx}) distributions along plate half width (aspect ratio k = 3) (Lines without markers are two-stress-function solution results)

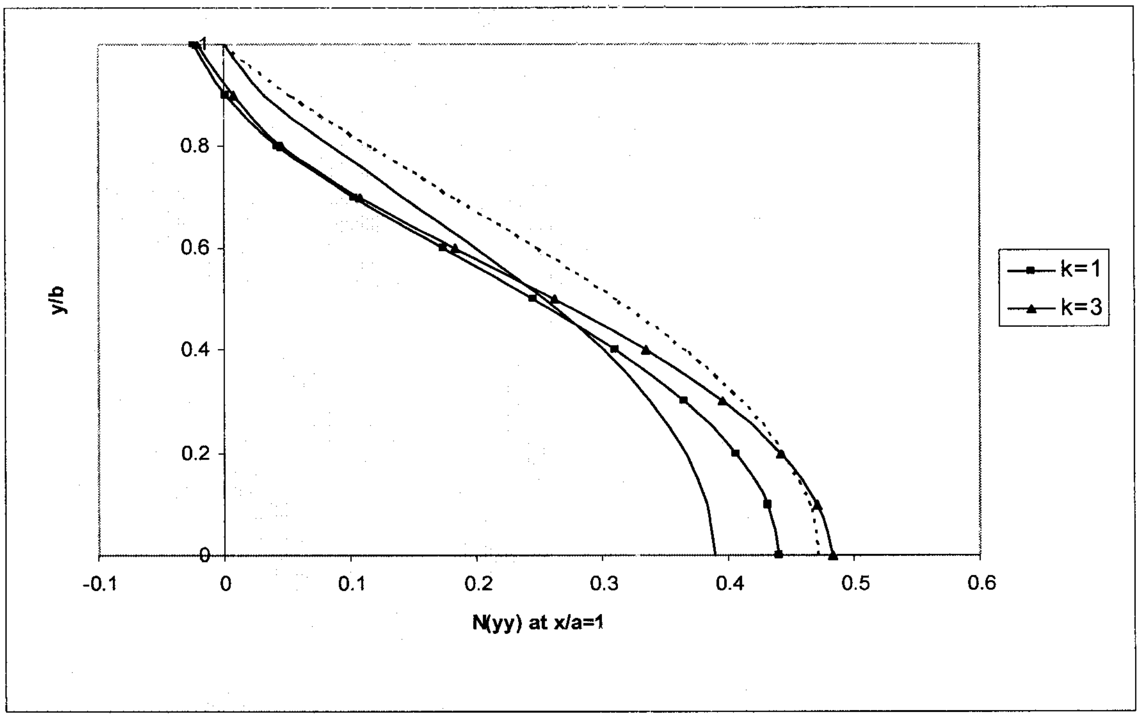

Figure 2.20: Comparative N_{yy} distributions at x/a=±1 edges across plate half width (Lines without markers are two-stress-function solution results)

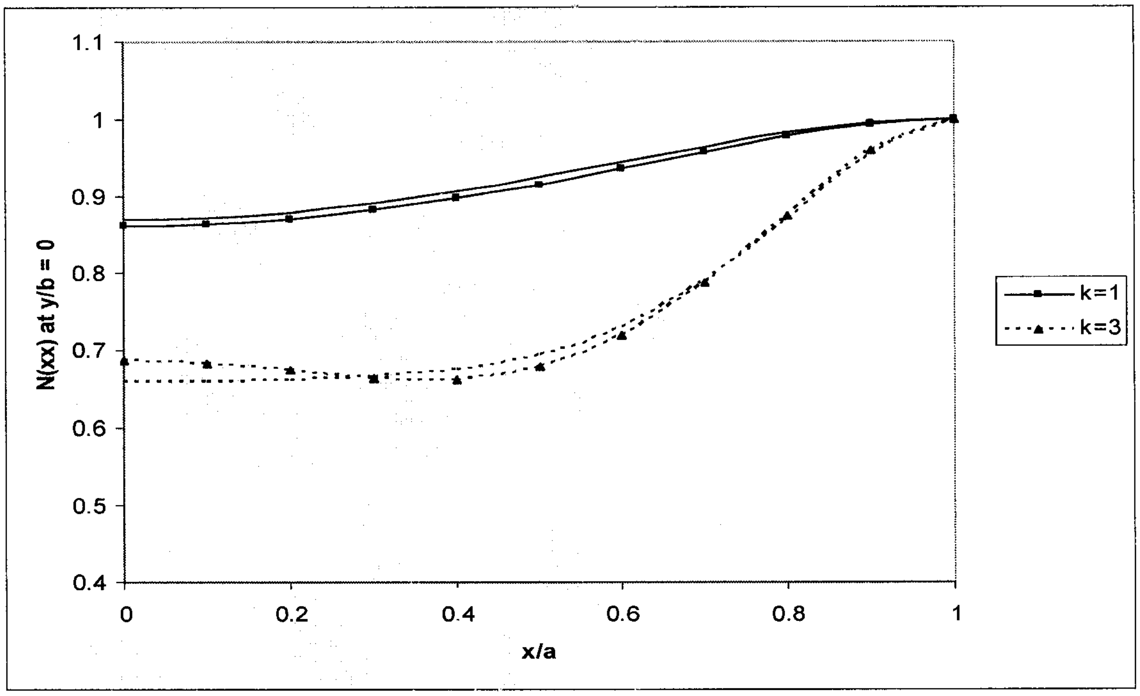

Figure 2.21: Comparative N_{xx} distributions at y/b=0 along plate half length (Lines without markers are two-stress-function results)

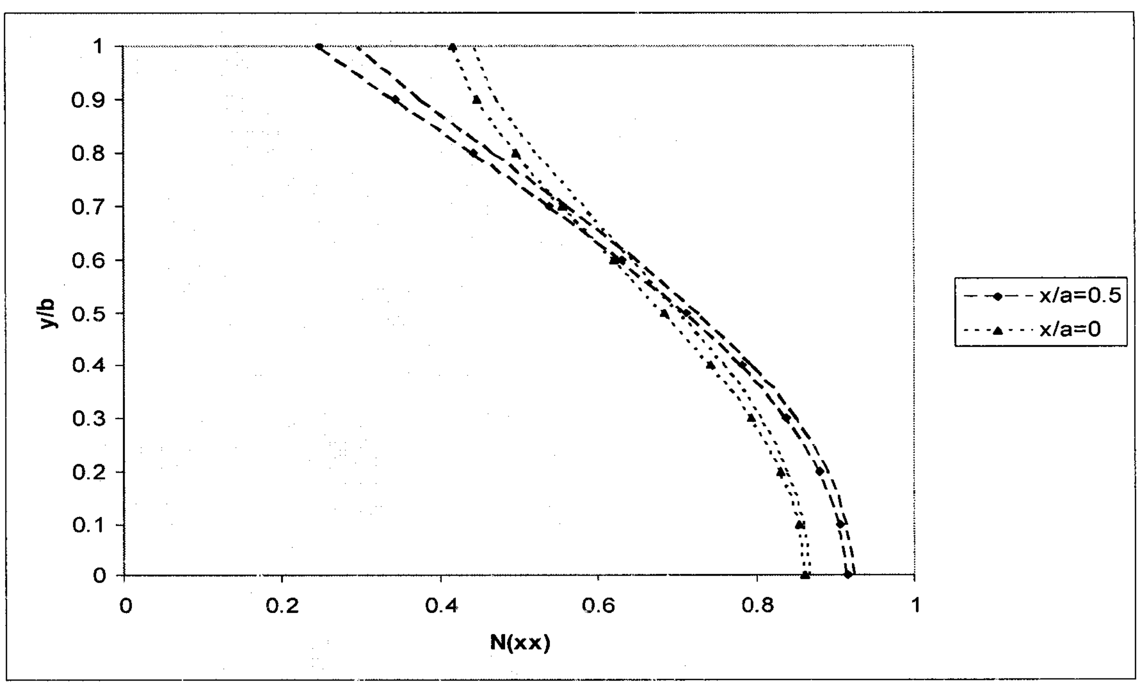

Figure 2.22a: Comparative N_{xx} distributions along plate half width (aspect ratio k = 1) (Lines without markers are two-stress-function solution results)

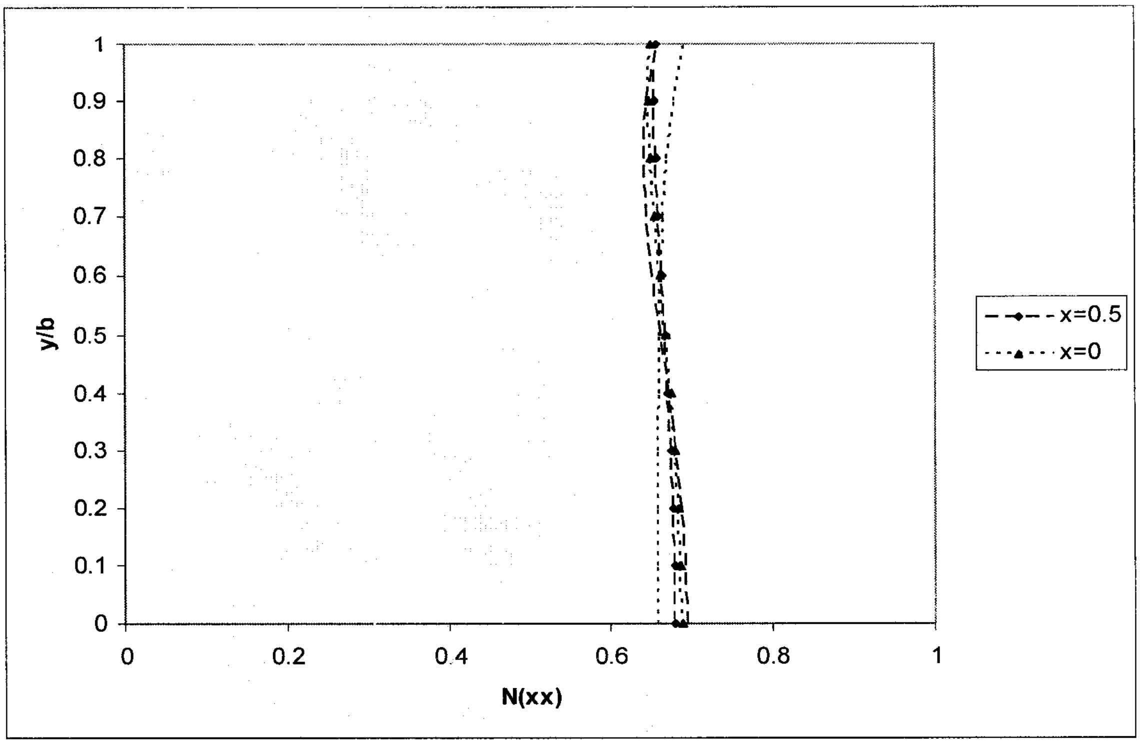

Figure 2.22b: Comparative N_{xx} distributions along plate half width (aspect ratio k = 2)
(Lines without markers are two-stress-function solution results)

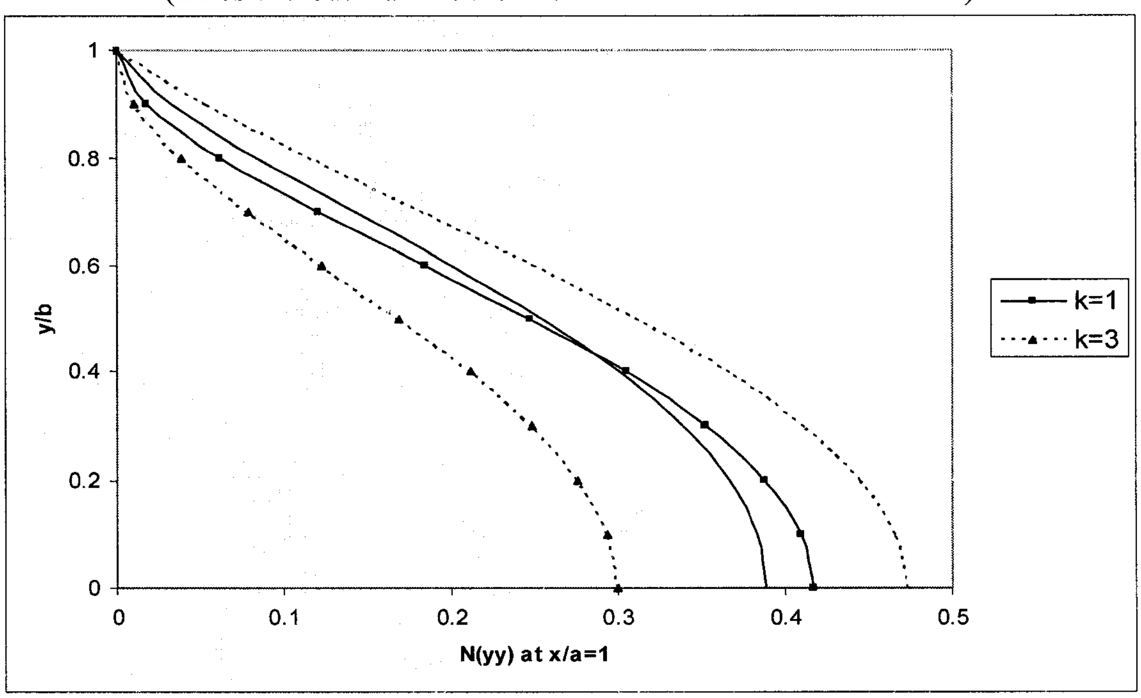

Figure 2.23: Comparative N_{yy} distributions at x/a = ± 1 edges across plate half width
(Lines without markers are two-stress-function solution results)

Pickett solution results

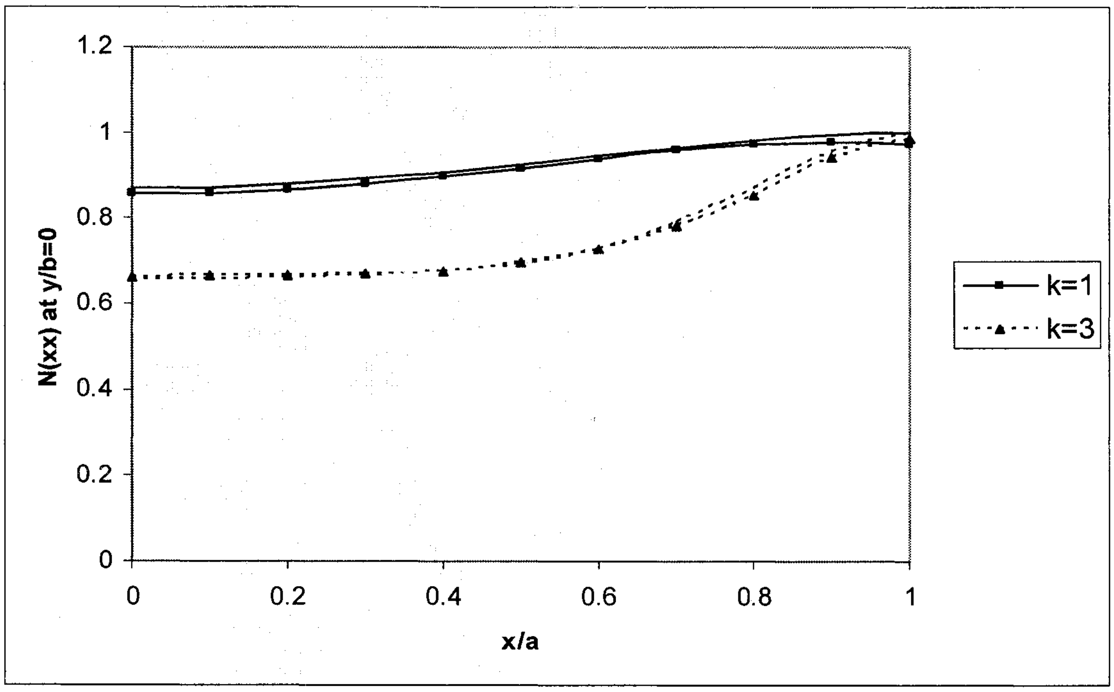

Figure 2.24: Comparative N_{xx} distributions at y/b=0 along plate half length
(Lines without markers are two-stress-function solution results)

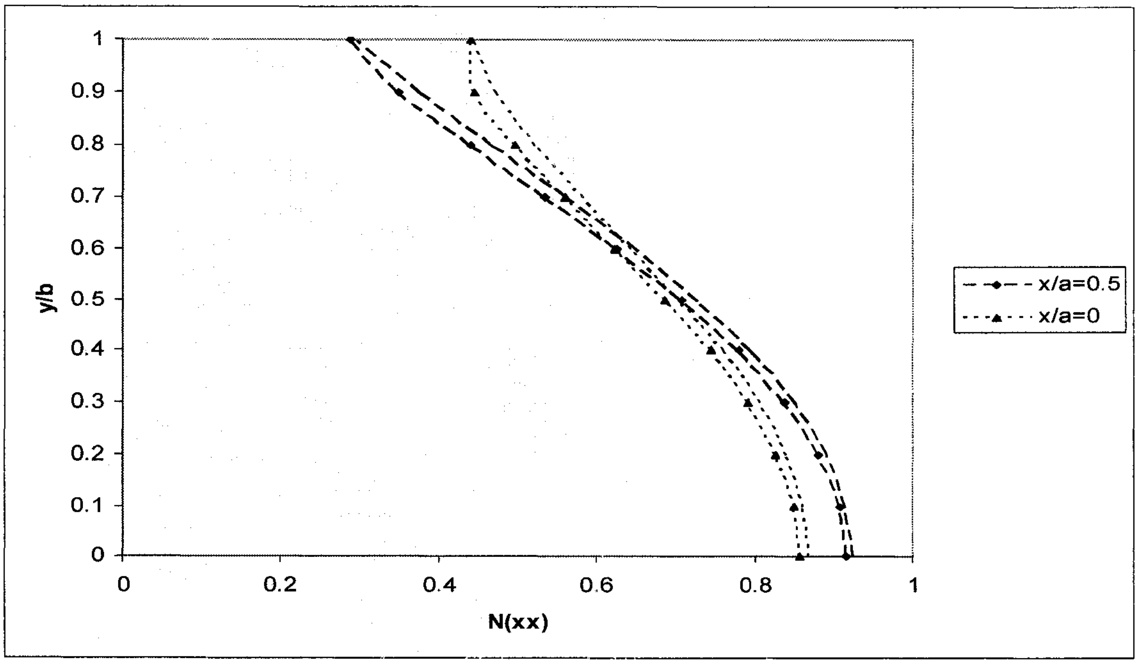

Figure 2.25a: Comparative N_{xx} distributions along plate half width (aspect ratio k = 1)
(Lines without markers are two-stress-function solution results)

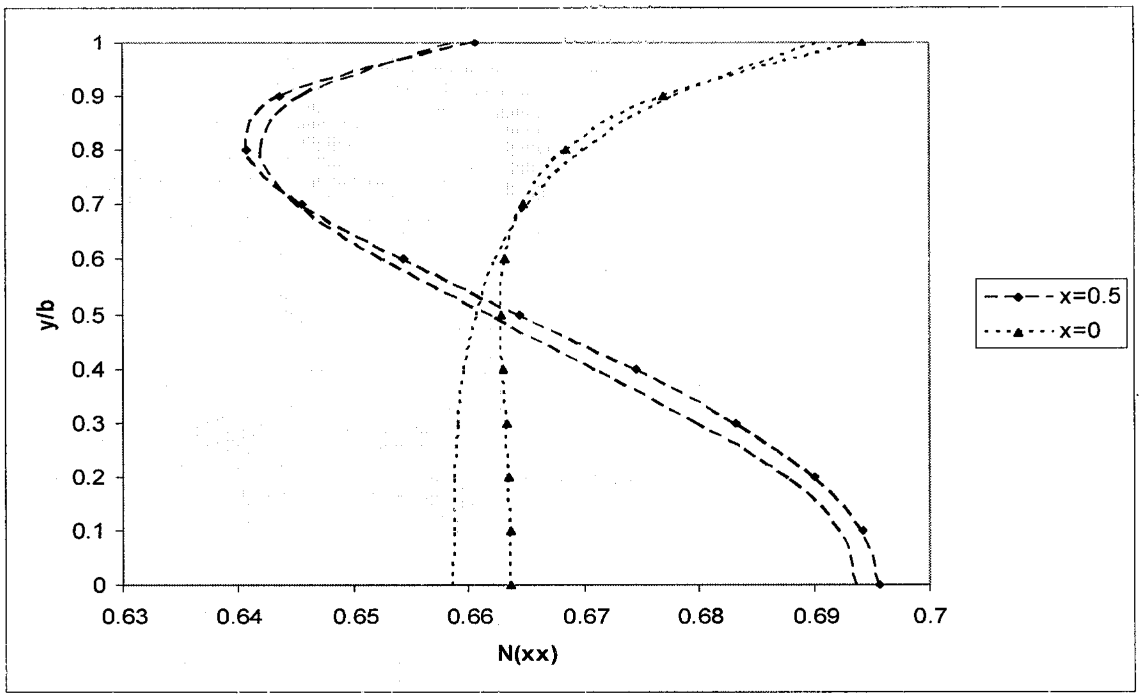

Figure 2.25b: Comparative N_{xx} distributions along plate half width (aspect ratio k = 3)
(Lines without markers are two-stress-function solution results)

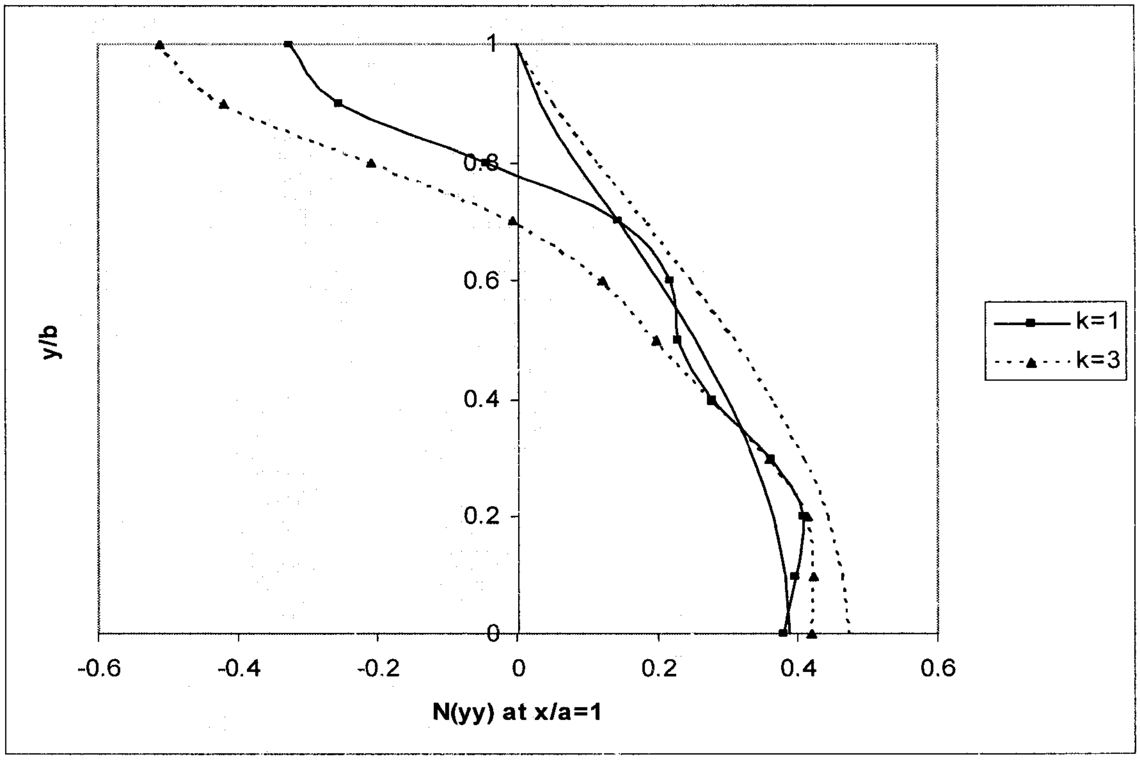

Figure 2.26: Comparative N_{yy} distributions at x/a = ±1 edges across plate half width
(Lines without markers are two-stress-function solution results)

CHAPTER THREE

BUCKLING AND VIBRATION ANALYSIS

3.1 Buckling Analysis

Using the in-plane elasticity solutions as developed in the previous chapter, buckling and vibration analyses of thin rectangular plates subjected to uniaxial half-sinusoidal edge loads are considered in this chapter. Once again, analytical solutions and a numerical solution by finite element analysis are carried out and the results are compared.

The governing differential equation for thin isotropic plate buckling is

$$\nabla^4 w - \frac{h}{D}\left(\sigma_x \frac{\partial^2 w}{\partial x^2} + 2\tau_{xy}\frac{\partial^2 w}{\partial x \partial y} + \sigma_y \frac{\partial^2 w}{\partial y^2}\right) = 0 \tag{3.1}$$

where D = flexural rigidity,

h = plate thickness,

w = transverse deflection

σ_x, σ_y, and τ_{xy} are the in-plane normal and shear stresses

Owing to the complexity of the resulting plate buckling equation when each of the in-plane stress components is a series sum, an exact analytical solution may not be possible. Therefore, the buckling solution is obtained by using the Galerkin method for the following four symmetric boundary conditions:

1. All edges simply supported
2. All edges clamped
3. Loaded edges simply supported and other edges clamped

4. Loaded edges clamped and other edges simply supported

For simply supported rectangular plates with a central coordinate system, the trial functions in Equation (3.2a) below satisfy all the required boundary conditions. However, in order to obtain consecutive modes, trial functions involving sinusoidal terms have to be considered as shown in Equation (3.2b). The trial functions for clamped plates are shown in Equation (3.3a,b).

$$\varphi_{1,3,5...} = \cos(m\pi x/2a)\cos(n\pi y/2b),\ \{m,n = 1,3,5,...\} \quad (3.2a)$$

$$\varphi_{2,4,6..} = \sin(j\pi x/a)\sin(k\pi y/b),\ \{j,k = 1,2,3,...\} \quad (3.2b)$$

$$\phi_{1,3,5..} = \cos\frac{m\pi x}{a} + \cos\frac{(m+1)\pi x}{a}\{m = 0,1,2..\} \quad (3.3a)$$

$$\phi_{2,4,6..} = -\left(\sin\frac{n\pi x}{2a} + \sin\frac{(n+2)\pi x}{2a}\right)\{n = 1,3,5..\} \quad (3.3b)$$

Numerical calculations were conducted using the symbolic math package Mathematica (Version 4.0) as well as Matlab (Version 6.0).

3.1.1 Convergence Analysis

As the Galerkin method is an approximate method involving predetermined trial functions, one has to consider numerical convergence in terms of number of trial functions in arriving at the necessary parameters. However, in the present case, as the trial functions are trigonometric terms which represent the buckling modes very accurately, one can expect to obtain sufficiently accurate results for fewer terms. Table 3.1 shows dimensionless buckling loads obtained using four and six trial functions for the case of all simply supported plates. Except for the aspect ratio of 3, the buckling load essentially remained constant. Even for an aspect ratio of 3, the buckling load changed by only about 1.2 percent. Due to the additional complexity of the numerical computations and based on the results from the six-term solution, the four-term Galerkin solution is considered sufficient in the subsequent analyses.

3.1.2 Finite Element Analysis

Using the previously obtained in-plane analysis results in time step one, buckling analysis is performed in time step two using the inverse power sweep method as well as the Lanczos method. It is observed that both methods show identical numerical buckling loads. Once again, mesh sizes consisting of up to 1200 elements (depending on the plate aspect ratio) were used and the results are compared with the analytical solution. From the buckling loads, normalized buckling loads are calculated, and the results are tabulated for plate aspect ratios of one, two and three.

3.1.3 Convergence Analysis of the Finite Element Method

Various mesh sizes from coarse to fine are considered for a plate involving all edges clamped and the buckling loads are plotted against the number of elements. As the clamped edge condition is much more stringent, it is assumed that the numerical convergency achieved is similar for the other boundary conditions as well. Figure 3.1 is a plot of dimensionless buckling load for various mesh sizes of a plate with all edges clamped. It is to be noted that the number of elements in the x-direction is proportionately equal to the aspect ratio times the number of elements in the y-direction. From this figure, it is evident that the dimensionless buckling load remained constant for a mesh size consisting of about 15 elements in the y-direction. In comparison, the rate of convergency is better at lower plate aspect ratio (k=2) than for a plate of higher aspect ratio (k=3). In view of these results, in the present work, the finite element analysis is carried out using 20 elements in the y-direction with proportional number of elements in the x-direction.

3.1.4 Numerical Results of Buckling Analysis

In all the following results, the boundary condition type is indicated by grouping opposite x-type edges followed by y-type edges. With this convention the following four edge conditions are used:

SSSS – All edges simply supported

CCCC – All edges clamped

SSCC – loaded edges (x-type) simply supported and other edges clamped

CCSS – loaded edges (x-type) clamped and other edge simply supported.

Numerical computations are carried out using the first four consecutive modes in the x-direction while keeping the first mode in the y-direction. Numerical results are compared between the finite element analysis and the analytical solutions using all in-plane elasticity solutions. Some comparative results for dimensionless buckling loads using various in-plane solutions for various plate edge conditions are presented in Tables 3.2 through 3.5.

Although the results obtained by Benoy (1969) are for the case of a parabolic loading, one can compare the solutions due to the close similarity of sinusoidal and parabolic stress distributions. Also, it is to be noted that the Timoshenko solution and the Pickett solution are for parabolic loading, whereas the two-stress-function solution, the FE solution, and the four-stress-function solution are for half-sinusoidal in-plane loading.

For the simply supported and clamped edge conditions, the Benoy solution underestimated the buckling loads considerably from the present solution. This difference is higher for higher plate aspect ratios and for clamped edge conditions. In case of clamped edges (Table 3.3), the differences between the present solution and the Benoy solution is of the order of 20 percent even for a plate aspect ratio of 1.

The reasons for the higher buckling loads can be explained by the following reasoning. In the present analysis, the in-plane stress solution contains both σ_y normal stress and τ_{xy} shear stresses which were neglected previously. Moreover, the σ_x stress distribution shows stress diffusion from the loaded edges towards the middle of the plate. As a result, the maximum stress is reduced (see Figure 2.6) and stresses near the edges $y/b = \pm 1$ are increased (see Figure 2.7a,b,c). As the plate edges are supported, this stress increase near the edges would cause the plate to sustain higher buckling loads. As the stress diffusion is higher at higher plate aspect ratios (Figure 2.7b,c) the buckling loads are progressively higher at higher plate aspect ratios. Also, the more stringent the boundary condition, the more buckling load the plate can withstand and, thus, the buckling loads are much higher for the case of clamped edges than of simply supported edges. It is to be noted that, for SSCC and CCSS mixed edge conditions, no existing results are available in the literature.

Figure 3.2 shows the comparative dimensionless buckling loads using the two-stress-function approach and the Benoy's results for clamped and simply supported edges. In both cases, the numerical difference is uniformly increased with the plate aspect ratio. Interestingly, the active buckling mode change occurred for a lower aspect ratio in case of the two-stress-function solution. This implies that the difference between the two methods for any given buckling mode is very much higher at higher plate aspect ratios. In case of simply supported edges, the buckling mode change occurred at similar plate aspect ratios. However, the Benoy's results indicated an almost constant dimensionless buckling load for any active mode whereas the two-stress-function solution showed an increasing buckling load with increasing mode number.

Using the four-stress-function solution, the buckling loads are (ref: Tables 3.2 through 3.5) always higher than from the two-stress-function solution for all plate edge conditions. This may be attributed to the presence of additional terms in the in-plane solution as well as the presence of some residual stresses at the boundaries as noted in the previous chapter.

Interestingly, the Timoshenko solution and the two-stress-function solution are in excellent agreement for all plate edge conditions and for all plate aspect ratios. Using the Timoshenko solution, higher buckling loads are obtained for lower plate aspect ratios and lower buckling loads are obtained for an aspect ratio of 3 in comparison with the two-stress-function solution. Also one can notice that the Timoshenko solution resulted in buckling loads that are both higher and lower than the corresponding two-stress-function solution. Upon closer observation reveals that the Timoshenko solution estimated lower buckling loads for a plate with aspect ratio of 3 irrespective of the edge conditions.

However the numerical difference between two methods is considerably small for all plate aspect ratios with all edge conditions.

The finite element solution also resulted in mostly higher buckling loads than the two-stress-function solution with the only exception in case of SSCC plates. Although numerical values of the buckling loads are in close agreement with the corresponding two-stress-function results, one can see larger differences in certain instances. The maximum difference however is obtained for SSCC type edge conditions for a plate aspect ratio of 3. It is to be noticed that, for this particular case, the FE solution is somewhat lower than all corresponding analytical solutions.

In view of the scattered nature of the buckling loads, it is thought to be helpful to tabulate the lowest buckling load for various plate edge conditions and is shown in Table 3.6. Although the buckling loads as calculated by Benoy are lower than all the present values, they were omitted from this table due to the erroneous nature of his calculations.

Figure 3.3 is a plot of dimensionless buckling load against aspect ratio for various edge conditions using the two-stress-function solution. It is interesting to note that, for the case of CCSS and SSSS boundary conditions, the minimum buckling load associated with any buckling mode is increased with plate aspect ratio whereas the reverse happens in the case of CCCC and SSCC edge conditions.

3.2 Vibration Analysis

The governing differential equation for the transverse (out-of-plane) vibration of thin isotropic plates subjected to compressive in-plane loading is

$$\nabla^4 w+\frac{h}{D}\left(\sigma_x \frac{\partial^2 w}{\partial x^2}+2\tau_{xy}\frac{\partial^2 w}{\partial x \partial y}+\sigma_y \frac{\partial^2 w}{\partial y^2}+\rho\frac{\partial^2 w}{\partial t^2}\right)=0 \tag{3.4}$$

where D is the flexural rigidity, h is the plate thickness, w is the normal deflection, and ρ is the plate density. After considering

$$w(x,y,t)=\overline{w}(x,y)\sin \omega t \tag{3.5}$$

one can write the above equation as

$$\nabla^4 \overline{w}+\frac{h}{D}\left(\sigma_x \frac{\partial^2 \overline{w}}{\partial x^2}+2\tau_{xy}\frac{\partial^2 \overline{w}}{\partial x \partial y}+\sigma_y \frac{\partial^2 \overline{w}}{\partial y^2}-\rho\omega^2 \overline{w}\right)=0 \tag{3.6}$$

As the in-plane stress solution is a series solution, exact analytical solutions may not be possible due to the complexity of the resulting plate vibration equation. Therefore, approximate solutions using the Galerkin method are obtained for combinations of simply supported and clamped rectangular plate edges. For simply supported and clamped rectangular plates with a central coordinate system, the trial functions in equations (3.2a,b) and equations (3.3a,b), respectively, satisfy the boundary conditions.

Free-vibration frequencies are obtained at various relative load (buckling load fraction) increments. Four trial functions involving (1,1), (2,1) (3,1), (4,1) vibration modes are considered in the present analysis.

3.2.1 Finite Element Analysis

As explained before, convergence of the finite element model is established using the buckling loads. For vibration analysis, frequency analysis is specified instead of buckling analysis in the second time step. Using the previously found buckling loads, various in-plane loads representing various load ratios are applied in the first time step and vibration frequencies are extracted. Frequencies up to first ten consecutive modes are extracted and the results are compared with the analytical results and tabulated.

3.2.2 Numerical Results of Vibration Analysis

Numerical computations are carried out using the first four consecutive modes in the x-direction while keeping the first mode in the y-direction, and the results are compared with those from finite element analysis. Figures 3.4 through 3.7 show the dimensionless frequency ratio (Ω^2/Ω_s^2) against dimensionless in-plane load (σ_0 h b^2/D) for various combinations of simply supported and clamped plate edges. The quantities Ω and Ω_s are nondimensionlized as shown in Equation (3.7). The dimensionless quantity Ω_s is the dimensionless fundamental frequency of an unloaded square plate with the corresponding edge condition.

$$\Omega^2 = \frac{\rho h \omega^2 a^2 b^2}{D} \tag{3.7}$$

In all the edge conditions, the plate frequencies of vibration using the two-stress-function and four-stress-function methods showed close agreement with the finite element results only at lower plate aspect ratios. As the aspect ratio increased, some differences were observed.

At higher aspect ratios, the two-stress-function method results appeared to be closer to the finite element results for the SSSS and CCCC plates. It is interesting to note that the finite element frequencies are lower than the analytical results in the case of CCCC, SSCC plates, and vice versa for the case of SSSS and CCSS plates.

Only in the case of SSCC plates having an aspect ratio of 3, the two-stress-function solution results and the four-stress-function results showed relatively close agreement compared with the finite element frequencies throughout the in-plane load range. In general, the differences in frequency ratios between the various methods increased uniformly as the in-plane load was increased towards the fundamental buckling load. Also, these differences are more pronounced at higher plate aspect ratios. Thus, one can see from these figures that larger differences in numerical values among the various methods of solution occurred for higher loads and higher plate aspect ratios.

It is interesting to note that the use of a nondimensional frequency, as defined in Equation (3.7), resulted in lower values of the fundamental frequency for a plate aspect ratio of 2 than that for a square plate for CCSS plates. All the remaining edge conditions gave higher frequencies than the fundamental frequency for the corresponding square plate.

Obviously, one can anticipate much closer agreement of the numerical values if one considers the nondimensional frequency itself, rather than the square of the frequency. Tables 3.7a through 3.10c show the numerical values of the nondimensional frequency at various in-plane load ratios. From these tables, the excellent agreement between the two-stress-function and the four-stress-function results is easily evident. Although there are minor differences in buckling loads (Devarakonda and Bert) between these analytical methods, the vibration frequencies are almost identical for each relative load ratio.

It is to be noted that, in all the tables, the numerical values for nondimensional frequency are given based on the definition of Equation (3.7). Also, the mode number shown in brackets for the finite element results is applicable to the entire row (i.e., for both of the analytical methods). The only exception is for the case of the CCSS plate (Table 3.10a) with an aspect ratio of 1.

As the Galerkin method is an assumed mode approximate method, one generally does not know beforehand whether or not the assumed modes yield consecutive modes. However, the finite element analysis arranges the modes consecutively based on the ascending order of the numerical value of the frequency. For comparison purposes, only those modes that are used for the analytical method are shown in all of these tables. The only exception is the lowest frequency for any given relative load ratio where all of the methods considered in the present study gave identical modes. Thus, with the exception of the lowest frequency, one can anticipate additional vibration modes active between the tabulated values. As a result of these additional modes, the frequency corresponding to the vibration mode (4,1) in Table 3.10a is not shown for the finite element results.

Tables 3.11 through 3.13 list the vibration frequencies in ascending order for various plate edge conditions (aspect ratios: 1,2,3) subjected to a relative in-plane load of 0.5. It is to be noted that these values are listed based on the finite element analysis.

For most in-plane load cases, the vibration modes contain integer wave numbers in the x and y co-ordinate directions. However, using the finite element solution, one can find certain modes which do not have waves coinciding with the co-ordinate directions. Such mode rearrangement occurs at various in-plane load ratios. In reference to Tables 3.11 through 3.13, one can see the mode rearrangement with increasing in-plane load ratio for any given plate. Figures 3.8 through 3.13 show the first six vibration modes (using finite element analysis) for a CCSS plate of aspect ratio 1 and Figures 3.14 through 3.19 are the first six vibration modes of a SSCC plate of aspect ratio 3. In both cases the in-plane load ratio is 0.9. In Figure 3.15, the mode number in the x-direction is not well defined due to the small positive deflection at the center followed by negative deflections in either direction. In Figure 3.16 such additional deflections can be found near the plate edges. It is to be noted that these modes appeared at this particular in-plane load ratio of 0.9 only. In Figure 3.11, the modes seem to be aligned towards the plate corners, and Figure 3.13 shows deflections near the edges although the active mode looks like (3,1).

3.3 Summary

The thin rectangular plate buckling and transverse vibration problem subjected to a half sinusoidal in-plane load is solved using the various in-plane elasticity solutions obtained previously. The buckling results indicated higher loads than those available in the literature which can be explained by the stress diffusion phenomenon and the presence of σ_y and τ_{xy} stresses throughout the plate. The buckling loads showed higher difference with the available results from the literature (incorrect) as the aspect ratio was increased and for the case of clamped edge conditions. A maximum difference of about 30 percent was obtained between the present analyses and Benoy's (incorrect) results. In general, excellent agreement between the analytical methods and the finite element solution was observed. The analytical solution was obtained using two-stress-function, four-stress-function and Timoshenko in-plane elasticity solutions, and all methods showed close agreement. The four-stress-function solution showed higher buckling loads for all plate aspect ratios and all plate edge conditions. From the plot of dimensionless buckling load against plate aspect ratios, the active buckling mode change occurred at lower plate aspect ratios in the present analysis than in Benoy's solution.

Extensive flexural vibration results were obtained for various in-plane load ratios for all plate edge conditions. It is to be noted that no results are available in the literature for such nonlinear in-plane load conditions. From the results obtained using the finite element analysis, it is observed that most of the mode numbers had integer wave numbers and were aligned along the x, y co-ordinate axes with some exceptions. Also, with increasing in-plane load ratios, the modes were rearranged, and such rearrangement was different for each plate. Extensive flexural vibration results were tabulated for reference.

Table 3.1: Comparative dimensionless ($\sigma_0 hb^2/\pi^2D$) buckling loads for simply supported edges.

Aspect ratio k (a/b)	FEA	Two-stress-function solution	
		4-term Galerkin	6-term Galerkin
1	5.41	5.14	5.14
2	5.73	5.43	5.43
3	5.83	5.74	5.67

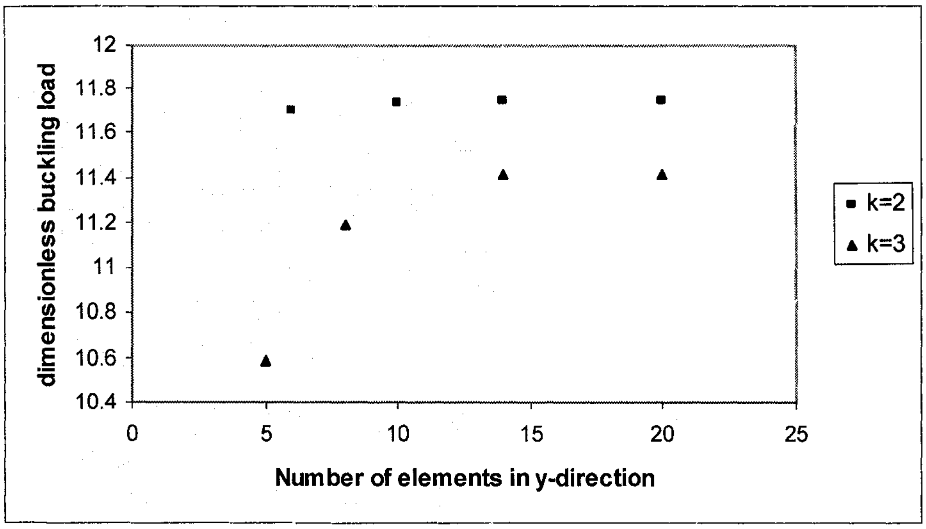

Figure 3.1: Convergence analysis of the finite element method

Table 3.2: Dimensionless ($\sigma_0 hb^2/\pi^2 D$) buckling loads for simply supported edges.

(Terms in brackets are percentage differences to two-stress-function solution)

Aspect ratio k (a/b)	Four-stress-function solution	FEA	Two-stress-function solution[1]	Based on Timoshenko solution (Parabolic)	Based on Pickett solution (Parabolic)	Benoy (Parabolic)[2]
1	5.42 (+5.44%)	5.41 (+5.25%)	5.14	5.24 (+1.94%)	5.24 (+1.94%)	4.59 (-10.7%)
2	5.75 (+5.89%)	5.73 (+5.52%)	5.43	5.54 (+2.02%)	5.54 (+2.02%)	4.59 (-15.4%)
3	6.04 (+5.22%)	5.83 (+1.56%)	5.74	5.66 (-1.39%)	5.72 (-0.348%)	4.59 (-20.0%)

[1] Refer Bert and Devarakonda (2003), [2] Refer Benoy (1963)

Table 3.3: Dimensionless ($\sigma_0 hb^2/\pi^2 D$) buckling loads for clamped edges.

Aspect ratio k (a/b)	Four-stress-function solution	FEA	Two-stress-function solution[1]	Based on Timoshenko solution (Parabolic)	Benoy (Parabolic)[2]
1	14.74 (+5.89%)	14.16 (+1.72%)	13.92	14.21 (+2.08%)	11.06 (-20.5%)
2	12.26 (+6.70%)	11.75 (+2.26%)	11.49	11.71 (+1.91%)	8.667 (-24.5%)
3	12.02 (+4.34%)	11.54 (+0.17%)	11.52	11.39 (-1.12%)	8.021 (-30.3%)

[1] Refer Devarakonda and Bert (to appear), [2] Refer Benoy (1963)

Table 3.4: Dimensionless ($\sigma_0 hb^2/\pi^2 D$) buckling loads for loaded edges clamped and other edges simply supported

Aspect ratio k (a/b)	Four-stress-function solution	FEA	Two-stress-function solution	Based on Timoshenko solution (Parabolic)	Benoy (Parabolic)
1	9.40 (+5.85%)	9.46 (+6.53%)	8.88	9.07 (+2.13%)	NA
2	7.47 (+7.02%)	7.46 (+6.87%)	6.98	7.16 (+2.57%)	NA
3	7.04 (+6.50%)	6.89 (+4.23%)	6.61	6.53 (-1.21%)	NA

NA – Not Available

Table 3.5: Dimensionless ($\sigma_0 hb^2/\pi^2 D$) buckling loads for loaded edges simply supported and other edges clamped

Aspect ratio k (a/b)	Four-stress-function solution	FEA	Two-stress-function solution[1]	Based on Timoshenko solution (Parabolic)	Benoy (Parabolic)
1	9.68 (+3.75%)	9.47 (+1.50)	9.33	9.45 (+1.28%)	NA
2	10.05 (+5.34%)	9.41 (-1.36%)	9.54	9.69 (+1.57%)	NA
3	10.79 (+3.55%)	9.65 (-7.38%)	10.42	10.23 (-1.82%)	NA

[1] Refer Devarakonda and Bert (to appear)

Table 3.6: Lowest buckling loads (dimensionless) for various edge conditions

Edge condition	Aspect ratio	Dimensionless buckling load	Mode	In-plane elasticity solution method
SSSS	1	5.14	(1,1)	Two-stress-function
	2	5.43	(2,1)	Two-stress-function
	3	5.66	(3,1)	Timoshenko solution
CCCC	1	13.92	(1,1)	Two-stress-function
	2	11.49	(3,1)	Two-stress-function
	3	11.39	(4,1)	Timoshenko solution
SSCC	1	9.33	(1,1)	Two-stress-function
	2	9.41	(2,1)	FEA
	3	9.65	(3,1)	FEA
CCSS	1	8.88	(2,1)	Two-stress-function
	2	6.98	(3,1)	Two-stress-function
	3	6.53	(4,1)	Timoshenko solution

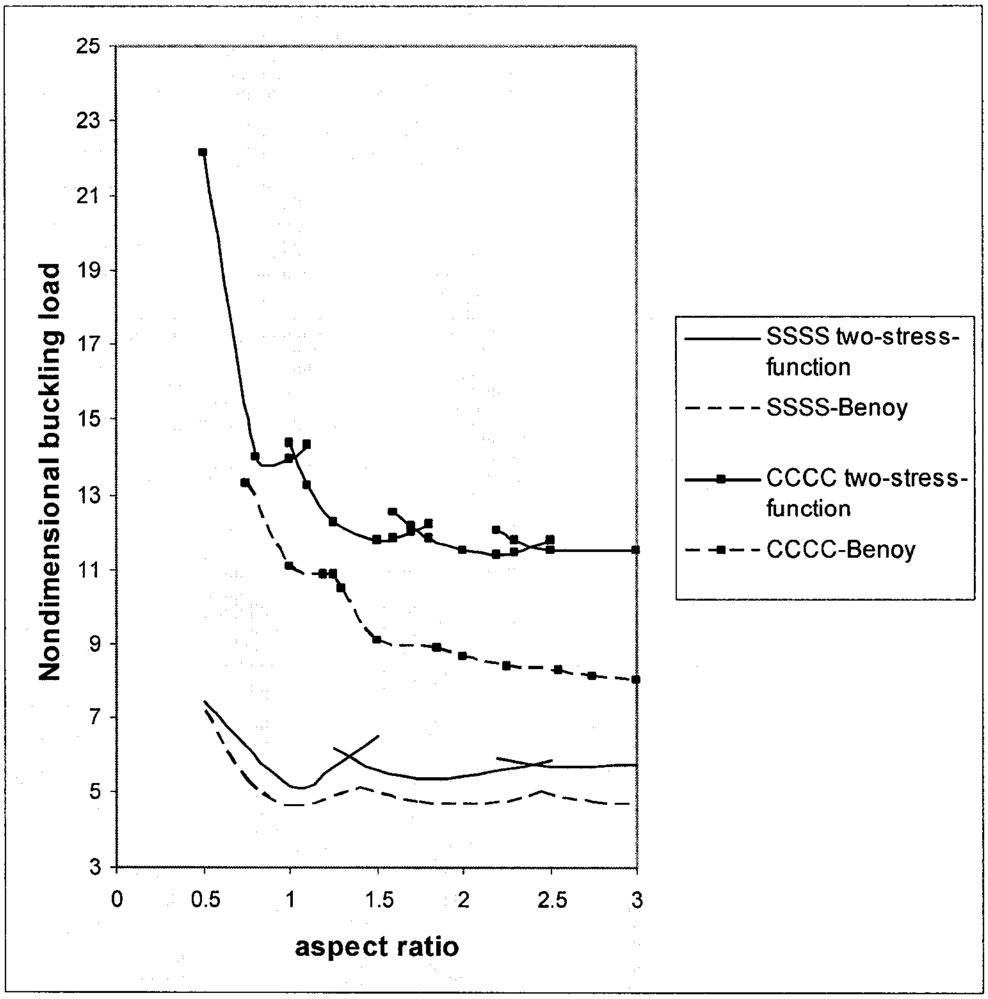

Figure 3.2: Comparative buckling loads

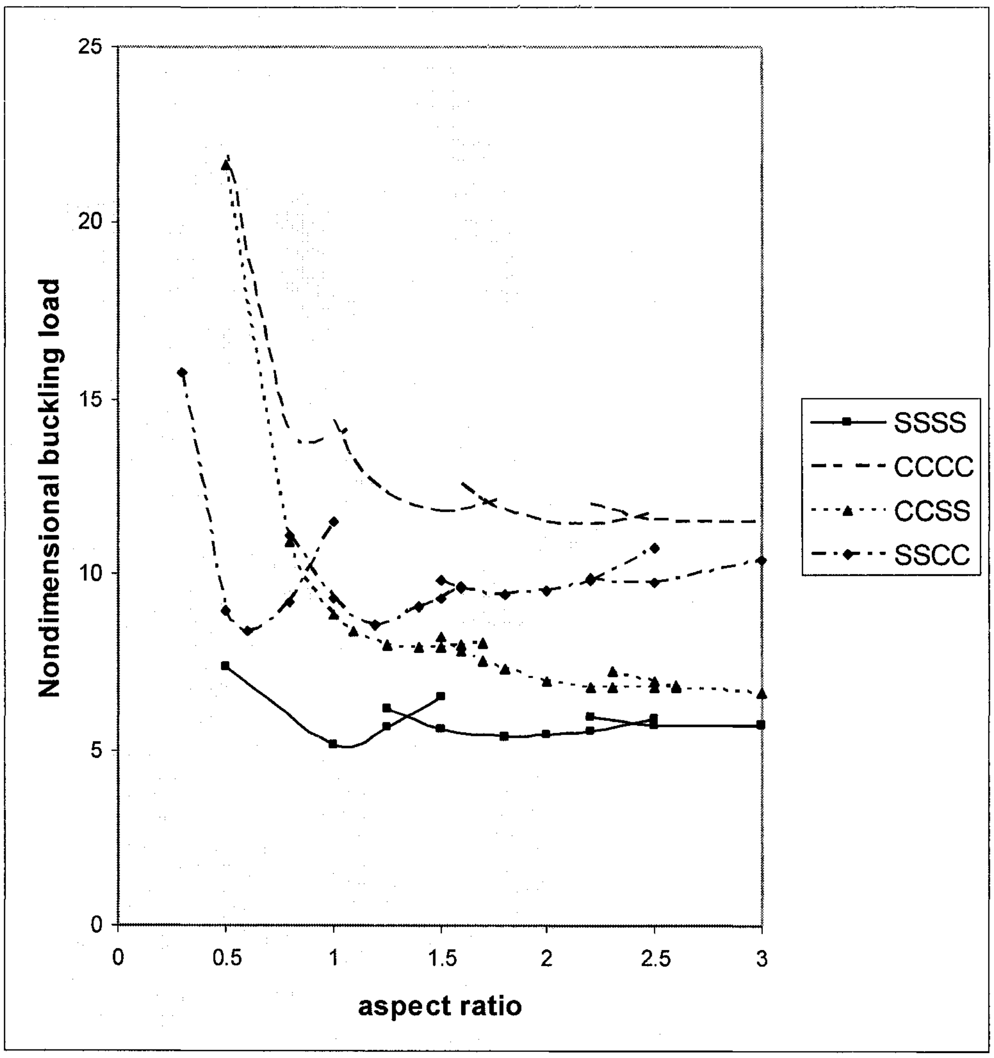

Figure 3.3: Nondimensional buckling loads using two-stress-function approach

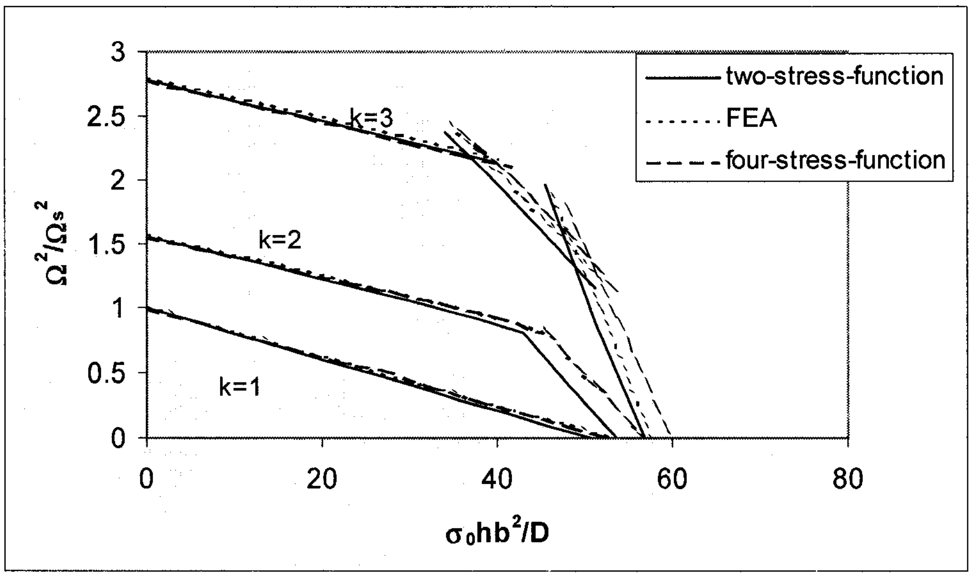

Figure 3.4: Frequency ratio against dimensionless in-plane load (SSSS); k = a/b (aspect ratio)

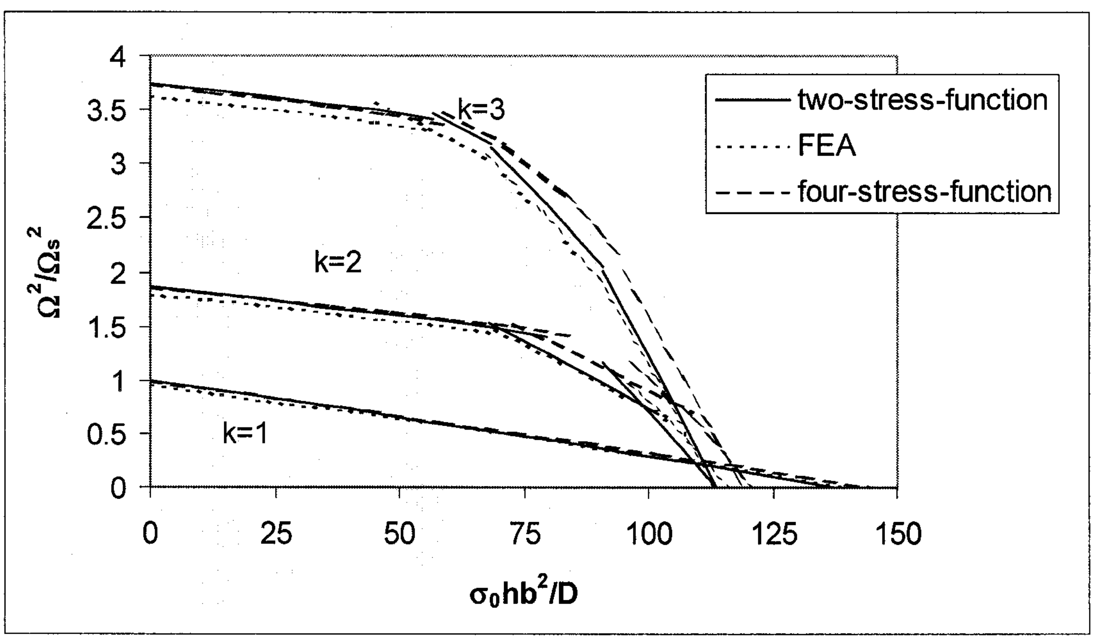

Figure 3.5: Frequency ratio against dimensionless in-plane load (CCCC)

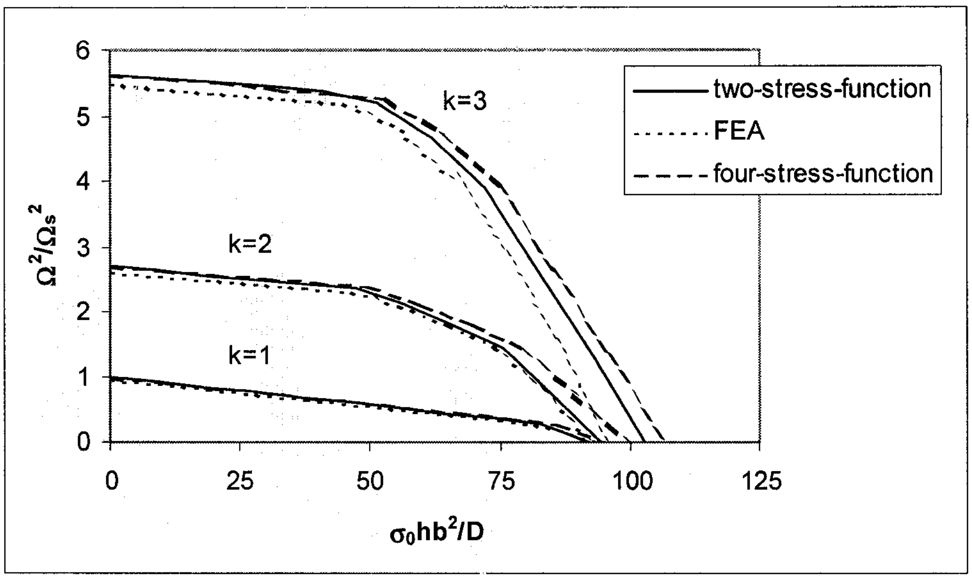

Figure 3.6: Frequency ratio against dimensionless in-plane load (SSCC)

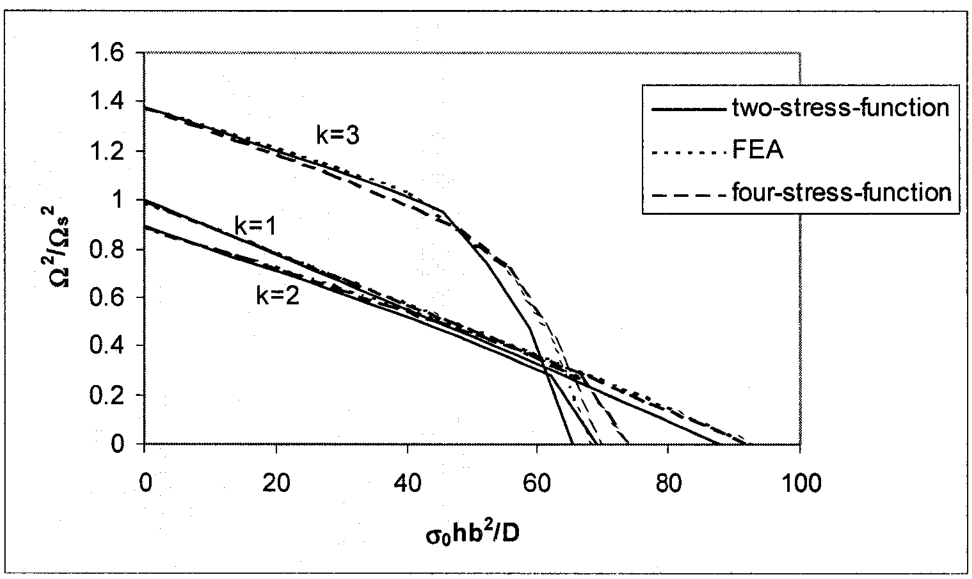

Figure 3.7: Frequency ratio against dimensionless in-plane load (CCSS)

Table 3.7a: Dimensionless frequency $\Omega = \omega ab\sqrt{\frac{\rho h}{D}}$, all edges simply supported (SSSS), aspect ratio: 1 (modes are not consecutive)

a/b=1				
σ_0/σ_{cr}	Two-stress-function	Four-stress-function	Finite element analysis	Mode
0.1	18.72	18.72	18.80	(1,1)
	47.64	47.63	48.05	(2,1)
	96.78	96.77	98.59	(3,1)
	165.7	165.7	171.3	(4,1)
0.5	13.96	13.96	14.03	(1,1)
	40.12	40.05	40.43	(2,1)
	88.74	88.66	90.41	(3,1)
	157.5	157.5	162.9	(4,1)
0.9	6.248	6.250	6.312(1,1)	(1,1)
	30.82	30.65	30.97(2,1)	(2,1)
	79.89	79.73	81.39	(3,1)
	148.9	148.7	154.1	(4,1)
$\sigma_{cr}hb^2/D$	50.78	53.49	53.75	(1,1)

Table 3.7b: Dimensionless frequency $\Omega = \omega ab\sqrt{\frac{\rho h}{D}}$, all edges simply supported (SSSS), aspect ratio: 2

a/b=2				
σ_0/σ_{cr}	Two-stress-function	Four-stress-function	Finite element analysis	Mode
0.1	23.95	23.96	24.06	(1,1)
	37.47	37.47	37.64	(2,1)
	61.30	61.30	61.67	(3,1)
	95.40	95.40	96.25	(4,1)
0.5	20.81	20.89	20.97	(1,1)
	28.00	28.04	28.16	(2,1)
	48.30	48.29	48.56	(3,1)
	80.94	80.90	81.68	(4,1)
0.9	12.59	12.63	12.76	(2,1)
	16.90	17.00	17.04	(1,1)
	30.23	30.24	30.17	(3,1)
	63.30	63.23	63.84	(4,1)
$\sigma_{cr}hb^2/D$	53.64	56.77	56.55	(2,1)

Table 3.7c: Dimensionless frequency $\Omega = \omega ab\sqrt{\frac{\rho h}{D}}$, all edges simply supported (SSSS), aspect ratio: 3

a/b=3				
σ_0/σ_{cr}	Two-stress-function	Four-stress-function	Finite element analysis	Mode
0.1	32.36	32.33	32.53	(1,1)
	40.98	40.99	41.20	(2,1)
	56.17	56.17	56.51	(3,1)
	78.31	78.29	78.96	(4,1)
0.5	30.12	29.96	30.31	(1,1)
	32.83	32.89	33.20	(2,1)
	41.88	41.87	42.35	(3,1)
	60.05	59.94	60.91	(4,1)
0.9	18.70	18.72	19.36	(3,1)
	21.17	21.12	21.73	(2,1)
	27.75	27.40	27.99	(1,1)
	33.32	33.09	34.53	(4,1)
$\sigma_{cr}hb^2/D$	56.73	59.69	57.54	(3,1)

Table 3.8a: Dimensionless frequency $\Omega = \omega ab\sqrt{\frac{\rho h}{D}}$, loaded edges simply supported and other edges clamped, aspect ratio: 1

a/b=1				
σ_0/σ_{cr}	Two-stress-function	Four-stress-function	Finite element analysis	Mode
0.1	28.40	28.42	27.86	(1,1)
	52.97	52.97	52.25	(2,1)
	100.2	100.2	100.5	(3,1)
	168.3	168.3	172.1	(4,1)
0.5	22.96	23.07	22.42	(1,1)
	39.49	39.50	38.99	(2,1)
	84.93	84.92	85.69	(3,1)
	152.7	152.6	157.1	(4,1)
0.9	15.65	15.90	15.12	(1,1)
	17.67	17.68	17.58	(2,1)
	66.26	66.24	67.67	(3,1)
	135.2	135.2	140.1	(4,1)
$\sigma_{cr}hb^2/D$	92.10	95.56	93.50	(2,1)

Table 3.8b: Dimensionless frequency $\Omega = \omega ab\sqrt{\frac{\rho h}{D}}$, loaded edges simply supported and other edges clamped, aspect ratio: 2

a/b=2				
σ_0/σ_{cr}	Two-stress-function	Four-stress-function	Finite element analysis	Mode
0.1	48.03	48.06	47.31	(1,1)
	56.89	56.91	55.86	(2,1)
	75.83	75.84	74.54	(3,1)
	106.4	106.3	105.1	(4,1)
0.5	45.62	45.74	44.98	(1,1)
	46.32	46.40	45.76	(2,1)
	56.64	56.69	56.17	(3,1)
	82.13	82.12	82.09	(4,1)
0.9	25.18	25.15	25.56	(3,1)
	30.24	29.67	30.58	(2,1)
	43.45	43.79	42.99	(1,1)
	48.40	48.52	50.06	(4,1)
$\sigma_{cr}hb^2/D$	94.20	99.19	92.96	(3,1)

Table 3.8c: Dimensionless frequency $\Omega = \omega ab\sqrt{\frac{\rho h}{D}}$, loaded edges simply supported and other edges clamped, aspect ratio: 3

a/b=3				
σ_0/σ_{cr}	Two-stress-function	Four-stress-function	Finite element analysis	Mode
0.1	69.93	69.87	68.93	(1,1)
	75.02	75.06	73.82	(2,1)
	85.19	85.25	83.75	(3,1)
	102.2	102.1	100.6	(4,1)
0.5	67.61	67.92	66.96	(2,1)
	68.31	68.07	67.40	(1,1)
	68.75	69.06	68.53	(3,1)
	76.40	76.30	76.93	(4,1)
0.9	33.966	34.00	36.71	(4,1)
	46.877	47.85	39.60	(3,1)
	59.91	60.30	59.83	(2,1)
	66.662	66.09	66.04	(1,1)
$\sigma_{cr}hb^2/D$	102.8	106.5	95.31	(4,1)

Table 3.9a: Dimensionless frequency $\Omega = \omega ab\sqrt{\frac{\rho h}{D}}$, all edges clamped (CCCC), aspect ratio: 1

a/b=1				
σ_0/σ_{cr}	Two-stress-function	Four-stress-function	Finite element analysis	Mode
0.1	34.97	34.97	34.38	(1,1)
	71.27	71.21	70.44	(2,1)
	132.19	132.1	130.0	(3,1)
	212.74	212.6	213.2	(4,1)
0.5	26.54	26.54	26.24	(1,1)
	54.04	53.66	54.08	(2,1)
	112.12	111.66	111.5	(3,1)
	191.64	191.1	193.8	(4,1)
0.9	12.31	12.32	12.35	(1,1)
	27.17	25.80	29.11	(2,1)
	87.76	86.70	89.30	(3,1)
	167.9	166.9	172.4	(4,1)
$\sigma_{cr}hb^2/D$	137.3	145.5	139.8	(1,1)

Table 3.9b: Dimensionless frequency $\Omega = \omega ab\sqrt{\frac{\rho h}{D}}$, all edges clamped (CCCC), aspect ratio: 2

a/b=2				
σ_0/σ_{cr}	Two-stress-function	Four-stress-function	Finite element analysis	Mode
0.1	49.45	49.48	48.63	(1,1)
	62.51	62.52	61.11	(2,1)
	88.92	88.63	85.39	(3,1)
	126.0	126.0	121.9	(4,1)
0.5	46.00	46.17	45.28	(1,1)
	49.44	49.55	48.50	(2,1)
	66.39	66.36	64.37	(3,1)
	99.05	98.84	96.15	(4,1)
0.9	28.90	28.97	28.37	(3,1)
	30.25	30.76	29.37	(2,1)
	43.72	43.90	43.03	(1,1)
	61.54	60.87	60.56	(4,1)
$\sigma_{cr}hb^2/D$	113.4	121.0	116.0	(3,1)

Table 3.9c: Dimensionless frequency $\Omega = \omega ab\sqrt{\dfrac{\rho h}{D}}$, all edges clamped (CCCC), aspect ratio: 3

a/b=3				
σ_0/σ_{cr}	Two-stress-function	Four-stress-function	Finite element analysis	Mode
0.1	70.50	70.42	69.42	(1,1)
	77.45	77.50	75.88	(2,1)
	91.60	91.72	88.58	(3,1)
	113.0	113.0	109.0	(4,1)
0.5	67.91	67.44	66.88	(1,1)
	68.30	68.49	67.10	(2,1)
	72.52	73.33	71.00	(3,1)
	84.72	84.87	82.41	(4,1)
0.9	37.20	37.09	36.68	(4,1)
	44.44	46.31	40.90	(3,1)
	59.37	60.19	57.81	(2,1)
	66.39	65.83	66.30	(1,1)
$\sigma_{cr}hb^2/D$	113.7	118.7	112.6	(4,1)

Table 3.10a: Dimensionless frequency $\Omega = \omega ab\sqrt{\frac{\rho h}{D}}$, loaded edges clamped and other edges simply supported (CCSS), aspect ratio: 1

a/b=1				
σ_0/σ_{cr}	Two-stress-function	Four-stress-function	Finite element analysis	Mode
0.1	27.65	27.65	27.61	(1,1)
	67.48	67.46	67.59	(2,1)
	129.7	129.69	128.9	(3,1)
	210.8	210.8	-*	(4,1)
0.5	20.76	20.75	20.83	(1,1)
	56.77	56.65	56.97	(2,1)
	117.5	117.4	117.1	(3,1)
	198.0	197.9	-*	(4,1)
0.9	9.382	9.379	9.537	(1,1)
	43.41	43.12	43.62	(2,1)
	104.0	103.7	104.4	(3,1)
	184.4	184.1	186.9	(4,1)
$\sigma_{cr}hb^2/D$	87.70	92.84	93.36	(1,1)

* See text, page 66

Table 3.10b: Dimensionless frequency $\Omega = \omega ab\sqrt{\frac{\rho h}{D}}$, loaded edges clamped and other edges simply supported (CCSS), aspect ratio: 2

a/b=2				
σ_0/σ_{cr}	Two-stress-function	Four-stress-function	Finite element analysis	Mode
0.1	26.52	26.54	26.52	(1,1)
	45.30	45.30	45.10	(2,1)
	76.22	76.21	74.58	(3,1)
	116.6	116.6	114.5	(4,1)
0.5	22.03	22.11	22.18	(1,1)
	33.90	33.88	33.91	(2,1)
	61.00	60.91	59.78	(3,1)
	99.77	99.59	97.99	(4,1)
0.9	15.27	15.25	15.44	(2,1)
	15.57	15.82	15.70	(1,1)
	40.70	40.45	39.89	(3,1)
	79.45	79.02	77.94	(4,1)
$\sigma_{cr}hb^2/D$	68.92	73.81	73.72	(2,1)

Table 3.10c: Dimensionless frequency $\Omega = \omega ab\sqrt{\frac{\rho h}{D}}$, loaded edges clamped and other edges simply supported (CCSS), aspect ratio: 3

a/b=3				
σ_0/σ_{cr}	Two-stress-function	Four-stress-function	Finite element analysis	Mode
0.1	33.50	33.39	33.54	(1,1)
	45.02	45.02	44.86	(2,1)
	64.98	65.02	63.61	(3,1)
	91.47	91.36	89.61	(4,1)
0.5	30.40	29.73	30.53	(1,1)
	35.19	35.10	35.26	(2,1)
	48.75	49.01	48.12	(3,1)
	71.64	71.01	70.41	(4,1)
0.9	20.01	19.07	19.88	(2,1)
	20.52	19.98	20.53	(3,1)
	28.89	28.80	29.09	(1,1)
	44.12	42.56	43.60	(4,1)
$\sigma_{cr}hb^2/D$	65.28	69.55	68.05	(3,1)

Table 3.11: Dimensionless frequency $\Omega = \omega ab\sqrt{\frac{\rho h}{D}}$ of a plate with an aspect ratio of 1 and relative in-plane load ratio of 0.5 (from FE analysis)

Mode sequence	SSSS	SSCC	CCCC	CCSS
1	14.03(1,1)	22.42(1,1)	26.24(,1,1)	20.82(1,1)
2	40.45(2,1)	38.99(2,1)	54.08(2,1)	52.85(1,2)
3	48.58(1,2)	68.68(1,2)	71.81(1,2)	56.97(2,1)
4	75.13(2,2)	85.69(3,1)	98.77(2,2)	87.97(2,2)
5	90.41(3,1)	88.26(2,2)	111.5(3,1)	103.4(1,3)
6	100.3(1,3)	130.7(3,2)	134.3(1,3)	117.1(3,1)
7	123.7(3,2)	131.7(1,3)	151.7(3,2)	137.3(2,3)
8	127.5(2,3)	153.0(2,3)	161.2(2,3)	146.9(3,2)
9	162.9(4,1)	157.1(4,1)	193.8(4,1)	176.0(1,4)
10	173.4(1,4)	194.9(3,3)	211.5(3,3)	194.7(3,3)

Table 3.12: Dimensionless Frequency $\Omega = \omega ab\sqrt{\frac{\rho h}{D}}$ of a plate with an aspect ratio of 2 and relative in-plane load ratio of 0.5 (from FE analysis)

Mode sequence	SSSS	SSCC	CCCC	CCSS
1	20.97(1,1)	44.98(1,1)	45.28(1,1)	22.18(1,1)
2	28.16(2,1)	45.76(2,1)	48.50(2,1)	33.91(2,1)
3	48.56(3,1)	56.17(3,1)	64.37(3,1)	59.78(3,1)
4	81.67(4,1)	82.08(4,1)	96.15(4,1)	85.36(1,2)
5	84.36(1,2)	122.5(5,1)	129.1(1,2)	97.99(4,1)
6	96.48(2,2)	128.42(1,2)	139.0(2,2)	99.98(2,2)
7	117.8(3,2)	136.5(2,2)	142.1(5,1)	125.1(3,2)
8	126.1(5,1)	151.7(3,2)	157.1(3,2)	147.5(5,1)
9	149.7(4,2)	175.7(6,1)	186.4(4,2)	161.6(4,2)
10	181.7(6,1)	177.0(4,2)	200.6(6,1)	187.4(1,3)

Table 3.13: Dimensionless Frequency $\Omega = \omega ab\sqrt{\frac{\rho h}{D}}$ of a plate with an aspect ratio of 3 and relative in-plane load ratio of 0.5 (from FE analysis)

Mode sequence	SSSS	SSCC	CCCC	CCSS
1	30.31(1,1)	66.96(2,1)	66.88(1,1)	30.53(1,1)
2	33.20(2,1)	67.40(1,1)	67.10(2,1)	35.26(2,1)
3	42.35(3,1)	68.53(3,1)	71.00(3,1)	48.12(3,1)
4	60.91(4,1)	76.93(4,1)	82.41(4,1)	70.41(4,1)
5	88.38(5,1)	95.45(5,1)	104.7(5,1)	101.5(5,1)
6	122.7(1,2)	124.7(6,1)	137.8(6,1)	123.0(1,2)
7	124.1(6,1)	163.9(7,1)	181.0(7,1)	132.2(2,2)
8	130.8(2,2)	189.5(1,2)	189.7(1,2)	140.8(6,1)
9	144.2(3,2)	195.2(2,2)	196.0(2,2)	147.5(3,2)
10	163.9(4,2)	204.1(3,2)	206.1(3,2)	169.6(4,2)

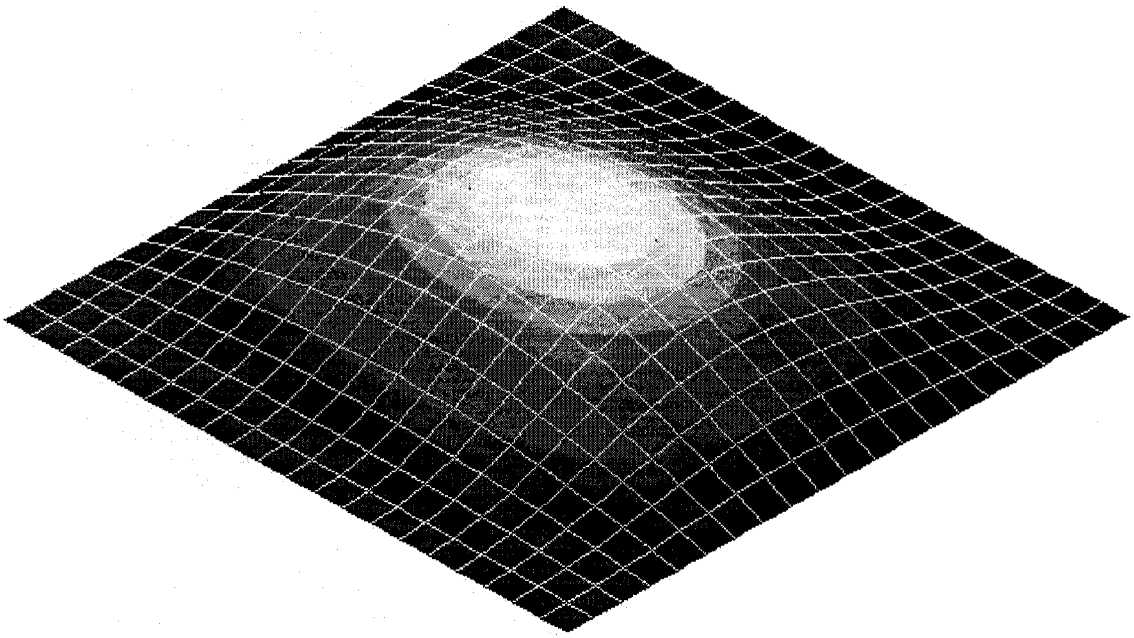

Figure 3.8: Mode 1 of CCSS plate with relative in-plane load of 0.9 (aspect ratio: 1)
Dimensionless frequency $\Omega = 9.537$

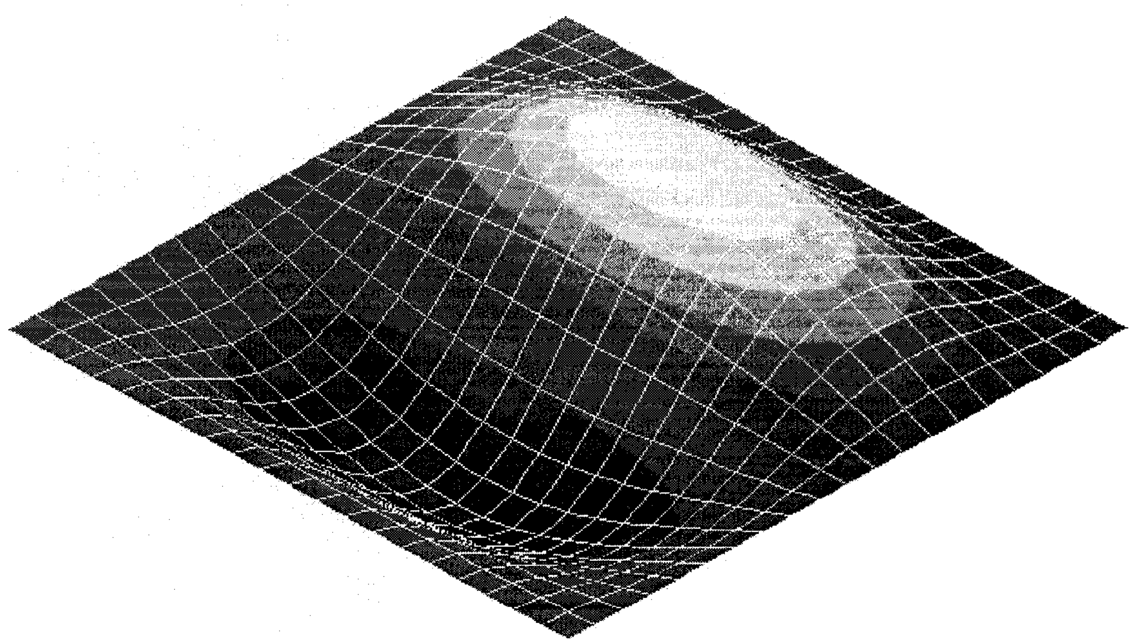

Figure 3.9: Mode 2 of CCSS plate with relative in-plane load of 0.9 (aspect ratio: 1)
Dimensionless frequency $\Omega = 43.62$

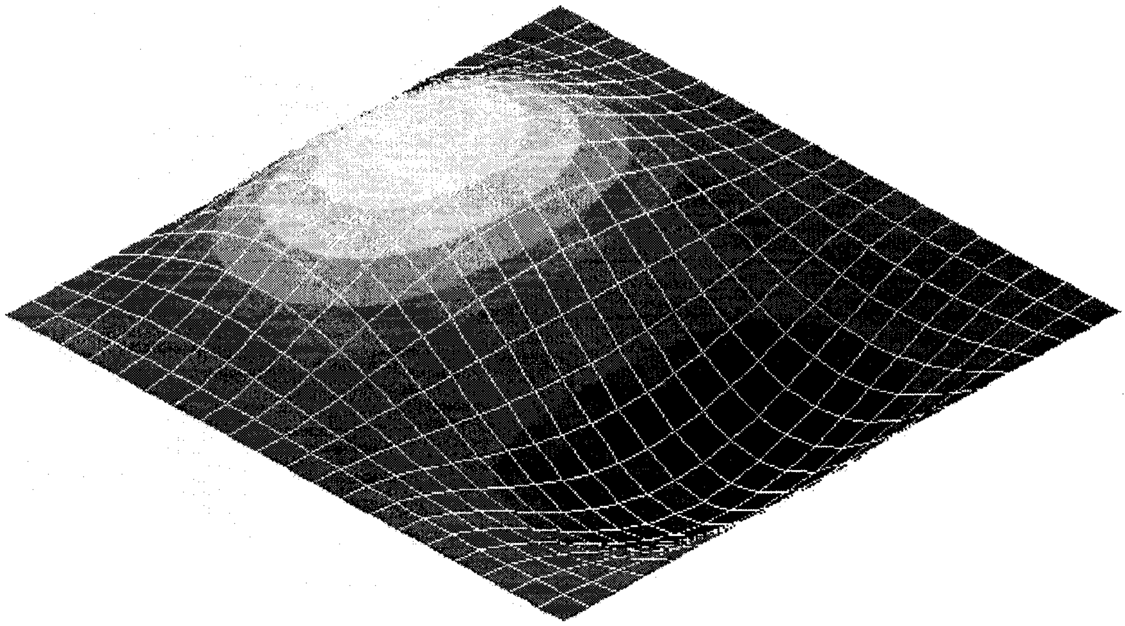

Figure 3.10: Mode 3 of CCSS plate with relative in-plane load of 0.9 (aspect ratio: 1)
Dimensionless frequency $\Omega = 50.98$

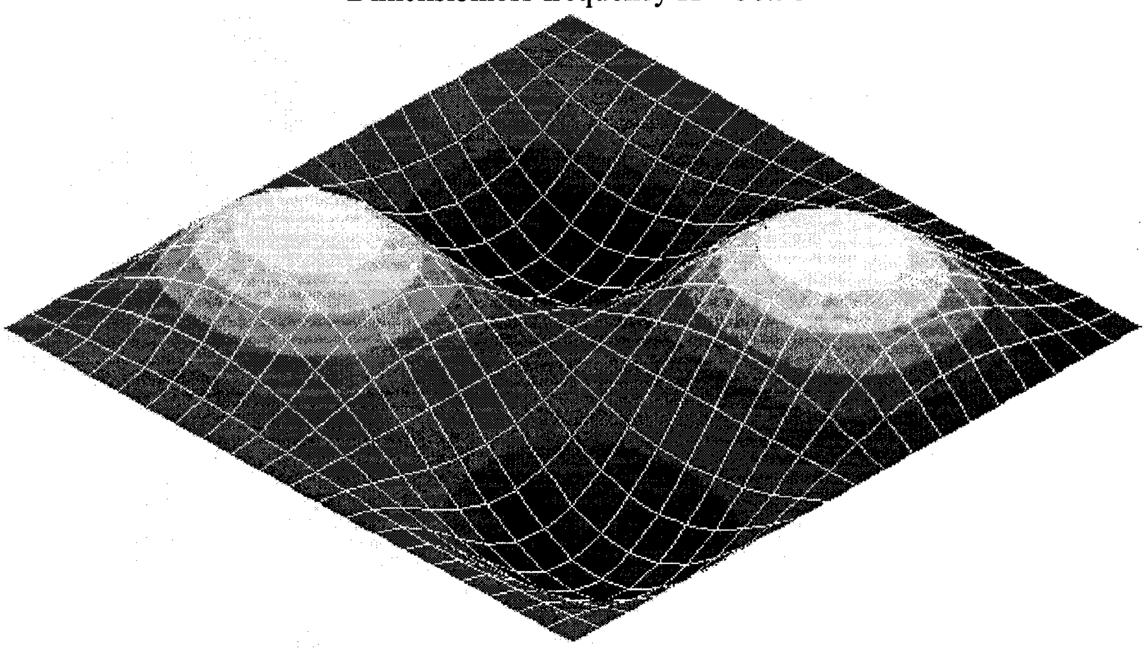

Figure 3.11: Mode 4 of CCSS plate with relative in-plane load of 0.9 (aspect ratio: 1)
Dimensionless frequency $\Omega = 81.72$

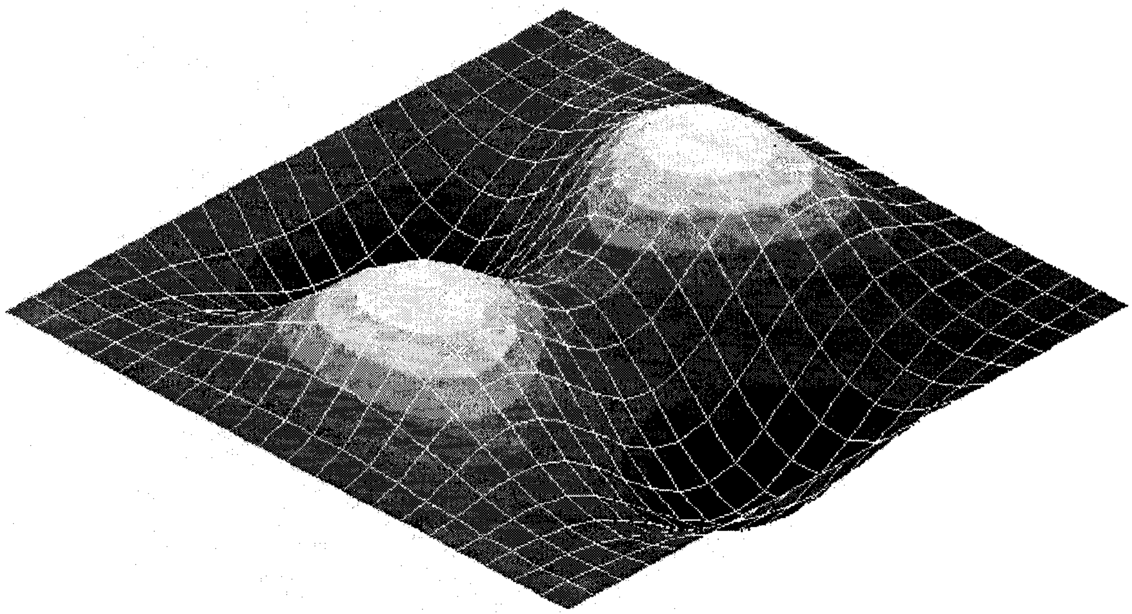

Figure 3.12: Mode 5 of CCSS plate with relative in-plane load of 0.9 (aspect ratio: 1)
Dimensionless frequency $\Omega = 102.6$

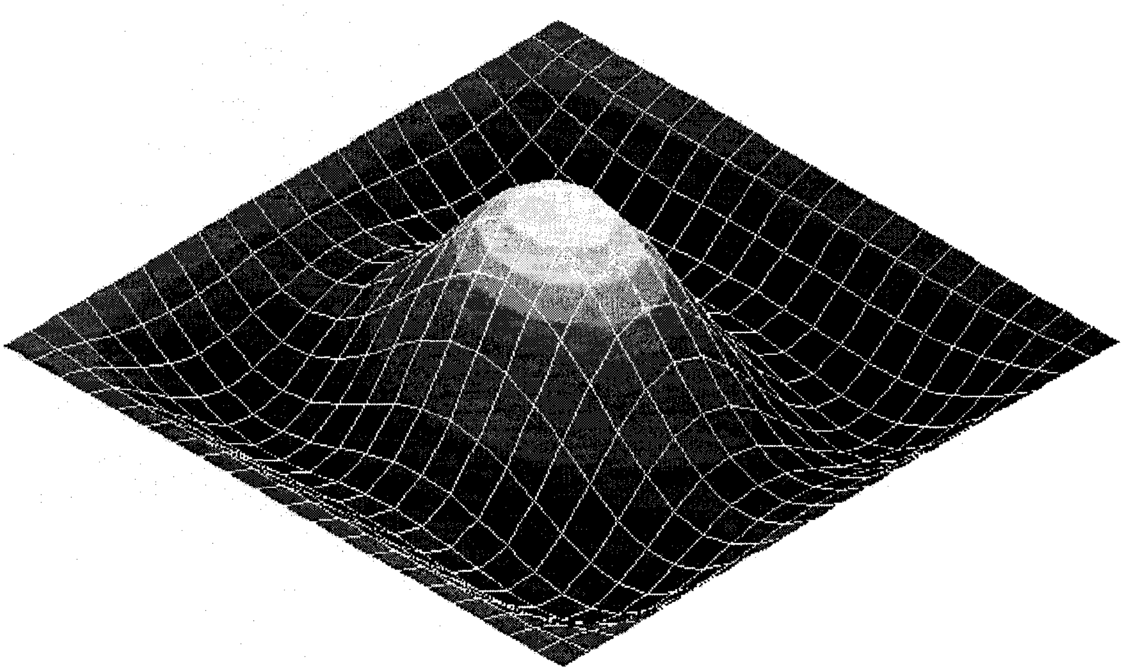

Figure 3.13: Mode 6 of CCSS plate with relative in-plane load of 0.9 (aspect ratio: 1)
Dimensionless frequency $\Omega = 104.4$

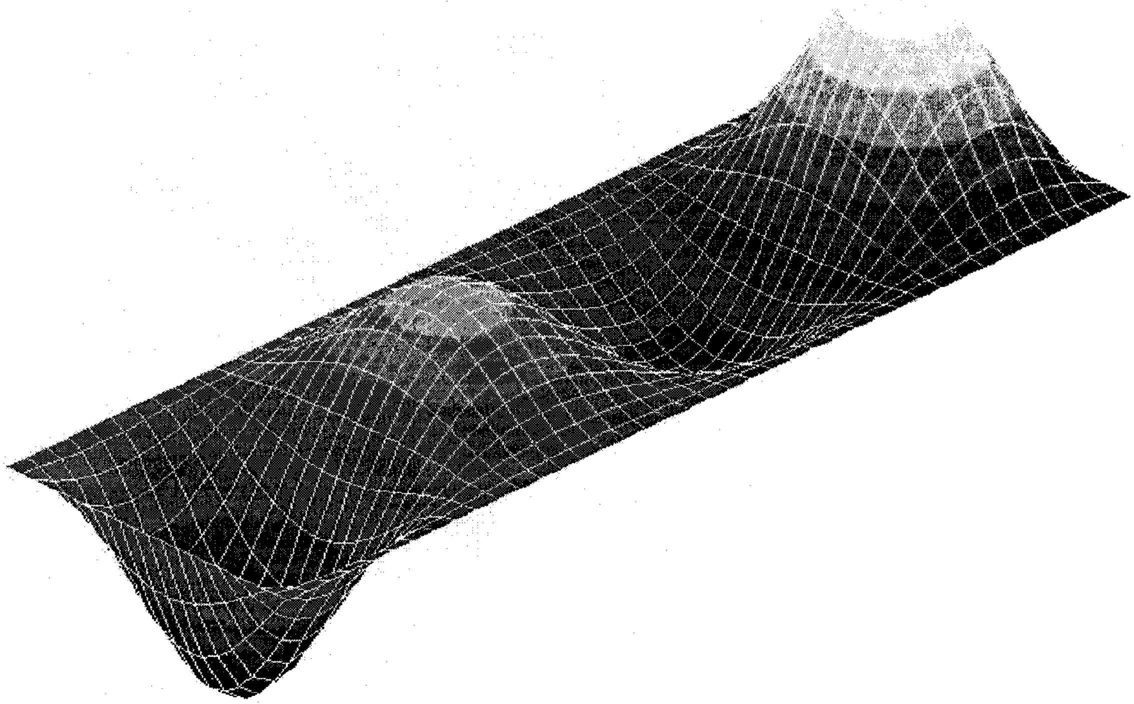

Figure 3.14: Mode 1 of SSCC plate with relative in-plane load of 0.9 (aspect ratio: 3)
Dimensionless frequency $\Omega = 36.71$

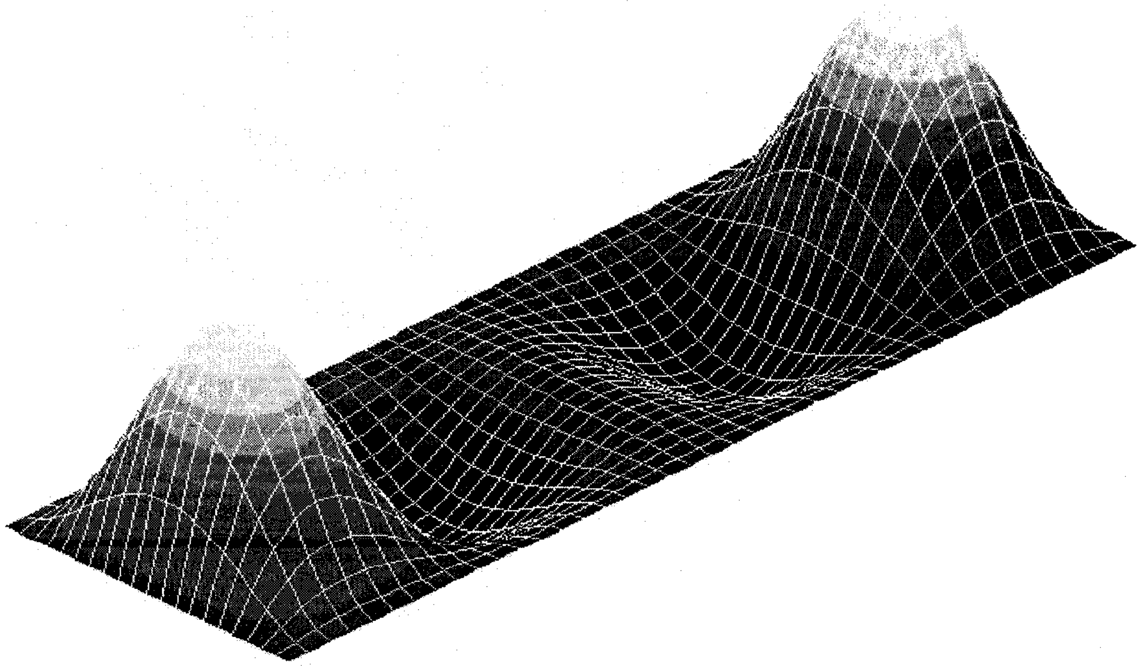

Figure 3.15: Mode 2 of SSCC plate with relative in-plane load of 0.9 (aspect ratio: 3)
Dimensionless frequency $\Omega = 39.60$

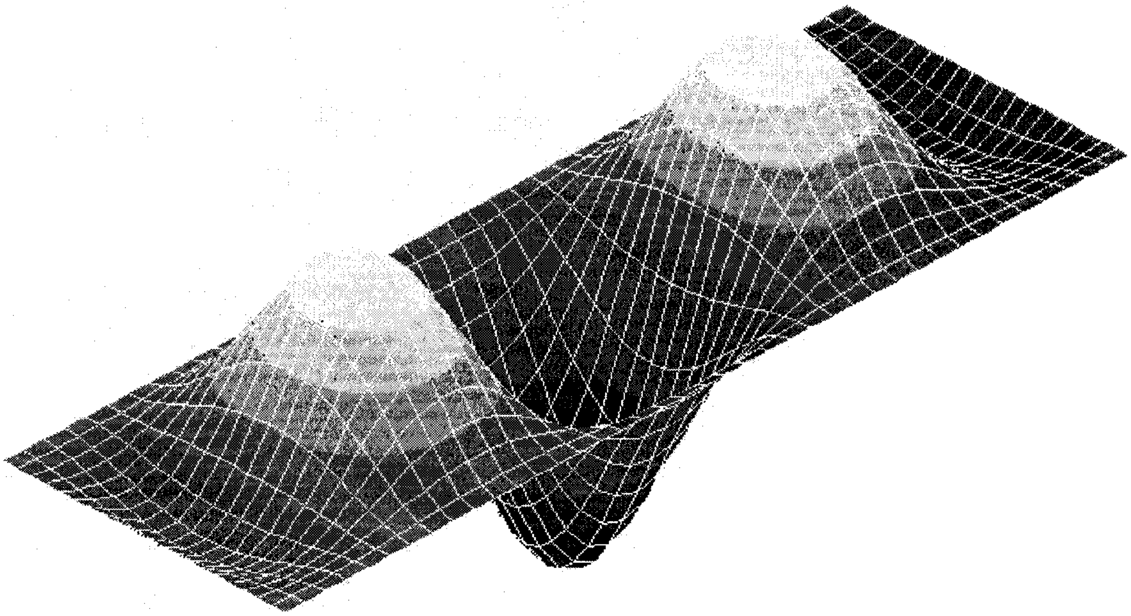

Figure 3.16: Mode 3 of SSCC plate with relative in-plane load of 0.9 (aspect ratio: 3)
Dimensionless frequency $\Omega = 55.29$

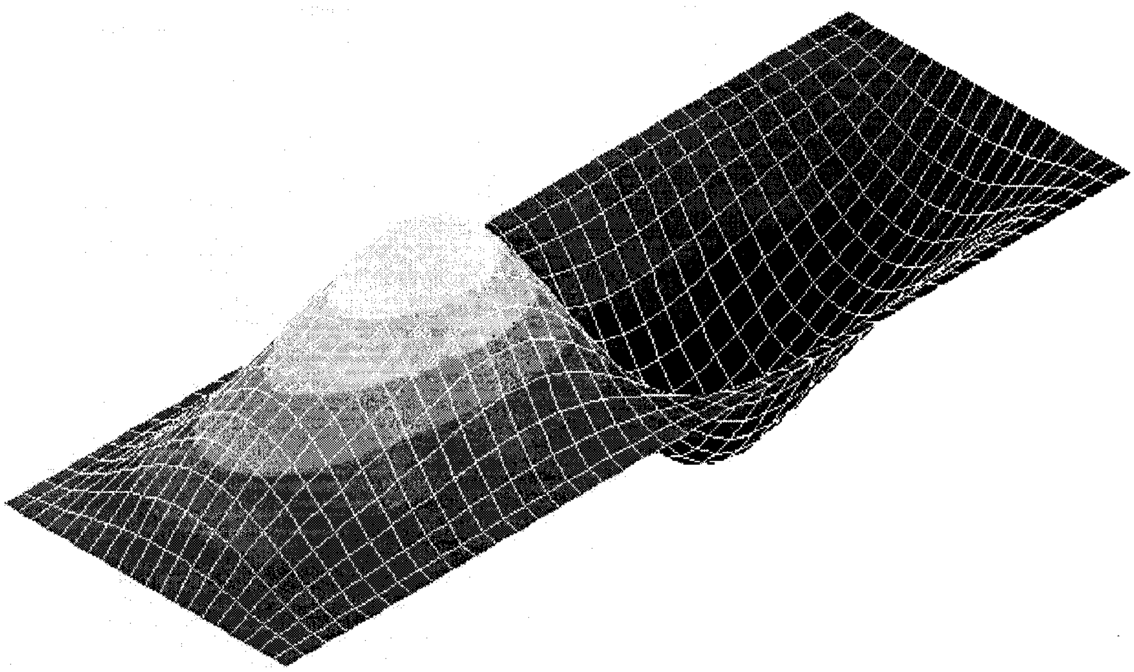

Figure 3.17: Mode 4 of SSCC plate with relative in-plane load of 0.9 (aspect ratio: 3)
Dimensionless frequency $\Omega = 59.84$

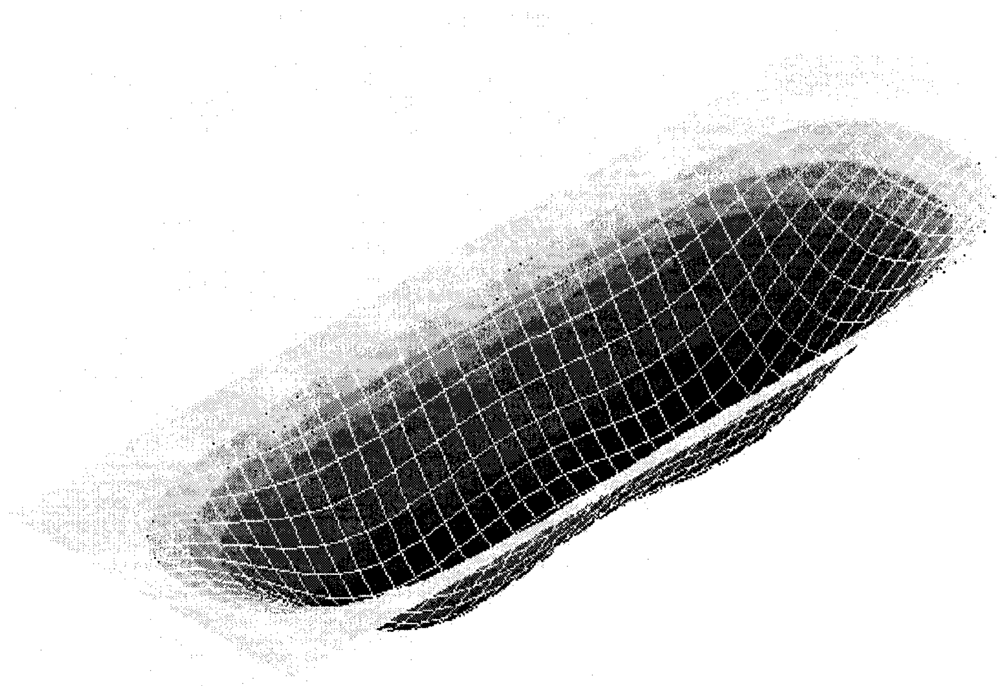

Figure 3.18: Mode 5 of SSCC plate with relative in-plane load of 0.9 (aspect ratio: 3)
Dimensionless frequency $\Omega = 66.05$

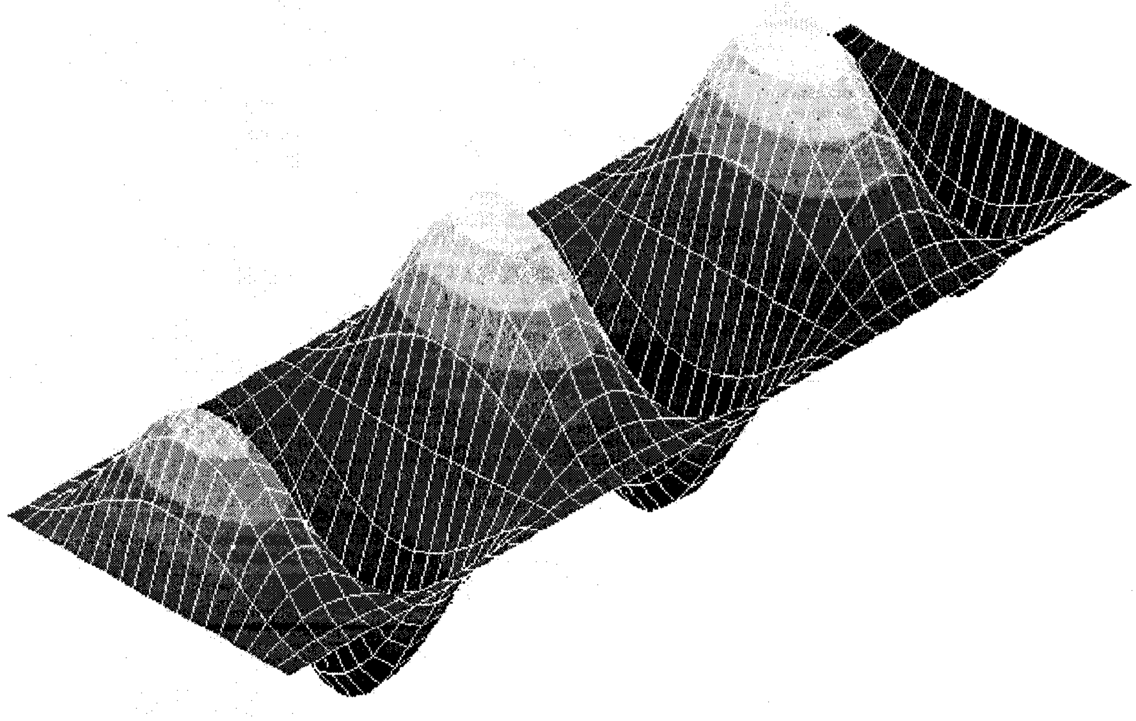

Figure 3.19: Mode 6 of SSCC plate with relative in-plane load of 0.9 (aspect ratio: 3)
Dimensionless frequency $\Omega = 77.74$

CHAPTER FOUR

CONCLUSIONS AND RECOMMENDATIONS

4.1 Conclusions

The present work proposed in-plane elasticity solutions for thin isotropic rectangular plates subjected to half-sinusoidal in-plane edge loads on two opposite edges. From the various in-plane elasticity solutions developed, it was evident that the polynomial method did not give a satisfactory solution due to the presence of excessive edge stresses. Consequently, by considering a superposition method and Fourier expansions, two different in-plane elasticity solutions are obtained: where the first solution is a simplified two-stress-function solution and the second is the four-stress-function solution. The present elasticity solutions exhibit the stress diffusion phenomenon at higher plate aspect ratios, in accordance with Saint-Venant's principle. As a result of this phenomenon, the in-plane x-direction stresses become uniform for most part of the plate at higher plate aspect ratios. Also the present solutions result in y-direction normal stresses as well as in-plane shear stresses which are of considerable magnitude throughout the plate.

Although in-plane elasticity solutions for the case of parabolically loaded rectangular plates are available in the literature, they were found to be either approximate or violate the boundary conditions at the plate corners. In the present analysis, only the four-stress-function superposition method showed similar boundary condition violations at the plate corners. The in-plane elasticity solutions are compared with finite element analysis results and found to be in very good agreement for various plate aspect ratios.

In the second part of the present analysis, buckling loads are estimated using the in-plane elasticity solutions, and the results are compared against each other and with those from finite element analysis. Owing to the complexity of the resulting governing differential equation, an approximate method of solution using Galerkin's method is used for estimating the buckling loads. Convergence of the trial functions considered is established for all plate edge conditions. The buckling results are tabulated for combinations of simply supported and clamped edge conditions. Once again, close agreements of the buckling results is observed between all the methods considered. Owing to the stress diffusion phenomenon, at higher plate aspect ratios, relatively higher magnitudes of stresses act near the edges. This behavior is very different than when one considers a stress distribution which is the same at all plate sections. As a result of this, the plate sustains higher buckling loads than were obtained in the literature. Buckling loads of up to 30 percent higher are observed in the present analysis.

The third part of the present work deals with the flexural vibration characteristics of rectangular plates under half-sinusoidal loads as described above. Once again, using the Galerkin method, frequencies are obtained for various edge conditions and using all in-plane elasticity solutions. The results are compared with those from finite element analysis and excellent agreement is observed for all plate sizes and edge conditions. Extensive results are tabulated for reference.

4.2 Recommendations

From the in-plane elasticity solution, it is apparent that one cannot ignore the contribution of the y-direction normal stresses as well as the shear stresses in general as they are of considerable magnitude relative to the applied in-plane edge loads. Owing to the relatively large magnitudes of the edge stresses, the polynomial solution is not recommended for plate aspect ratios of more than 1. Among the other solutions, the two-stress-function and the Timoshenko solutions showed no spurious edge stresses at the boundaries. In this regard, the two-stress-function solution can be considered superior as it satisfied the governing differential equation. The four-stress-function solution is more complicated than the two-stress-function solution due to the additional stress functions and the associated Fourier expansions. All of the in-plane elasticity solutions developed in this study including the finite element method clearly exhibited the stress diffusion phenomenon at higher plate aspect ratios and therefore can not be neglected for estimating the buckling loads and the flexural vibration characteristics of the plate.

In the buckling analysis, all the current in-plane elasticity solutions yield loads higher than the corresponding values from the literature. The dimensionless buckling loads are plotted for various plate edge conditions and the use of these plots is recommended in place of the existing plots in the literature. Also, the buckling loads obtained clearly indicate that the plate under such loading conditions can sustain higher buckling loads, which enables the designer to select plate sizes more efficiently. Clearly the stress diffusion phenomenon at higher plate aspect ratios caused the plate to sustain higher buckling loads. Also from the present study it was observed that various methods estimate the lowest buckling load for various plate edge conditions with the exception of the four-stress-function solution. In general the two-stress-function solution estimate the lowest buckling load for most of the cases.

Extensive flexural vibration frequencies are tabulated for all the plate edge conditions and with varying in-plane load ratios. All the analytical solutions and finite element solution show excellent agreement especially near smaller in-plane load ratios. From the results of the flexural vibration analysis, one can estimate the resonant frequencies of plate structures from the present results which are plotted for various in-plane load ratios.

4.3 Future work

The present work can be extended in many facets to include other complexities involving geometry and material behavior. However, as a first step towards establishing the present behavior, one can conduct experimental analysis confirming the in-plane and buckling characteristics of rectangular plates with sinusoidal edge loads. . In a similar fashion, the present work can be extended to include combinations of other edge conditions such as free and guided edges. In general the Rayleigh-Ritz method seems to be promising owing to boundary condition relaxation for the trial functions.

Furthermore anisotropic and laminated composite plates could be considered as an extension of the material behavior. It is also possible to extend the present analysis for various applications involving spherical or cylindrical shell panels.

REFERENCES

Bassily, S.F., and Dickinson, S.M., 1973, Vibration of plates subject to arbitrary in-plane loads-A perturbation approach, Journal of Applied Mechanics, 40, pp.1023-1028.

Bassily, S.F., and Dickinson, S.M., 1978, Buckling and vibration of in-plane loaded plates treated by a unified Ritz approach, Journal of Sound and Vibration, 59(1), pp.1-14.

Bazant, Z., and Cedolin, L., 1991, Stability of Structures, Oxford University Press, New York.

Benoy, M.B., 1969, An energy solution for the buckling of rectangular plates under non-uniform in-plane loading, Aeronautical Journal, 73, pp.974-977.

Bert, C.W., and Devarakonda, K.K., 2003, Buckling of rectangular plates subjected to nonlinearly distributed in-plane loading, International Journal of Solids and Structures, 40(16), pp. 4097-4106.

Bloom, F., and Coffin, D., 2001, Handbook of Thin Plate Buckling and Postbuckling, Chapman & Hall/CRC, Boca Raton.

Brown, C.J., 1991, Elastic buckling of plates subjected to distributed tangential loads, Computers and Structures, 41(1), pp.151-155.

Brush, D.O., and Almroth, B.O., 1975, Buckling of Bars, Plates and Shells, McGraw-Hill Inc., New York.

Bryan (1890-91), On the stability of a plane plate under thrusts in its own plane, with applications to the "buckling" of the sides of a ship. Proceedings of the London Mathematical Society 22, pp.54-67.

Chan, H.C., and Foo, O., 1979, Vibration of rectangular plates subjected to in-plane forces by the finite strip method, Journal of Sound and Vibration, 64(4), pp.583-588.

Chen, Y.Z., 1998, Evaluation of buckling loading of rectangular bending plate by using an iterative approach, Computer Methods in Applied Mechanics and Engineering, 167, pp.91-99.

Devarakonda, K.K., and Bert, C.W., Buckling of rectangular plate with nonlinearly distributed compressive loading on two opposite edges: comparative analysis and results, (in press in Mechanics of Advanced Materials and Structures).

Dickinson, S.M., 1971, Lateral vibration of rectangular plates subject to in-plane forces, Journal of Sound and Vibration, 16(4), pp.465-472.

Dickinson, S.M., 1975, Bolotin's method applied to the buckling and lateral vibration of stressed plates, AIAA Journal, 13(1), pp.109-110.

Dickinson, S.M., and Di Blasio, A., 1986, On the use of orthogonal polynomials in the Rayleigh-Ritz method for the study of the flexural vibration and buckling of isotropic and orthotropic rectangular plates, Journal of Sound and Vibration, 108(1), pp.51-62.

El-Bayoumy L., 1971, Buckling of clamped rectangular plates, Journal of the Engineering Mechanics Division, Proceedings of the ASCE, pp.1277-1289.

Favre, H., 1948, The influence of its own weight on the stability of a rectangular plate. In: Proceedings of 7th International Congress of Applied Mechanics, London, 1, pp.151-159.

Gorman, D.J., 1976, Free vibration analysis of cantilever plates by the method of superposition, Journal of Sound and Vibration, 49(4), pp.453-467.

Gorman, D.J., and Singhal, R.K., 1993, A superposition-Rayleigh-Ritz method for free vibration analysis of non-uniformly tensioned membranes, Journal of Sound and Vibration 162(3), pp.489-501.

Gorman, D. J., 2000, Free vibration and buckling of in-plane loaded plates with rotational elastic edge support, Journal of Sound and Vibration, 229(4), pp.755-773.

Grimm, T.R., and Gerdeen, J.C., 1975, Instability analysis of thin rectangular plates using the Kantorovich method, Journal of Applied Mechanics, 42, pp.110-114.

Grossman, N., 1949. Elastic stability of simply supported flat rectangular plates under critical combinations of transverse compression and longitudinal bending, Journal of the Aeronautical Sciences, 16, pp.272-276.

Guran, A., and Inman, D.J., ed., 1999, Buckling of Plates with In-Plane Forces, World Scientific, Series A, Volume 3, Singapore.

Hu, H., Abatan, A., and Badir, A., 1999, Effect of material anisotropy on buckling behavior of plates under parabolically varying load, 31st International SAMPE Technical Conference, October 26-30, Atlanta.

Kang, J.H., and Leissa, A.W., 2001, Vibration and buckling of SS-F-SS-F rectangular plates loaded by in-plane moments, International Journal of Structural Stability and Dynamics, 1, pp.527-543.

Kaul, R.K., and Tewari, S.G., 1958, On the bounds of eigenvalues of a clamped plate in tension, Journal of Applied Mechanics, 25, pp.52-54

Kerr, A.D., 1969, An extended Kantorovich method for the solution of eigenvalue problems, International Journal of Solids and Structures, 5, pp.559-572.

Kielb, R. E., and Han, L.S., 1980, Vibration and buckling of rectangular plates under in-plane hydrostatic loading, Journal of Sound and Vibration, 70(4), pp.543-555.

Laura, P.A.A., Luisoni, L.E., and Gutierrez, R.H., 1977, Vibrations of rectangular plates elastically restrained against rotation along the edges and subjected to a non-uniform state of in-plane stress, Recent Advances in Engineering Science, ed., Sih, G.C., Proceedings of 14th Annual Meeting of the Society of Engineering Science, November 14-16, Bethlehem, PA, pp.155-158.

Leissa, A.W., 1969, Vibration of Plates, U.S. Government Printing Office, NASA SP-160.

Leissa, A.W., 1973, The free vibration of rectangular plates, Journal of Sound and Vibration, 31, pp.257-293.

Leissa, A.W., and Kang, J.H., 2001. Exact solutions for the free vibrations and buckling of rectangular plates with linearly varying in-plane loading, Proceedings, 2001 ASME International Mechanical Engineering Congress and Exhibition, New York; ASME Paper IMECE2001/AD-23758.

Lurie, H., 1952, Lateral vibrations as related to structural stability, Journal of Applied Mechanics, 19, pp.195-198

MARC element library Volume B, 1994, MARC Analysis Research Corporation, Palo Alto, CA.

Massonnet, C., 1962, Two-dimensional problems (Chapter 37), Handbook of Engineering Mechanics, W.Flugge, ed., McGraw-Hill Inc., New York.

McKenzie, K.I., 1964, The buckling of a rectangular plate under combined biaxial compression, bending and shear, Aeronautical Quarterly, 15, pp.239-246.

Mei, C., and Yang, T.Y., 1972, Free vibrations of finite element plates subjected to complex middle-plane force systems, Journal of Sound and Vibration, 23(2), pp.145-156.

Niedenfuhr, F.W., 1957, On choosing stress functions in rectangular coordinates, Journal of Aeronautical Sciences, 24, pp.460-461.

Neou, C.Y., 1957, A direct method for determining Airy polynomial stress functions, ASME Journal of Applied Mechanics, 24, pp.387-390.

Noel, R.G., 1952, Elastic stability of simply supported flat rectangular plates under critical combinations of longitudinal bending, longitudinal compression, and lateral compression, Journal of the Aeronautical Sciences, 19, pp.829-834.

Pickett, G., 1944, Application of the Fourier Method to the solution of certain boundary problems in the theory of elasticity, Journal of Applied Mechanics, 11, pp.176-182.

Reddy, J.N., 1999, Theory and analysis of elastic plates, Taylor & Francis, Philadelphia, PA.

Shuleshko, P., 1956, Buckling of rectangular plates uniformly compressed in two perpendicular directions with one free edge and opposite edge elastically restrained, Journal of Applied Mechanics, 23, pp.359-363.

Shuleshko, P., 1957, Buckling of rectangular plates with two unsupported edges, Journal of Applied Mechanics, 24, pp.537-540.

Simons, D.A., and Leissa, A.W., 1971, Vibrations of rectangular cantilever plates subjected to in-plane acceleration loads, Journal of Sound and Vibration, 17(3), pp.407-422.

Sundararajan, C., 1980, Stability analysis of plates by a complementary energy method, International Journal for Numerical Methods in Engineering, 15, pp.343-349.

Szilard, R., 1974, Theory and Analysis of Plates: Classical and Numerical Methods, Prentice-Hall Inc., New Jersey.

Taylor, G.I., 1933, The buckling load for a rectangular plate with four clamped edges, Zeitschrift für angewandte Mathematik und Mechanik, 13(2), pp.147-152.

Timoshenko, S.P., 1924, The approximate solution of two-dimensional problems in elasticity, Philosophical Magazine, 47, pp.1095-1101.

Timoshenko, S.P., and Gere, J.M., 1961, Theory of elastic stability, 2nd ed., McGraw-Hill Inc., New York.

Timoshenko, S.P., and Goodier, J.N., 1970, Theory of Elasticity, 3rd ed., McGraw-Hill Inc., New York.

van der Neut, A., 1958, Buckling caused by thermal stresses, High temperature effects in aircraft structures, AGARDograph No.28, pp.215-247.

Walker, A.C., 1984, A brief review of plate buckling research, Behavior of Thin-walled Structures, ed., Rhodes, J., and Spence, J., Elsevier Applied Science Publishers, New York, pp.375-398.

Wang, C.M., Chen, Y., and Xiang, Y., 2002, Exact buckling solutions for simply supported rectangular plates under intermediate and end uniaxial loads, Proceedings of the Second International Conference on Structural Stability and Dynamics, ed., Wang, C.M., Liu, G.R., and Ang, K.K., World Scientific, New Jersey, pp.424-429.

Way, S., 1936, Stability of rectangular plates under shear and bending forces, Journal of Applied Mechanics, 3, pp.A131-A135.

Weinstein, A., and Chien, W.Z., 1943, On the vibrations of a clamped plate under tension, Quarterly Applied Mathematics, 1, pp.61-66.

APPENDIX I

Computer code for two-stress-function in-plane solution written in Matlab

Notes: The following code is run on Matlab (Version 6.0.1). The constants t1, t2 and t3 are the Fourier expansions of the shear stress due to stress function φ_1. These constants are to be calculated separately and are to be changed for any plate aspect ratio. Here "k" is the plate aspect ratio.

```
% This program calculates the constants of in-plane analysis
% for two stress function approach.
k=1.2;
c=1.5707963;
pi=c*2.0;
denm=sinh(k*c)*cosh(k*c) + k*c;
f1=(sinh(k*c) + k*c*cosh(k*c))/denm;
f4= -1.0*k*c*sinh(k*c)/denm;
% t1,t2,t3 are Fourier expansions of the shear stress due
% to stress function phi-1 at y/b=+/- 1 edges
t1=2.0159e-1;
t2=-3.923e-2;
t3=1.2771e-2;
c41=-1.0/(tanh(pi/k));
```

```
c42=-1.0/(tanh(2.0*pi/k));

c43=-1.0/(tanh(3.0*pi/k));

p1=(pi/k+c41)*sinh(pi/k) + c41*pi*cosh(pi/k)/k;

p2=((2.0*pi/k)+c42)*sinh(2.0*pi/k) + c42*2.0*pi*cosh(2.0*pi/k)/k;

p3=((3.0*pi/k)+c43)*sinh(3.0*pi/k) + c43*3.0*pi*cosh(3.0*pi/k)/k;

c11=-1.0*t1/p1;

c12=-1.0*t2/(2.0*p2);

c13=-1.0*t3/(3.0*p3);

c41=c11*c41;

c42=c12*c42;

c43=c13*c43;

q11= (c11*((pi/k)^2) + c41*2.0*pi/k)*k/pi;

q41= c41*((pi/k)^2)*k/pi;

q12= (c12*((2.0*pi/k)^2) + c42*4.0*pi/k)*k/pi;

q42= c42*((2.0*pi/k)^2)*k/pi;

q13= (c13*((3.0*pi/k)^2) + c43*6.0*pi/k)*k/pi;

q43= c43*((3.0*pi/k)^2)*k/pi;

sum=-1.0*(q11*cosh(pi/k) + q41*sinh(pi/k));

sum = sum + (q12*cosh(2.0*pi/k) + q42*sinh(2.0*pi/k));

sum = sum - (q13*cosh(3.0*pi/k) + q43*sinh(3.0*pi/k));

% R = Uniform stress, r = multiplication factor

R=sum;

sum=-1.0 - q11 + q12 - q13 - R;
```

```
r= -1.0/sum;

tmp1=f1 + (4.0*f4/(k*pi));

tmp2=f1 + (2.0*f4/(k*pi));

fprintf(1,'R = %e\n',R);

fprintf(1,'r = %e\n',r);

% Following stresses are compressive which can be directly

% substituted into the Mathematica files in the same order

fprintf(1,'sigma x\n');

fprintf(1,'%e\t%e\n',f1*r,f4*r);

fprintf(1,'%e\t%e\n',-1.0*q11*r,-1.0*q41*r);

fprintf(1,'%e\t%e\n',-1.0*q12*r,-1.0*q42*r);

fprintf(1,'%e\t%e\n',-1.0*q13*r,-1.0*q43*r);

fprintf(1,'%e\n',R*r);

fprintf(1,'sigma y\n');

fprintf(1,'%e\t%e\n',-1.0*tmp1*r,-1.0*f4*r);

fprintf(1,'%e\t%e\n',c11*pi*r/k,c41*pi*r/k);

fprintf(1,'%e\t%e\n',c12*4.0*pi*r/k,c42*4.0*pi*r/k);

fprintf(1,'%e\t%e\n',c13*9.0*pi*r/k,c43*9.0*pi*r/k);

fprintf(1,'sigma xy\n');

fprintf(1,'%e\t%e\n',-1.0*tmp2*r,-1.0*f4*r);

fprintf(1,'%e\t%e\n',-1.0*r*(c11*pi/k+c41),-1.0*r*c41*pi/k);

fprintf(1,'%e\t%e\n',-2.0*r*(c12*2.0*pi/k+c42),-2.0*r*c42*2.0*pi/k);

fprintf(1,'%e\t%e\n',-3.0*r*(c13*3.0*pi/k+c43),-3.0*r*c43*3.0*pi/k);
```

APPENDIX II

Computer code for calculating the in-plane stresses written in Matlab

```
fid=fopen('c:\twostressplotinput.txt','r');

% vector A contains elements for sig xx coefficients

A = fscanf(fid,'%e',9);

% vector B contains elements for sig yy coeff

B = fscanf(fid,'%e',8);

% vector C contains elements for sig xy coeff

C = fscanf(fid,'%e',8);

fclose(fid);

k=3;

pby2 = 1.5707963;

% N(xx) plot

z = 1.0;

j = 1;

for eta = 0.0:0.1:1.0

   y(j) = eta;

   s1 = ( A(1)*cosh(k*pby2*z) + A(2)*z*sinh(k*pby2*z) )*cos(pby2*eta);

   s2 = ( A(3)*cosh(2.0*pby2*eta/k) + A(4)*eta*sinh(2.0*pby2*eta/k)
)*cos(2.0*pby2*z);

   s3 = ( A(5)*cosh(4.0*pby2*eta/k) + A(6)*eta*sinh(4.0*pby2*eta/k)
)*cos(4.0*pby2*z);
```

```
s4 = ( A(7)*cosh(6.0*pby2*eta/k) + A(8)*eta*sinh(6.0*pby2*eta/k)
)*cos(6.0*pby2*z);
    x(j) = s1 + s2 + s3 + s4 + A(9);
    j = j+1;
end
plot(x,y)
% N(yy) plot
z = 1.0;
j = 1;
for eta = 0.0:0.1:1.0
    x1(j) = eta;
    s1 = ( B(1)*cosh(k*pby2*z) + B(2)*z*sinh(k*pby2*z) )*cos(pby2*eta);
    s2 = ( B(3)*cosh(2.0*pby2*eta/k) + B(4)*eta*sinh(2.0*pby2*eta/k)
)*cos(2.0*pby2*z);
    s3 = ( B(5)*cosh(4.0*pby2*eta/k) + B(6)*eta*sinh(4.0*pby2*eta/k)
)*cos(4.0*pby2*z);
    s4 = ( B(7)*cosh(6.0*pby2*eta/k) + B(8)*eta*sinh(6.0*pby2*eta/k)
)*cos(6.0*pby2*z);
    y1(j) = s1 + s2 + s3 + s4;
    j = j + 1;
end
% N(xy) plot
eta = 1.0;
```

```
j = 1;

for z = 0.0:0.1:1.0

   x2(j) = z;

   s1 = ( C(1)*sinh(k*pby2*z) + C(2)*z*cosh(k*pby2*z) )*sin(pby2*eta);

   y3(j) = s1;

   s2 = ( C(3)*sinh(2.0*pby2*eta/k) + C(4)*eta*cosh(2.0*pby2*eta/k)
)*sin(2.0*pby2*z);

   s3 = ( C(5)*sinh(4.0*pby2*eta/k) + C(6)*eta*cosh(4.0*pby2*eta/k)
)*sin(4.0*pby2*z);

   s4 = ( C(7)*sinh(6.0*pby2*eta/k) + C(8)*eta*cosh(6.0*pby2*eta/k)
)*sin(6.0*pby2*z);

   y2(j) = s1 + s2 + s3 + s4;

   j = j+1;

end
```

APPENDIX III

Sample finite element analysis input data for MSC-MARC

Notes on the input data

The data file given below is only a sample file in which only part of the nodal and element input data is shown for brevity. However, all the remaining data fields are shown exactly. Although this input data file is generated by the software, certain fields can be edited using a text processor. The data set can be divided in two major groups in which the first sub group contains all the element geometry and boundary condition parameters in addition to the analysis options. In the second part all load cases are defined in the order in which they are applied. For the elastic buckling analysis, the option "large disp" has to be specified in addition to the "buckle" option at the beginning of the file. With these two options, the software superimposes the second load case (which is buckling) on the first load case (named Prestress in the present analysis) and solves the whole system.

Prior to the "Loadcase" option, a "dist loads" option can be seen towards the end of the first group which represents the loading condition at zero time step. Typically the loads applied using this option will be applied at zero time step and the loads specified using the "Load case" option are applied at any other time step that can be defined. In a static stress analysis, either option will give the same results. However, for buckling analysis, only those loads that are specified using the "Load case" option are considered for prestress condition upon which the buckling analysis will be superposed.

The element 72 (rectangular plate element) has 4 corner nodes and 4 nodes at the mid side of the edges. Each mid node has a degree of freedom which is rotation of the edge about itself. In order to model the clamped edge condition, one has to specify this DOF (degree of freedom) to be zero.

In case of dynamic analysis, the buckle option will be replaced by the modal frequency option with number of frequencies to be extracted as a parameter. The frequencies are always arranged starting from the lowest one. The important difference in case of the dynamic analysis is the inclusion of an additional load case with "zero" in-plane loads. This causes the software to superpose the first load case (Prestress in the present case) with the dynamic modal analysis load case.

```
title     Sinusoidal load (trial 2)
$....MARC input file produced by MSC.Marc Mentat 2001r2
sizing      1000000  800 2521  302
elements     72
processor    1   1   1
large disp
buckle       2   2   1   0   0   0
all points
dist loads   20   2   0
shell sect   3
setname       7
end
$..................
solver
   4   0   0   0   0   0   0   0
optimize    10
connectivity
   0   0   0
   1   72   1   2   43   42  862  863  864  865
   2   72   2   3   44   43  866  867  868  863
   3   72   3   4   45   44  869  870  871  867
   4   72   4   5   46   45  872  873  874  870
   5   72   5   6   47   46  875  876  877  873
   6   72   6   7   48   47  878  879  880  876
   7   72   7   8   49   48  881  882  883  879
   8   72   8   9   50   49  884  885  886  882
   9   72   9  10   51   50  887  888  889  885
  10   72  10  11   52   51  890  891  892  888
coordinates
   3 2521   0   0
   1 0.00000+0 0.00000+0 0.00000+0
   2 3.75000-2 0.00000+0 0.00000+0
   3 7.50000-2 0.00000+0 0.00000+0
   4 1.12500-1 1.1102-16 0.00000+0
   5 1.50000-1 0.00000+0 0.00000+0
   6 1.87500-1 0.00000+0 0.00000+0
   7 2.25000-1 0.00000+0 0.00000+0
   8 2.62500-1 0.00000+0 0.00000+0
   9 3.00000-1 0.00000+0 0.00000+0
  10 3.37500-1 0.00000+0 0.00000+0
2510 1.31250+0 4.87500-1 0.00000+0
 2511 1.29375+0 4.99219-1 0.00000+0
 2512 1.35000+0 4.87500-1 0.00000+0
 2513 1.33125+0 4.99219-1 0.00000+0
```

```
2514 1.38750+0 4.87500-1 0.00000+0
2515 1.36875+0 4.99219-1 0.00000+0
2516 1.42500+0 4.87500-1 0.00000+0
2517 1.40625+0 4.99219-1 0.00000+0
2518 1.46250+0 4.87500-1 0.00000+0
2519 1.44375+0 4.99219-1 0.00000+0
2520 1.49766+0 4.87500-1 0.00000+0
2521 1.48125+0 4.99219-1 0.00000+0
isotropic

  1              0   0   0   0material1
 2.0000+11 3.00000-1 7.80000+3 0.00000+0 0.00000+0 0.00000+0 0.00000+0
0.00000+0
    1    to    800
geometry

 1.00000-2 0.00000+0 0.00000+0 0.00000+0 0.00000+0 0.00000+0 0.00000+0
    1    to    800
fixed disp

 0.00000+0
   1
   21    62   103   144   185   226   267   308   349     c
   390   431   472   513   554   595   636   677   718     c
   759   800   841
 0.00000+0
   3
    1     2     3     4     5     6     7     8     9     c
    10    11    12    13    14    15    16    17    18     c
    19    20    21    22    23    24    25    26    27     c
    28    29    30    31    32    33    34    35    36     c
    37    38    39    40    41    42    82    83   123     c
   124   164   165   205   206   246   247   287   288     c
   328   329   369   370   410   411   451   452   492     c
   493   533   534   574   575   615   616   656   657     c
   697   698   738   739   779   780   820   821   822     c
   823   824   825   826   827   828   829   830   831     c
   832   833   834   835   836   837   838   839   840     c
   841   842   843   844   845   846   847   848   849     c
   850   851   852   853   854   855   856   857   858     c
   859   860   861
 0.00000+0
   2
   411    to    451
 0.00000+0
   1
```

```
  862   865   866   869   872   875   878   881   884    c
  887   890   893   896   899   902   905   908   911    c
  914   917   920   923   926   929   932   935   938    c
  941   944   947   950   953   956   959   962   965    c
  968   971   974   977   980   981   985   1062  1066    c
 1143  1147  1224  1228  1305  1309  1386  1390  1467    c
 1471  1548  1552  1629  1633  1710  1714  1791  1795    c
 1872  1876  1953  1957  2034  2038  2115  2119  2196    c
 2200  2277  2281  2358  2362  2439  2442  2443  2445    c
 2447  2449  2451  2453  2455  2457  2459  2461  2463    c
 2465  2467  2469  2471  2473  2475  2477  2479  2481    c
 2483  2485  2487  2489  2491  2493  2495  2497  2499    c
 2501  2503  2505  2507  2509  2511  2513  2515  2517    c
 2519  2520  2521
dist loads

  21 0.00000+0 0.00000+0 0.00000+0   4
    40    800
  41 0.00000+0 0.00000+0 0.00000+0   4
     1    761
  21 0.00000+0 0.00000+0 0.00000+0   5
    80    760
  41 0.00000+0 0.00000+0 0.00000+0   5
    41    721
  21 0.00000+0 0.00000+0 0.00000+0   6
   120    720
  41 0.00000+0 0.00000+0 0.00000+0   6
    81    681
  21 0.00000+0 0.00000+0 0.00000+0   7
   160    680
  41 0.00000+0 0.00000+0 0.00000+0   7
   121    641
  21 0.00000+0 0.00000+0 0.00000+0   8
   200    640
  41 0.00000+0 0.00000+0 0.00000+0   8
   161    601
  21 0.00000+0 0.00000+0 0.00000+0   9
   240    600
  41 0.00000+0 0.00000+0 0.00000+0   9
   201    561
  21 0.00000+0 0.00000+0 0.00000+0  10
   280    560
  41 0.00000+0 0.00000+0 0.00000+0  10
   241    521
  21 0.00000+0 0.00000+0 0.00000+0  11
   320    520
```

```
  41 0.00000+0 0.00000+0 0.00000+0   11
    281     481
  21 0.00000+0 0.00000+0 0.00000+0   12
    360     480
  41 0.00000+0 0.00000+0 0.00000+0   12
    321     441
  21 0.00000+0 0.00000+0 0.00000+0   13
    400     440
  41 0.00000+0 0.00000+0 0.00000+0   13
    361     401
no print
summary
post
   1   16   17    0    0   19   20    0    1    0    0    0    0    0
  311    0
parameters
 1.00000+0 1.00000+9 1.00000+2 1.00000+6 2.50000-1 5.00000-1 1.50000+0-5.00000-1
 8.62500+0 2.00000+1 1.00000-4 1.00000-6 1.00000+0 1.00000-4
 8.31400+0 2.73150+2 0.00000+0 0.00000+0 5.67051-8
end option
$..................
$....start of loadcase Prestress
title     Prestress
control
99999   10    0    0    0    1    0    0    1    0    0
 1.00000-1 0.00000+0 0.00000+0 0.00000+0 0.00000+0 0.00000+0 0.00000+0
0.00000+0
parameters
 1.00000+0 1.00000+9 1.00000+2 1.00000+6 2.50000-1 5.00000-1 1.50000+0-5.00000-1
 8.62500+0 2.00000+1 1.00000-4 1.00000-6 1.00000+0 1.00000-4
 8.31400+0 2.73150+2 0.00000+0 0.00000+0 5.67051-8
auto load
   1    0   10
time step
 1.00000+0
dist loads    0

  21 6.54080+4 0.00000+0 0.00000+0    4
     40     800
  41 6.54080+4 0.00000+0 0.00000+0    4
      1     761
  21 1.94579+5 0.00000+0 0.00000+0    5
     80     760
  41 1.94579+5 0.00000+0 0.00000+0    5
     41     721
  21 3.19024+5 0.00000+0 0.00000+0    6
```

```
  120    720
  41 3.19024+5 0.00000+0 0.00000+0    6
   81    681
  21 4.35594+5 0.00000+0 0.00000+0    7
  160    680
  41 4.35594+5 0.00000+0 0.00000+0    7
  121    641
  21 5.41422+5 0.00000+0 0.00000+0    8
  200    640
  41 5.41422+5 0.00000+0 0.00000+0    8
  161    601
  21 6.33945+5 0.00000+0 0.00000+0    9
  240    600
  41 6.33945+5 0.00000+0 0.00000+0    9
  201    561
  21 7.10845+5 0.00000+0 0.00000+0   10
  280    560
  41 7.10845+5 0.00000+0 0.00000+0   10
  241    521
  21 7.70269+5 0.00000+0 0.00000+0   11
  320    520
  41 7.70269+5 0.00000+0 0.00000+0   11
  281    481
  21 8.10664+5 0.00000+0 0.00000+0   12
  360    480
  41 8.10664+5 0.00000+0 0.00000+0   12
  321    441
  21 8.31145+5 0.00000+0 0.00000+0   13
  400    440
  41 8.31145+5 0.00000+0 0.00000+0   13
  361    401
continue
$....end of loadcase Prestress
$..................
$....start of loadcase Buckle
title    Buckle
buckle
  40 1.00000-4    0
continue
recover
   1   2   2
continue
$....end of loadcase Buckle
$..................
```